NASA/TM—2011-215805

Statistical Models of Fracture Relevant to Nuclear-Grade Graphite: Review and Recommendations

Noel N. Nemeth
Glenn Research Center, Cleveland, Ohio

Robert L. Bratton
Idaho National Laboratory, Idaho Falls, Idaho

March 2011

NASA STI Program . . . in Profile

Since its founding, NASA has been dedicated to the advancement of aeronautics and space science. The NASA Scientific and Technical Information (STI) program plays a key part in helping NASA maintain this important role.

The NASA STI Program operates under the auspices of the Agency Chief Information Officer. It collects, organizes, provides for archiving, and disseminates NASA's STI. The NASA STI program provides access to the NASA Aeronautics and Space Database and its public interface, the NASA Technical Reports Server, thus providing one of the largest collections of aeronautical and space science STI in the world. Results are published in both non-NASA channels and by NASA in the NASA STI Report Series, which includes the following report types:

- TECHNICAL PUBLICATION. Reports of completed research or a major significant phase of research that present the results of NASA programs and include extensive data or theoretical analysis. Includes compilations of significant scientific and technical data and information deemed to be of continuing reference value. NASA counterpart of peer-reviewed formal professional papers but has less stringent limitations on manuscript length and extent of graphic presentations.

- TECHNICAL MEMORANDUM. Scientific and technical findings that are preliminary or of specialized interest, e.g., quick release reports, working papers, and bibliographies that contain minimal annotation. Does not contain extensive analysis.

- CONTRACTOR REPORT. Scientific and technical findings by NASA-sponsored contractors and grantees.

- CONFERENCE PUBLICATION. Collected papers from scientific and technical conferences, symposia, seminars, or other meetings sponsored or cosponsored by NASA.

- SPECIAL PUBLICATION. Scientific, technical, or historical information from NASA programs, projects, and missions, often concerned with subjects having substantial public interest.

- TECHNICAL TRANSLATION. English-language translations of foreign scientific and technical material pertinent to NASA's mission.

Specialized services also include creating custom thesauri, building customized databases, organizing and publishing research results.

For more information about the NASA STI program, see the following:

- Access the NASA STI program home page at *http://www.sti.nasa.gov*

- E-mail your question via the Internet to *help@sti.nasa.gov*

- Fax your question to the NASA STI Help Desk at 443–757–5803

- Telephone the NASA STI Help Desk at 443–757–5802

- Write to:
  NASA Center for AeroSpace Information (CASI)
  7115 Standard Drive
  Hanover, MD 21076–1320

NASA/TM—2011-215805

Statistical Models of Fracture Relevant to Nuclear-Grade Graphite: Review and Recommendations

Noel N. Nemeth
Glenn Research Center, Cleveland, Ohio

Robert L. Bratton
Idaho National Laboratory, Idaho Falls, Idaho

National Aeronautics and
Space Administration

Glenn Research Center
Cleveland, Ohio 44135

March 2011

Acknowledgments

The authors thank Prof. S. Leigh Phoenix and Dr. Phani Nukala for providing helpful correspondence and publications of their research and Andrew Walker for assistance in preparing this manuscript. This manuscript was funded by Battelle Energy Alliance, LLC, under Contract No. DE–AC07–05ID14517 with the U.S. Department of Energy.

Level of Review: This material has been technically reviewed by technical management.

Available from

NASA Center for Aerospace Information
7115 Standard Drive
Hanover, MD 21076–1320

National Technical Information Service
5301 Shawnee Road
Alexandria, VA 22312

Available electronically at http://gltrs.grc.nasa.gov

Contents

Statistical Models of Fracture Relevant to Nuclear-Grade Graphite: Review and Recommendations

Noel N. Nemeth
National Aeronautics and Space Administration
Glenn Research Center
Cleveland, Ohio 44135

Robert L. Bratton
Idaho National Laboratory
Idaho Falls, Idaho 83415

Summary

The nuclear-grade (low-impurity) graphite needed for the fuel element and moderator material for next-generation (Gen IV) reactors displays large scatter in strength and a nonlinear stress-strain response from damage accumulation. This response can be characterized as quasi-brittle. In this expanded review, relevant statistical failure models for various brittle and quasi-brittle material systems are discussed with regard to strength distribution, size effect, multiaxial strength, and damage accumulation. This includes descriptions of the Weibull, Batdorf, and Burchell models as well as models that describe the strength response of composite materials, which involves distributed damage. Results from lattice simulations are included for a physics-based description of material breakdown. Consideration is given to the predicted transition between brittle and quasi-brittle damage behavior versus the density of damage (level of disorder) within the material system. The literature indicates that weakest-link-based failure modeling approaches appear to be reasonably robust in that they can be applied to materials that display distributed damage, provided that the level of disorder in the material is not too large. The Weibull distribution is argued to be the most appropriate statistical distribution to model the stochastic-strength response of graphite. This report is an expanded version of Nemeth and Bratton (2010).

1.0 Introduction

1.1 Graphite and Next-Generation Nuclear Reactors

At present, 10 countries, including the United States, have agreed to cooperate on the development of the fourth generation (Gen IV) nuclear energy system (Generation IV International Forum (2009)). Figure 1 shows the evolution of reactors since their introduction in the 1950s. The Gen IV system is expected to come into service in 2030. In the United States, Gen IV research is being conducted by the U.S. Department of Energy for development of the Very High Temperature Reactor design concept for the Next Generation Nuclear Plant Project (Idaho National Laboratory et al. (2005)). The design will have a graphite-moderated reactor, either a prismatic graphite-block-type core or pebble-bed core that will produce process heat in a highly efficient manner, reducing the need to burn fossil fuels to produce process heat and thereby reducing green house emissions. The application of heat is essential to nearly all basic material and commodity manufacturing processes, and heating processes account for about 17 percent of all industrial energy use (U.S. Department of Energy (2008)). Figure 2 shows a schematic of the Gen IV Very High Temperature Reactor gas-cooled reactor.

The Next Generation Nuclear Plant will have a projected service life of 30 to 60 years and be designed to ensure passive decay heat removal without fuel damage or radioactive material releases during accidents. The development of the design methods and validation of the graphite structures used in the reactor are important to the Next Generation Nuclear Plant Project because large amounts of graphite (up to thousands of tons) would be required for the reactor core and the individual graphite bricks that

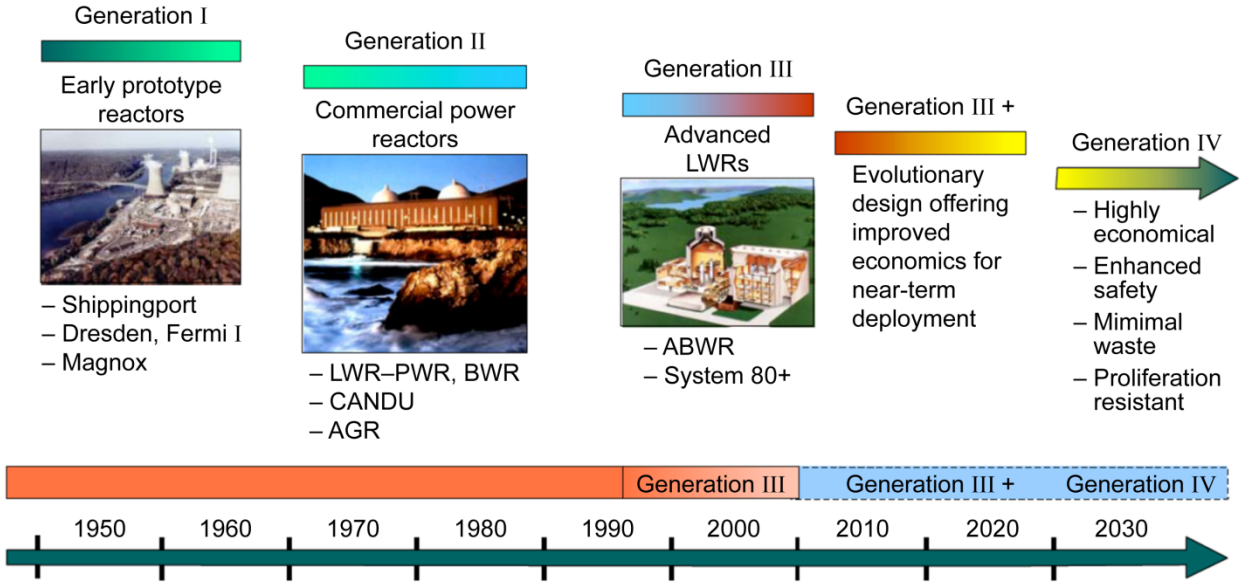

Figure 1.—Generation I to IV development time line. LWR, light water reactor; PWR, pressurized heavy water reactor; BWR, boiling water reactor; CANDU, Canada Deuterium Uranium reactor; AGR, advanced gas-cooled reactor; ABWR, Advanced Boiling Water Reactor. Reproduced from U.S. DOE Nuclear Energy Research Advisory Committee and Generation IV International Forum (2002).

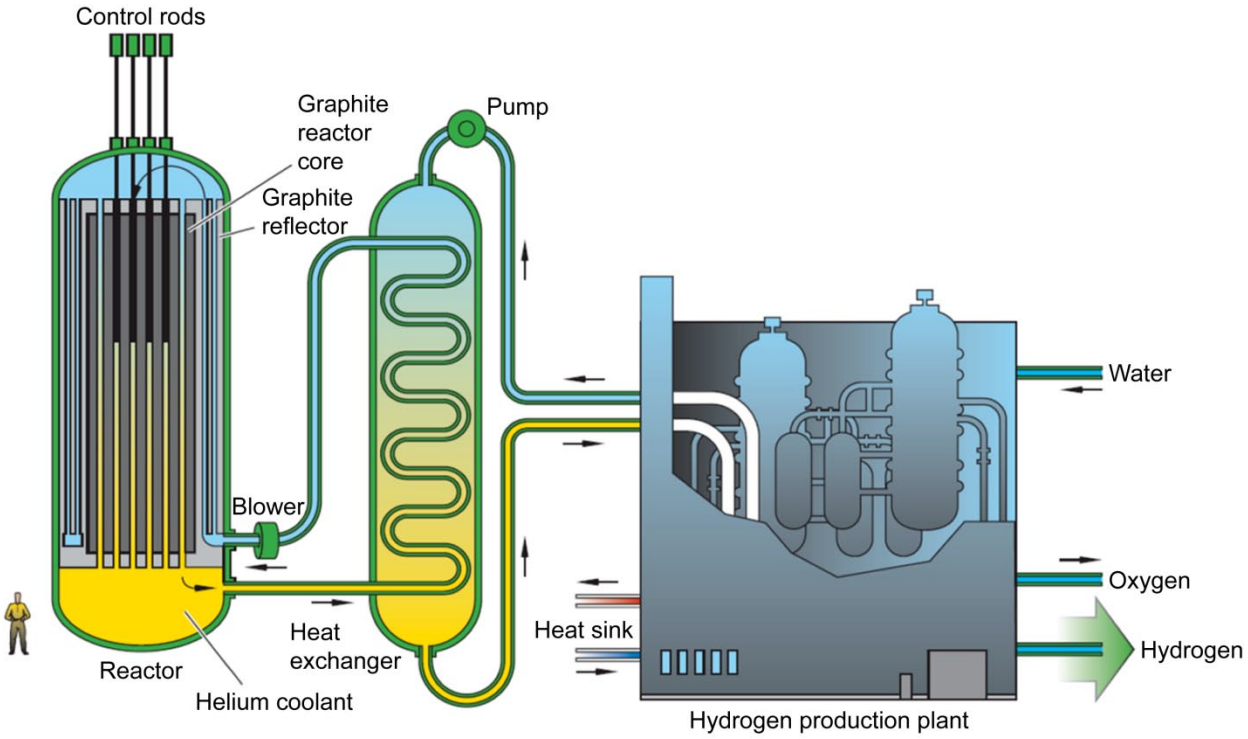

Figure 2.—Generation IV very high temperature gas-cooled reactor using graphite for neutron reflection and moderation within the reactor core. Reproduced from U.S. DOE Nuclear Energy Research Advisory Committee and Generation IV International Forum (2002).

surround the nuclear fuel may experience significant loads. Figure 3 shows an example of in-core graphite components for an earlier generation II reactor design. Of particular concern is the potential for crack formation and even rupture in individual blocks. Therefore, failure theories—and/or effective design strategies that can predict and mitigate failure from fracture—are needed. NASA has complementary interest in this endeavor with regards to the development of Moon and Mars surface power generation and nuclear propulsion for interplanetary missions. The Department of Defense would have interest with regards to a graphite nozzle throat in a solid rocket motor.

An important characteristic of graphite is that its strength is stochastic—an individual specimen can show a large random fluctuation in strength from a population mean. Graphite also can have a nonlinear stress-strain response because of distributed damage and damage accumulation within the material prior to rupture. This behavior can be described as "quasi-brittle" or "ductile-like." In contrast, classically brittle materials, such as ceramics and glasses, fail abruptly without prior damage accumulation, although they similarly display large scatter in strength. Other materials, such as fiber-reinforced composites, can accumulate significant damage prior to failure and have less scatter in strength than the individual constituents of the composite have. Graphite rupture behavior seemingly falls somewhere between the behaviors of ceramics and fiber-reinforced composites.

This report reviews some statistical failure models that may be relevant for the design of nonirradiated nuclear-grade graphite. This report is an expanded version of Nemeth and Bratton (2010), including additional details and models that were not included in the original journal article. Models for various brittle and quasi-brittle material systems are discussed with regard to strength distribution, size effect, multiaxial strength, anisotropic strength, and damage accumulation. Table I summarizes the models discussed in this report. This includes descriptions of the Weibull, Batdorf, and Burchell models as well as models that describe the strength response of composite materials, which involve distributed damage. Results from lattice simulations are included for a physics-based description of material breakdown, and consideration is given to the predicted transition between brittle and quasi-brittle damage behavior versus the density of damage (level of disorder) within the material system.

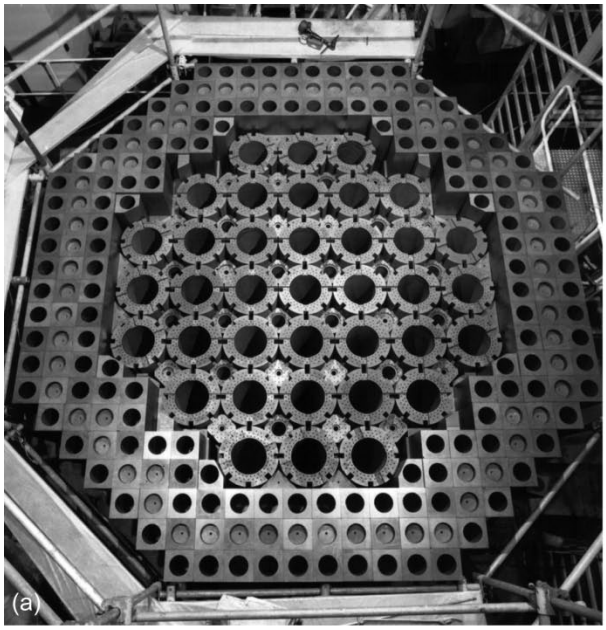

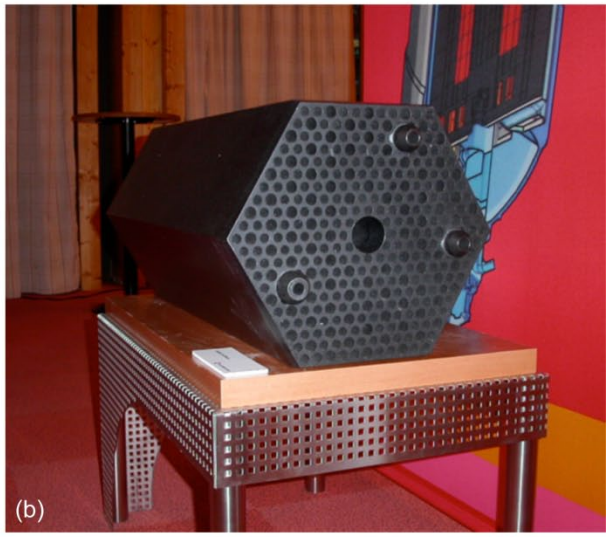

Figure 3.—Examples of graphite in-core reactor components. (a) Graphite components of United Kingdom advanced gas-cooled reactor (AGR) assembled with block-and-key construction before fuel insertion. Reproduced from Holt (2010). Copyright EDF Energy; used with permission. (b) Prismatic graphite fuel element from Fort St. Vrain research reactor (see Pinner (2000–2010)).

TABLE I.—SUMMARY OF FRACTURE MODELS DESCRIBED IN THIS REVIEW

Model	Section	Description	Material system	Weakest link	Size effect	Distribution type	Multiaxial
Weibull	2.1.1	Based on extreme-value distribution for classically brittle materials. Posits that scatter in strength and size effect is solely due to the presence of inherent flaws whereby the largest and weakest critically located flaw under load will cause rupture of the material.	Brittle	Yes	Yes, based on the weakest-link theory (WLT) mechanism	Weibull	No (Weibull's polyaxial theory is the same as Batdorf's for shear-insensitive cracks.)
Batdorf	2.1.2.1	Combines the Weibull distribution with linear elastic fracture mechanics (LEFM) to predict stochastic strength response under multiaxial loading. Originally developed for graphite and brittle materials in general.	Brittle	Yes	Yes, based on the WLT mechanism	Weibull	Yes, using principles of LEFM; assumes the random orientation of flaws
Principle of Independent Action (PIA)	2.1.2.2	Applies the Weibull distribution to individual principal stresses to predict stochastic strength response under multiaxial loading.	Brittle	Yes	Yes, based on the WLT mechanism	Weibull	Yes, using individual principal stresses
Margetson (anisotropy)	2.1.3	Applies a PIA style of methodology with the Weibull distribution to predict stochastic strength under multiaxial loading for an anisotropic material (transversely isotropic strength).	Brittle	Yes	Yes, based on the WLT mechanism	Weibull	Yes, using tensile stresses oriented relative to the material coordinate system and applied independently
Unit Sphere Strength Anisotropy Model	2.1.3 and Appendix B	Uses a Batdorf-style approach to combine LEFM with preferred flaw orientation or fracture toughness to predict stochastic strength under multiaxial loading for an anisotropic material (transversely isotropic strength).	Brittle	Yes	Yes, based on the WLT mechanism	Weibull	LEFM with preferred orientation of flaws or fracture toughness
R-curve	2.1.4	Fracture toughness changing with crack length affects stochastic strength distribution. R-curve is a characteristic material property.	Brittle	No	No, by itself R-curve does not imply a size effect with changing material volume	Deterministic material property unless the criterion of Planas (1995) and Bazant and Planas (1998) is considered	No
Ho	2.1.5	Empirical criterion to account for the reduction of strength due to grain size effects.	Brittle	Yes	Yes, size effect modified by grain size relative to specimen size	Modified Weibull	No
Schmidt	2.1.5	Modified Weibull methodology to allow a size effect between flexural and tension loading but allow a size effect with increasing volume of a specimen. This is an empirical criterion.	Brittle	Yes, but modified	Yes, but modified to be only a stress gradient effect	Modified Weibull methodology	Uses maximum deformation failure criterion
Li and Fok	2.1.5	Elastic damage model combined with the Weibull distribution for critical strain where damage is initiated. The difference in strength between tension and bending load is explained as being due to strain-softening behavior of quasi-brittle materials.	Quasi-brittle	No	Yes, size effect for a stress gradient	Weibull distribution coupled with nonlinear stress-strain response	No

TABLE I.—SUMMARY OF FRACTURE MODELS DESCRIBED IN THIS REVIEW

Model	Section	Description	Material system	Weakest link	Size effect	Distribution type	Multiaxial
Burchell	2.1.6	Graphite microstructure specific model; fracture initiates near pores and progresses through grains. Model depends on initial size distribution of pores and probability a crack can propagate through progressive rows of grains.	Brittle	Yes	Yes, but different from Weibull	Lognormal distribution of initial pore sizes	Yes, PIA-type methodology or Shetty (1987) based mixed-mode criterion
Uniform defect model	2.1.7	Model is based on a critical density of defects as a failure criterion. Does not consider flaw interaction. Assumes a Poisson process governing the general equation for the probability of occurrence of k inhomogeneities in the volume V.	Brittle	Yes, based on the critical number of defects within a given volume	Yes, but smaller than Weibull	Gamma distribution	No
Daniels	2.2.3	Fiber-bundle model based on equal load sharing. Based on an asymptotic analysis for a large number of fibers in a fiber bundle.	Composite/ quasi-brittle	No	No	Normal or Gaussian	No
Batdorf and Ghaffarian	2.2.5	Modeled the formation and growth of multiple fiber fractures as the basis of their failure criterion. In their model the Weibull relation for single fiber strength is used to determine the number of critical fiber fractures (singlets), double adjacent fractures (doublets), triple adjacent fractures (triplets), and so on as a function of stress and volume.	Composite/ quasi-brittle	Yes	Yes	Piecewise Weibull	No
Chain of Bundles	2.2.6	A composite is treated as a serial arrangement of independent bundles. Failure of a bundle causes failure of the composite.	Composite/ quasi-brittle	Yes	Yes	Not specified but likely asymptotically Weibull at small probabilities of failure	No
Watson-Smith	2.2.6	A modified Weibull distribution to decouple size effect from strength scatter.	Brittle	Yes	Yes, but not classically Weibull	Modified Weibull	No
Bazant and Pang	2.2.6	A multiscale model composed of mixed series and parallel systems that is argued to provide a physical underpinning to the Weibull distribution. In their model, quasi-brittle materials will have a two-parameter Weibull distribution at the lower probabilities of failure.	Quasi-brittle	Yes	Yes, but not classically Weibull	Normal or gaussian at higher levels of failure probability and Weibull at lower probabilities of failure	No
Lattice Models	2.3 to 2.3.3	Methodology to simulate material individual inhomogeneities with a stochastic distribution so as to investigate damage evolution with load for quasi-brittle materials	Quasi-brittle (flaw interaction accounted for)	Depends on input parameters	Yes, but response depends on input parameters	Not clearly established and depends also on input parameters	Response not investigated in this literature review
Watson-Smith & Chain of Bundles	3.7	A modified Weibull distribution to decouple size effect from strength scatter. Additional terms added to mimic a chain-of-bundles approach.	Brittle/ quasi-brittle	Yes	Yes, but not classically Weibull	Modified Weibull	No

More specifically, Section 1.2 describes the morphology and mechanical behavior of graphite, and Section 1.3 provides further detail regarding the fracture of graphite. Section 1.4 describes the effects of strength distribution and results from size-effect studies, and Section 2.0 introduces the two broad classes of statistical models of fracture: weakest-link series systems and parallel systems. Section 2.1 covers fracture models that fall under the weakest-link series system category of brittle material failure, and Section 2.2 covers the category for parallel systems, describing fracture models that involve distributed damage.

Section 2.1 describes the weakest-link theory (WLT) model. Section 2.1.1 describes extreme-value distributions and introduces the Weibull extreme-value distribution and the Weibull size-effect relationship. Section 2.1.2.1 primarily discusses the Batdorf model but also provides references for other models for predicting the effect on strength from multiaxial stress states, and Section 2.1.2.2 gives an example multiaxial strength prediction of the Batdorf model compared with the Principle of Independent Action model. Strength anisotropy models with regards to multiaxial stresses are discussed in Section 2.1.3. The effect of R-curve on strength distribution is provided in Section 2.1.4, and the Ho and Schmidt modified Weibull models for diminished size effect are provided in Section 2.1.5. The Burchell model, which considers how the graphite microstructure affects fracture, is described in Section 2.1.6, and the uniform defect model, which considers the effects of defect clusters, is described in Section 2.1.7.

Section 2.2 introduces the parallel system modeling category—specifically, composite material fiber-bundle models (Secs. 2.2.1 to 2.2.7) and lattice models of disordered materials (Secs. 2.3 and 2.3.1 to 2.3.3)—for describing fracture from distributed damage and how that is relevant to graphite. Section 2.2 discusses the important concept of the bounds of the applicability of WLT to distributed damage modeling. For composites, it describes the two extremes of composite failure modes (Sec. 2.2.1) and various fiber-bundle models—broadly classified as equal-load-sharing and local-load-sharing models (Sec. 2.2.2). The classical model of Daniels for a dry bundle of fibers is described in Section 2.2.3, and the chain-of-bundles equal-load-sharing model is described in Section 2.2.4. Local-load-sharing modeling with regards to size effect is described in Section 2.2.5, including the Batdorf and Ghaffarian model of multiplets. The Harlow and Phoenix WLT relation for composite materials is provided in Section 2.2.6, along with Watson-Smith's modified Weibull distribution and Bazant's interpretation of the Weibull distribution for mixed-series and parallel systems. Section 2.2.7 describes the brittle-to-ductile-like transition for composite bundle systems as it relates to the stochastic strength distribution of individual fibers.

Section 2.3 introduces lattice models of quasi-brittle materials. A discussion of the role of disorder on system breakdown is provided in Section 2.3.1, the brittle-to-ductile-like transition in lattice models is described in Section 2.3.2, and results of studies of strength distribution and size effect in lattice model simulations are given in Section 2.3.3.

Section 3.0 is devoted to further discussion and a summary of the previous sections in the context of developing a more comprehensive graphite design methodology. It primarily discusses the applicability, limitations, and recommendations regarding the use of the Weibull distribution but also summarizes the main points of the report. Sections include uncertainty in experimental data and the statistics-based argument for using the Weibull distribution at low probabilities of failure (Sec. 3.1), the role of large-size intrinsic flaws on strength distribution (Sec. 3.2), a summary of the physically based argument for the Weibull distribution at low probabilities of failure (Sec. 3.3), non-Weibull models and the brittle-to-ductile-like transition summary (Secs. 3.4 and 3.4.1 for bundle models and Sec. 3.4.2 for lattice models), the physical interpretation of the Weibull modulus (Sec. 3.5), a discussion of strength dispersion and size effect versus material volume (Sec. 3.6), the functional relationship between size effect and strength dispersion in WLT (Sec. 3.6.1), scaling issues and the Weibull modulus—models and experimental data (Sec. 3.6.2), a proposed Watson-Smith-style modified Weibull distribution for uniform uniaxial tensile loading (Sec. 3.7), the continuum assumption and stress gradient regarding the Weibull distribution (Sec. 3.8), issues and recommendations for predicting the effect of slots and notches on graphite component strength (Sec. 3.9), a very brief treatment of multiaxial stresses and anisotropic strength (Sec. 3.10), some comments on the Burchell model (Sec. 3.11), some brief comments regarding probabilistic design (Sec. 3.12), and final comments (Sec. 3.13). The conclusions are given in Section 4.0.

Appendix A shows a formulation of the uniform defect model of Section 2.1.7 approximated as a Weibull distribution (assumed for compressive stress states), Appendix B shows further detail regarding the development of a mechanistic model for describing anisotropic strength from multiaxial stresses from Section 2.1.3, and Appendix C shows the interchangeability of using the composite stress or the fiber stress in probability-of-failure calculations (applies to Sec. 2.2.6). To aid the reader, symbols used in this report are defined in Appendix D.

This report attempts to address the important question: What is the most appropriate probabilistic distribution that should be used in the design of graphite components? The authors draw attention to some unique aspects of graphite rupture behavior that make development of a comprehensive design methodology more challenging. However, only the problem of fast-fracture—the inherent rupture strength from the sudden, uncontrolled crack propagation of (pristine) graphite independent of any additional time- or cycle-dependent material degradation effects is addressed. Also, the methodologies in this report primarily describe failure with regards to the volume of the material or the imperfections (flaws) within the volume of the material. For the sake of brevity, only limited descriptions are given of these methodologies with regards to the surface of the material—imperfections residing on the surface (surface flaws) or edges (edge flaws)—because the modeling approach is similar. Awareness of these modeling problems and some of the modeling approaches available will be useful in the eventual selection and refinement of methodologies for designing graphite components by organizations such as ASME International (Boiler and Pressure Vessel Code) and the Nuclear Regulatory Commission.

1.2 Graphite Morphology and Characteristics

Nuclear-grade graphite refers to bulk graphite of accepted and characterized properties. One important area of investigation and subsequent design standards development such as the ASME's Boiler and Pressure Vessel Code for graphite-core structures involves the testing, qualification, and design methodology for new material grades of nuclear graphite. Graphite is a brittle material or quasi-brittle material, and brittle materials require a design methodology that is different from ductile materials (such as metals). Graphite is similar to other brittle materials in that it does not exhibit plastic deformation and shows wide scatter in strength. However, it differs from other classically brittle materials in that it can have a nonlinear stress-strain response and large amounts of acoustic emission (damage accumulation from microcracking) prior to rupture. (This is termed "quasi-brittle" behavior.)

Graphite and its properties are discussed in Burchell (1999), Smith (1972), and Greenstreet (1968). Greenstreet also provides an interesting historical perspective of graphite development. As used herein, nuclear-grade isotropic graphite is bulk graphite of accepted and characterized properties (both nonirradiated and irradiated) with high purity (such as low boron content) and certified for use inside a nuclear reactor core. Graphite is a monolithic material that, in some respects, is similar to ceramic materials, which are not processed via melting. All graphites are nearly pure carbon and are made by mixing a coke solid particulate filler with a liquid binder (usually coal tar pitch). The mixture is compacted and heated to expel volatiles and create the desired material phases. The coke filler particles are rigid and irregularly shaped such that the packing is inefficient, leaving a significant fraction of interparticle voids (particles pack at typically less than 70-percent full density). The binder is pyrolyzed during baking—losing mass and decreasing in volume—producing shrinkage cracks, shrinkage cavities, connected porosity, blowholes, and macrocracks. After baking, the carbon body is graphitized (the carbon atoms arrange into the layered hexagonal crystal structure of graphite) by exposing the formed body to temperatures in excess of 2700 °C. Although micrographs of graphite appear to show separate phases of particulates and binder, the binder does not exist as a separate phase; rather, the binder is also graphitized, just as the coke filler particles are. X-ray crystallography examination of various areas shows the material to be graphitic, regardless of where the binder or coke particles were in the original form of the article.

The degree of graphitization varies within the volume of the billet. Graphitization results in further shrinkage and the anisotropies of thermal contraction of individual misaligned graphite crystals (due to the differing thermal expansion coefficients of the a- and c-axis of the graphite's hexagonal lattice

structure) create Mrozowski stresses (Mrozowski (1956)). These stresses may be partially relieved by the formation of additional microcracks. The end result is that graphite contains a variety of defect structures and typically has between 15- and 25-percent void volume. There tends to be wide variation in the properties of graphite as a result of processing, although the chemical composition remains the same. This can be true not only from one material grade to another, but between different billets of the same material grade or within a billet.

Different grades of graphite can show widely different textures and pore-size distributions, as well as the presence of subcritical cracklike formations (see Figure 4). This cracklike porosity can range from being fairly planar to having an "onion skin" appearance. Pears and Sanders (1970) identified two classes of defects: background and disparate. Background defects are generally small relative to the size of the filler particles and are uniformly distributed. They include small blowholes, microcracks, locations of weak cleavage within filler particles, shrinkage cracks and cavities, and small gas pockets (connected or unconnected porosity) within the binder residue. Background defects are ever present. Disparate defects are much larger than background defects and are most commonly blowholes, which may be elongated defects created during extrusion. There may also be macrocracks, formed from a variety of processes involving gas entrapment. Other possible disparate defects include regions of binder deficiency, where cohesion between filler particles is poor; spongy regions of excess binder; inclusions, usually refractory metal carbides; voids left by the vaporization of inclusions; and "reorganized" graphite, where an impurity produces a region of ordered graphite unlike that of the filler and binder residue.

Graphite can be manufactured with different average grain sizes. Coarse-grained material has grains larger than 4 mm; medium-grained material has grains smaller than 4 mm; fine-grained material has grains smaller than 100 μm; and superfine, ultrafine, and microfine materials have grain sizes smaller than 50, 10, and 2 μm, respectively. Nuclear graphite typically has medium to ultrafine grains. Manufactured graphite is usually extruded or molded, and the resulting grain structure has a biased orientation. As such, material properties are often measured with the grain (parallel to the extrusion direction and perpendicular to the molding axis) or against the grain (perpendicular to the extrusion direction and parallel to the molding axis).

Graphite is similar to other brittle materials in that it does not exhibit plastic deformation (in the sense of metals) and shows wide scatter in strength. However, it differs from other classically brittle materials in that it can have a nonlinear stress-strain response and large amounts of acoustic emission (damage accumulation from microcracking) prior to rupture. This is termed "quasi-brittle" behavior. The amount of nonlinearity in the stress-strain response depends on the material microstructure. This nonlinearity is associated with the accumulation of mechanical damage within the material. When a material is stressed, micromechanical events such as slip, shear, cleavage, or microcracking are detected in the form of acoustic emission. In graphite, acoustic emission typically begins at the onset of loading with the frequency of events and energy per event increasing with load level. Kaiser (1950) found that, upon unloading, acoustic emission ceased and would not resume until the previous maximum stress was exceeded. This is known as the Kaiser effect, and the stress-strain effect is illustrated in Figure 5. A strain offset from damage accumulation under tensile load is indicated in the figure.

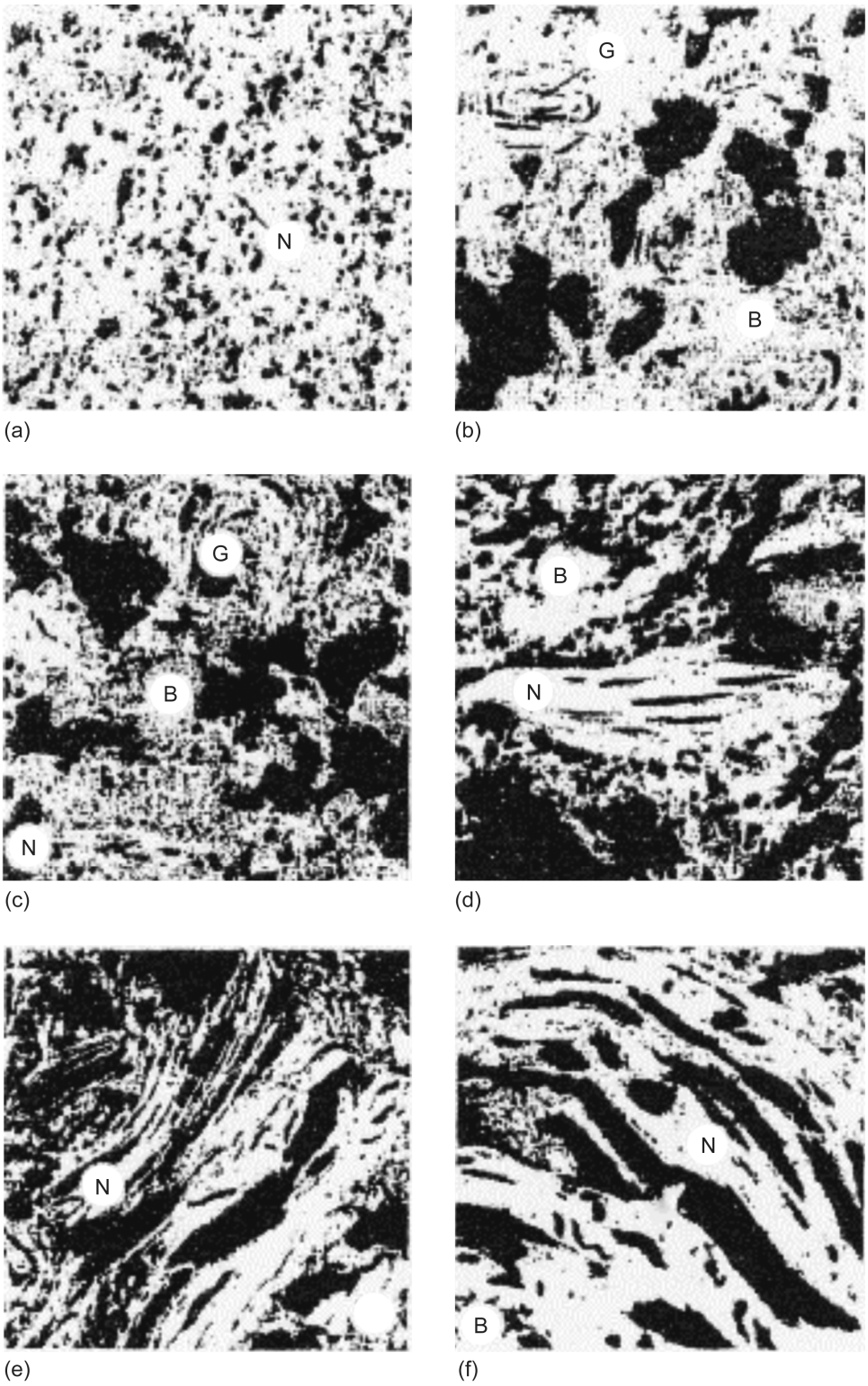

Figure 4.—Typical graphite microstructures showing N, needle-coke particles; G, gilsocarbon particles; and B, binder phase. The dark regions are pores. (a) High Density Graphite (HDG; Morganite Co.). (b) IM1–24 (Anglo Great Lakes Corporation). (c) SM2–24 (Anglo Great Lakes Corporation). (d) Pile Grade A (PGA). (e) Nipple stock. (f) Unimpregnated electrode graphite. Reproduced from Tucker et al. (1986). Copyright Elsevier; used with permission.

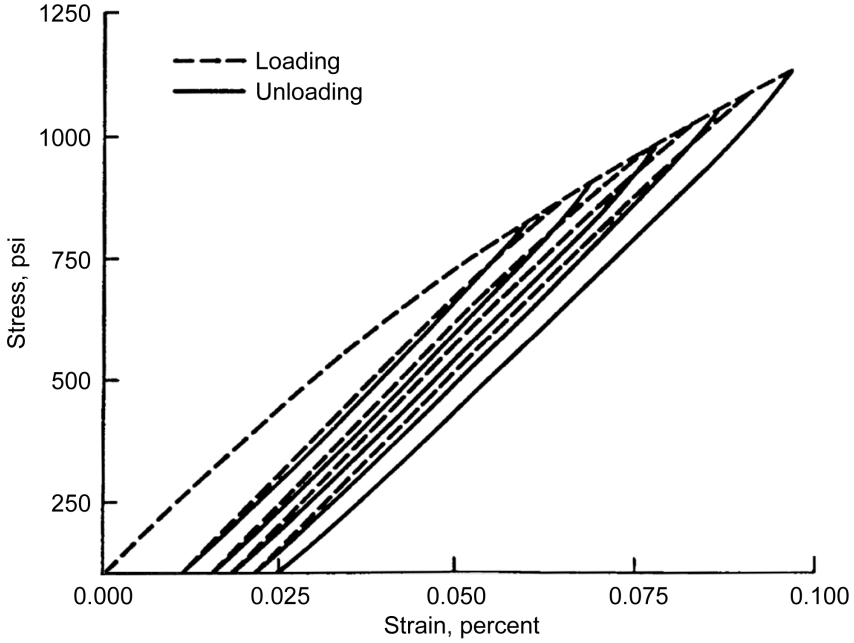

Figure 5.—Tensile stress-strain curve for repeated loading for an unspecified graphite. Reproduced from Losty and Orchard (1962). Copyright Elsevier; used with permission.

Graphite strain at failure is a few tenths of one percent in tension and 1 to 2 percent in compression; therefore, graphite is considerably stronger in compression than in tension. Deviation from stress-strain linearity is small for low stresses but more pronounced at higher stress levels. The stress-strain curve is continuous, without any abrupt transition point. The deviation from linearity may be more pronounced in tension than it is in compression as reported by Arai and Oku (1979). Also, there can be significant scatter in the material strain-response from specimen to specimen, again as shown in Arai and Oku. In nuclear-grade graphite, the compression strength is 3 or 4 times the tensile strength. Bulk graphite tends to be weak in tension—with strength on the order of 11 to 15 MPa, depending on whether it is measured against the grain or with the grain—and has low fracture toughness K_{Ic} (between 1.4 and 1.5 MPa-$m^{1/2}$, as reported by General Atomics (1988) for H–451 graphite). Hence, graphite strength is anisotropic (transversely isotropic). Newer grades of nuclear graphite tend to be more isotropic (within 10 percent or less)—which is desirable. Strength improves with temperature (in a nonoxidizing environment) up to 2500 °C, and there is high resistance to thermal shock. There is wide scatter in the strength of nominally identical graphite specimens, and therefore, graphite strength has to be described in terms of probability distributions such as the normal, lognormal, or Weibull (1951). The Weibull distribution is the distribution most often cited when reporting the strength behavior of specimen test data (see Sec. 2.1.1 for a description).

The strength variation observed in graphite is more pronounced in tension than in compression. The strength varies randomly from log to log and partly randomly, partly systematically within the log where the systematic part reflects a general increase in strength away from the center. When adjusted for the systematic spatial variation, the tensile strength can be approximated by a Weibull distribution or possibly by a bimodal Weibull distribution.

1.3 Fracture of Graphite

The fracture of graphite can be a complex process, with different grades of graphite potentially having different failure behaviors. A good treatise on the fracture of graphite can be found in Brocklehurst (1977). The fracture of graphite is nominally brittle or quasi-brittle with little or no plasticity

prior to failure. This means that fracture is influenced by preexisting flaws or inherently weak regions in the material. Porosity can be important in the fracture process. Stress concentrations at, or very near, pores can initiate cracking or influence the crack path, and conversely, crack growth may be arrested at a pore until a higher stress is applied. In the binder phase, there may be regions of common basal plane alignment extending over 100 μm in length. Cleavage in these regions can occur at stresses well below the fracture stress and can act as sites for crack initiation. Finally, coke filler particles with the proper orientation are highly susceptible to cleavage along basal planes at low stresses.

Tensile fracture occurs when a local concentration of microcracks develops and coalesces to form an unstable macrocrack of critical size. Microcracks, oriented approximately normal to the applied load, begin forming at low strain (relative to the ultimate strain) and preferentially form in regions of stress concentration adjacent to the large disparate defects. These grow to a limited size and stop growing. These defects or pores basically act as loci for crack initiation and termination. Knibbs (1967) observed that well-defined systems of secondary cracking arose when the crack tip entered a pore or defect and that locations of low-density material impede crack growth. Increasing the strain (load) causes new microcracks to form throughout the body that similarly reach a limiting size and stop growing. This process continues until the density of microcracks is such that they overlap, join, coalesce, and—at some location in the structure—create a fracture path.

As discussed in Tucker and McLachlan (1993), crack growth tends to be transgranular (through the grain), with the crack path within the individual grain corresponding to the crystallite cleavage plane (from Jenkins (1962) and Knibbs (1967)). Regions of similarly oriented crystallites are more likely to fail than collections of small randomly oriented crystals. The ultimate fracture path tends to extend from one large defect to another. It is interesting that the microcracks that form early in the process usually do not propagate directly to fracture. The fracture surface is rough, and the path is normally branching and irregular. In general, the fractography of fracture surfaces has not located the earliest initiating flaws. It can be concluded that the process of fracture in graphite falls somewhere between that of brittle monolithic ceramics and quasi-brittle materials such as brittle-fiber-reinforced composites.

For classically brittle materials, like ceramics and glasses, the science and art of fractography can often trace the source of fracture in a specimen or component to a single originating flaw (Quinn (2007)). These originating flaws can be from individual pores, porous regions, agglomerates, compositional inhomogeneities, inclusions, large grains, cracks, machining damage, handling damage, surface pits, surface pores, and damage or chipping along sharp corners. These flaw types (or flaw populations) are broadly classified as either volume distributed, surface distributed, or edge distributed and are considered to be separate and competing failure modes. When the probability of a component surviving loading is evaluated, it is done as a function of the component volume, the component surface (or even the component edges), or a combination of the two. This is referred to as volume-flaw reliability analysis or surface-flaw reliability analysis (e.g., see Nemeth et al. (2003, 2005) and Gyekenyesi and Nemeth (1987)). For graphite, the failure process is usually considered to be a function of the material volume; therefore, the reliability analysis is performed over the volume of the component. This assumption is made because the identity and location of the earliest flaws usually cannot be established and because the subsequent growth and accumulation of damage through microcracking can be diffusely distributed within the material volume (at least for uniform uniaxial tension) prior to a final coalescence of damage and formation of a macrocrack.

The role surface flaws may play in the fracture of graphite is not clearly established. One would expect that, under flexural loading, surface flaws would play some role in the fracture of the material. However, the authors of this report are not aware of any studies that have examined the strength of nuclear-grade graphite flexural specimens as a function of the grit size of the abrasive that was used to grind the specimen surface. Part of the reason for this may be that the size of exposed pores on the specimen surface is often larger than the grit size of the abrasive, making it pointless to characterize the surface roughness from the grinding process and indicating that the size of surface pores—rather than the damage caused by the grinding process—will control the strength response in flexure.

1.4 Overview of Experimental Studies, Strength Distribution, and Related Considerations

Graphite behavior ranges from brittle to quasi-brittle, depending on the processing of the material. Low-void-content, fine-grained materials would likely be more brittle than high-void-content, larger grained materials. Regardless of the processing, the strength of graphite is always stochastic—the strengths of nominally identical specimens fluctuate significantly from the population mean. Probability distributions can approximate this strength variability, but is one type of distribution more appropriate to use than another?

Often distributions such as normal (gaussian), lognormal, or Weibull can fit experimental data nearly equally well (within the range typically sampled between 1 and 99 percent). Figure 6(a) shows a schematic example of this, comparing a two-parameter Weibull distribution and a gaussian (normal) distribution having the same mean and standard deviation. The two curves appear to be similar in this limited range. Danzer et al. (2008) indicates that several thousand experimental tests may be required to discern a difference between a normal and a Weibull distribution.

A good example of this difficulty is shown in Kittl and Aldunate (1983), where despite a large amount of data (575 specimens), an appropriate distribution could not be established with high confidence for cement cylinders tested in compression (see Appendix A, Figure 30). Another more relevant example is the study by Price (1976) on nuclear graphite grade H–451 (Great Lakes Carbon Corporation) involving over 2000 tensile and four-point-bending specimens. In this study, both a normal (gaussian) and Weibull distribution were purported to fit equally well to the results of the various fracture experiments. Nemeth et al. (2011) reanalyzed these data by pooling (combining) the individual data sets into larger, more meaningful, data sets. Two- and three-parameter Weibull distributions fit very well to the data. A large international study by Tennery and Ferber (1989) with over 2500 four-point-bending specimens for three different ceramics indicated that the Weibull distribution generally fit the data better, although for one material, the gaussian and Weibull distributions fit equally well.

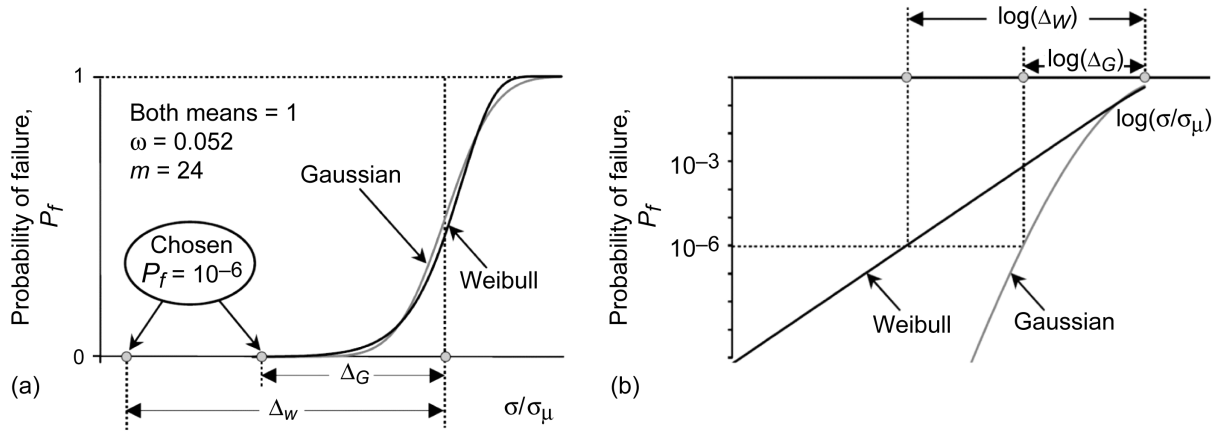

Figure 6.—Gaussian and two-parameter Weibull distribution with a mean of 1 and a 5.2-percent coefficient of variation ω, where *m* is the Weibull parameter, Δ_G is the difference in σ/σ_μ from the mean to the value of σ/σ_μ where the probability of failure is 10^{-6} for the gaussian distribution, Δ_W is the difference in σ/σ_μ from the mean to the value of σ/σ_μ where the probability of failure is 10^{-6} for the Weibull distribution, σ is the applied uniaxial stress, and σ_μ is the mean fracture strength. (a) Linear scale. (b) Log scale. Note the large difference in the abscissa for small probabilities of failure P_f. Reproduced from Bazant and Pang (2007). Copyright Elsevier; used with permission.

The deviations from one distribution to another only become apparent in the distribution tails (as shown schematically in Figure 6(b) for two-parameter Weibull and gaussian distributions with identical means and standard deviations). However, obtaining experimental data at low probabilities of failure (the lower tail of the distribution and the region of highest interest) requires prohibitively large numbers of specimens. Hence it is difficult or impractical to determine a best distribution based solely on fit to data. From a design perspective, the conservatism (or nonconservatism) of one distribution relative to another distribution can be an important differentiator since these distributions extrapolate differently at the lower tail, where confirmatory data do not exist (e.g., see Liu (1997)).

A further, and perhaps more fundamental, consideration is whether a physical basis consistent with graphite failure can be associated with a particular distribution and if that distribution or model can be used to make other predictions that can be experimentally verified, such as size effect, where average strength is affected by the size of the component. In fact, size effect has been investigated for graphite in several studies, including Brocklehurst and Darby (1974), Strizak (1991), Price (1976) (see also Nemeth et al. (2011)), and Department of Energy gas-cooled reactor reports from Homan and Kasten (1980), Kennedy (1987), and Kasten et al. (1989). Generally these investigations compared experimental results with predictions made using the Weibull distribution. The size effect and the Weibull distribution are discussed further in Section 2.1.1. The Weibull distribution predicts that average strength decreases with increasing volume (with the rate of decrease functionally related to the degree of strength scatter). However, many of the studies show inconsistent results with regard to this expectation. (Generally they show that flexural specimen tests follow Weibull distributions, whereas tensile specimen tests produce a smaller-than-expected size effect.)

Danzer et al. (2007, 2008) provide an excellent discussion regarding the applicability and problems of using the Weibull distribution to describe the strength response of brittle materials. Many of the same problems described by Danzer et al. (2007, 2008) for ceramics are relevant to graphite.

Note that the determination of graphite strength requires taking into account the nonlinear elastic response of the material. This was done in the following studies by using various approximations, including correction factors. The methods and accuracy of these approaches are not described herein.

Brocklehurst and Darby (1974) tested uniform tensile, four-point-bending, diametral compression, and internally pressurized specimens (the material source was not specified). Bending strength exceeded the tensile strength by a factor of 1.4 to 1.7, consistent with a lower Weibull modulus material; increasing the size of the specimen decreased strength, consistent with a higher Weibull modulus material. At any given strain, the elastic bend stress exceeded the tensile stress by about 35 percent, but the strain to failure in bending exceeded that in tension by about 10 percent. The resultant effect was that the bend strength was about 50 percent greater than the tensile strength. This is shown in Figure 7. Note the scatter in the stress-strain response as indicated by the arrows in the figure.

Brocklehurst (1977) examined tensile and bend strength as a function of the volume of cylindrical specimens and the inner beam span of four-point-bend flexural specimens, as shown in Figure 8. Each point shown represents the mean of six specimens. Standard deviations are also indicated. Figure 8(a) shows that, for flexural specimen volumes greater than 1 cm^3, strength decreased with increasing volume, consistent with a size effect for a Weibull modulus of $m = 16$. This value of Weibull modulus also was measured for 30 four-point flexural specimens with a constant inner span volume of 25 cm^3. Conversely, the tensile data showed an increasing strength with volume, although this trend leveled off at volumes greater than 8 cm^3. For smaller volumes, both the tensile and flexural specimens indicated decreasing strength with decreasing volume. In Figure 8(b) the fracture strength of the tensile specimens is shown to decrease with decreasing volume; the relative grain size of the material in comparison to the specimen dimensions likely played a role in this behavior. Ho (1979) applied an empirical correction to the Weibull distribution to account for grain size relative to specimen size (see Sec. 2.1.5), and this behavior may be due to the grain acting as a flaw or microcrack (Tucker et al. (1986)), whereby the grain size becomes an increasing larger fraction in comparison to a characteristic dimension of the specimen such as diameter (tensile specimen) or thickness (flexural specimen).

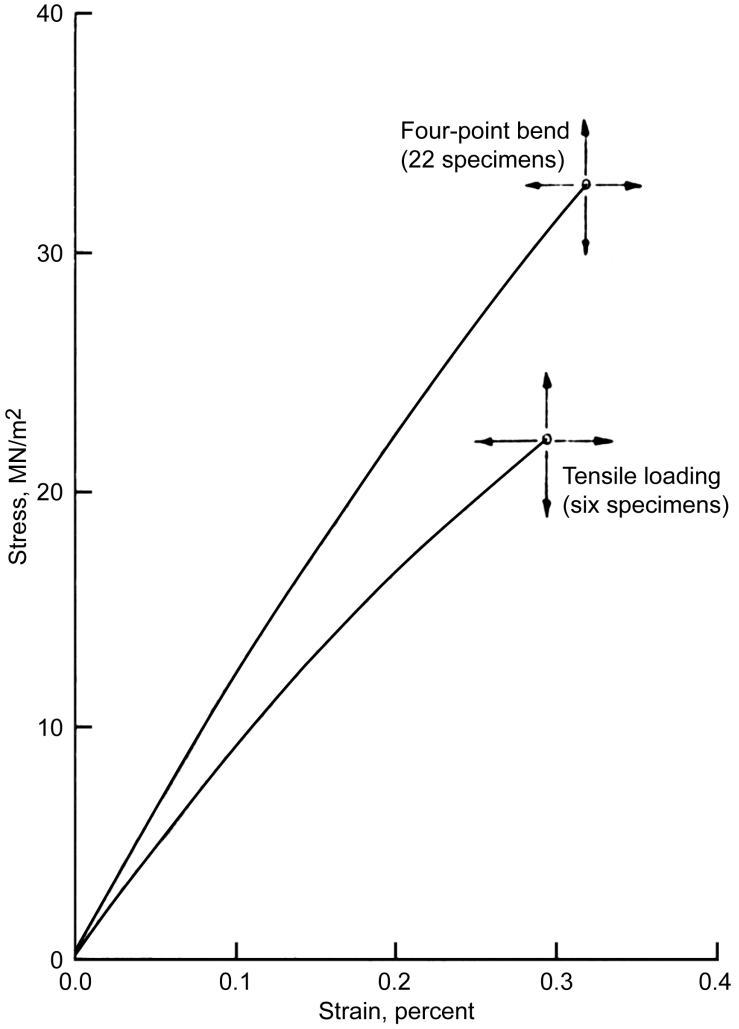

Figure 7.—Averaged stress-strain to failure relation of 22 specimens in four-point bending and six specimens under uniaxial tensile loading of a nuclear-grade graphite. Arrows indicate the standard deviation in the data. Reproduced from Brocklehurst and Darby (1974). Copyright Elsevier; used with permission.

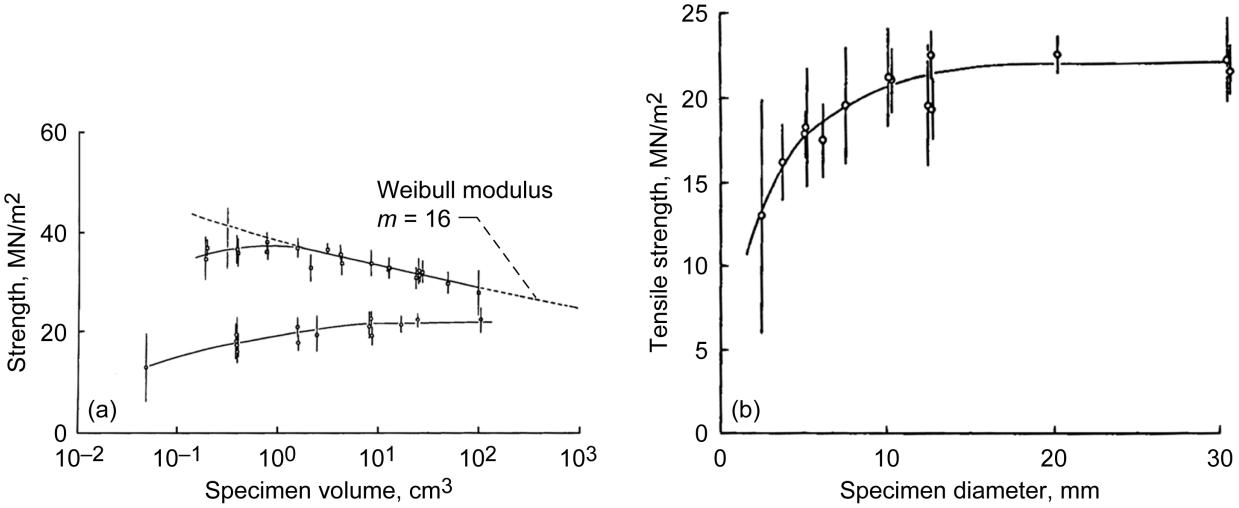

Figure 8.—Fracture strength of IM1–24 grade graphite (Anglo Great Lakes Corporation) and standard deviations of the data. (a) Tensile strength as a function of specimen volume of tensile specimens (circles) and four-point flexural specimens. (b) Tensile strength as a function of specimen diameter. Reproduced from Brocklehurst (1977). Copyright Taylor & Francis Group; used with permission.

Price (1976) ruptured over 2000 tensile and four-point bend specimens to examine size effect, strength anisotropy, and strength variation versus location within the billet on H–451 graphite. As previously mentioned, normal and Weibull distributions were stated to fit the data equally well. The mean strengths showed systematic dependence on orientation and location. Axial specimens (along the extrusion axes) were stronger than radial specimens (perpendicular to the extrusion axis). Specimens excised near the edge of the log (cylinder) were stronger than specimens taken from the center of the log. Strength fluctuations also were correlated with local density variations. The variation in strength was lower for axial specimens than for radial specimens and was lower for bend specimens than for tensile specimens. Flexural specimens averaged between 52 and 55 percent stronger than tensile specimens—consistent with predictions of 51 to 64 percent from the Weibull distribution, whereas the strength of small tensile specimens (724 mm^3 volumes) was 3 to 8 percent higher than that of larger tensile specimens (9847 mm^3 volumes)—which was significantly smaller than the expected 28- to 38-percent difference using the Weibull distribution.

There were 48 data sets generated in Price (1976), with an average of 42 specimens per data set (high value of 48 and low value of 24 specimens in the individual data sets). The average Weibull modulus *m*, which measures scatter in strength, was 8.6 and 9.7 for the small and large tensile specimens, respectively. The average Weibull modulus for the flexural specimens was 14.7 when the fracture stresses were corrected for nonlinear stress-strain response. Each average value was generated from 16 data sets. The Weibull modulus of 15 of 16 paired data sets (consisting of a small tensile, large tensile, and a flexural data set in a given billet, location, and orientation) was higher for the flexural specimens than for the tensile specimens, likely indicating that the flexural specimens had a different and higher Weibull modulus than the tensile specimens had. It is unknown if any experimental bias existed in the testing. The large tensile specimens had a slightly higher average Weibull modulus than the small tensile specimens did, where 10 out of 16 times the Weibull modulus of the large tensile specimen was larger than that of the small tensile specimen within a paired data set. The difference in the Weibull modulus between the large and small tensile specimens was likely not significant.

Ho (1979) comments that load eccentricity due to improper alignment of the load train may have contributed to the higher strength variability (and hence the lower Weibull modulus) of the tensile specimens relative to that of the bending specimens. Ho (1979) also applied an empirical correction to the

Weibull distribution scale parameter to account for grain size relative to specimen size (see Sec. 2.1.5). It is known that critical specimen dimensions, for example diameter in a tensile specimen, negatively affect strength when the specimen dimension is on the order of the grain size. Ho was able to show good correlation to the Weibull distribution size effect when the grain size to specimen size correction factor was applied for the tensile specimens, although this also may also have been a case of calibrating a theory to data.

Nemeth et al. (2011) reanalyzed the fracture data reported by Price (1976) for H–451 grade graphite, which involved over 2000 specimens tested in flexure and tension. Nemeth et al. (2011) used the WeibPar program (Connecticut Reserve Technologies, Inc., 2009) to pool (combine) the fracture data into larger sets to better identify and confirm trends. They used 90-percent confidence bounds on the Weibull parameters to examine if one set of data was statistically similar to another set of data. Figure 9 shows a Weibull plot of the pooled data of the large tensile specimens, the smaller tensile specimens, and the four-point flexural specimens from Nemeth et al. (2011) for specimens oriented axially (Figure 9(a)) and radially (Figure 9(b)) relative to the material extrusion direction. The solid lines represent the predicted strength response based on the Weibull distribution. The flexural specimen fracture stresses were not corrected for the nonlinear stress-strain response of the graphite. Further details and extensive Weibull plots of the data are provided in Nemeth et al. (2011). Similar to Price (1976), the results showed a much smaller size effect than would have been expected based on the Weibull distribution for the tensile specimens. A significant size effect was observed between the tensile and flexural specimens. The Weibull modulus m, which measures the scatter in the data, was consistent between the different sizes of tensile specimens but was higher for the flexural specimens. The difference in the Weibull moduli of the tensile and flexural specimens indicates that additional effects (e.g., see Li and Fok (2009) and Sec. 2.1.5) or different failure mechanisms were operating. The diameter of the small tensile specimen may have played a role in the lack of a significant size effect between the two different tensile specimen sizes because the grain size of the material was on the same order as the diameter (see Sec. 2.1.5 for a further explanation).

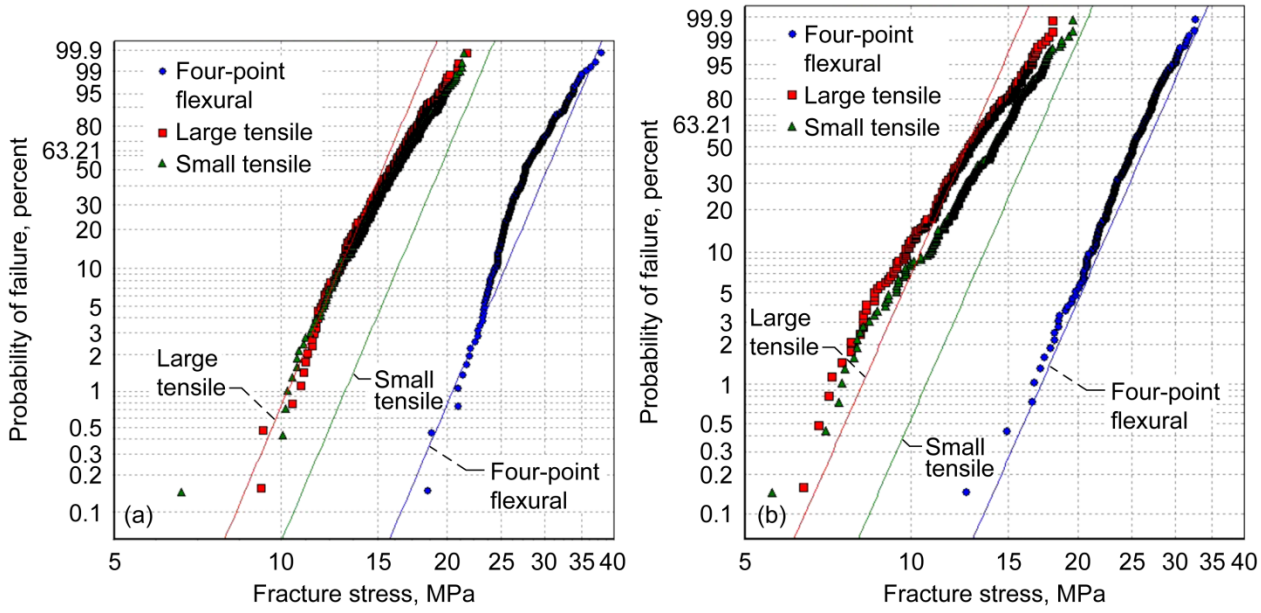

Figure 9.—Weibull plots of large-size tensile, small-size tensile, and four-point flexural specimens of graphite-grade H–451. The lines represent a best fit to the pooled data considering the size effect predicted from the Weibull distribution. Note that the fracture stresses for the flexural specimens were not corrected for the nonlinear stress-strain response of H–451. (a) Axial orientation of 317 large-size tensile, 346 small-size tensile, and 336 four-point flexural specimens. (b) Radial orientation of 311 large-size tensile, 343 small-size tensile, and 346 four-point flexural specimens. Reproduced from Nemeth et al. (2011).

Homan and Kasten (1980) used Stackpole 2020 and H–451 grade materials for their size-effect study of various sizes of O-ring, C-ring, and four-point-bending specimens. Good correlation was obtained for size effects corresponding to Weibull moduli of 16 and 6 for Stackpole 2020 and H–451, respectively. Homan and Kasten's study used a "95-percent stressed volume" (the volume under a stress of 95 percent or more of the highest stress in the specimen) in the effective volume calculations, it reused portions of previously fractured specimens, and it corrected for variations in the density of pores in the material. Size effect corresponding to high density, mean density, and low density within the billet were systematically examined.

In Kennedy (1987), a large study performed on Stackpole 2020, Union Carbide TS1792, and Toyo Tanso IG11 graphites examined billet-to-billet, within-billet, and size-effect strength variations. Kennedy concluded that the randomness of the mean strength in the billets made it unlikely that test results from small sample volumes removed from the billet would be representative of the billet as a whole. Size effect on grades TS1792 and 2020 was studied using the methods and specimen types described in Homan and Kasten (1980). Size effect consistent with the trends of the Weibull distribution was obtained. For grade 2020 this was shown to apply for up to 5 orders of magnitude difference in stressed-volume (by including tensile specimen results for a single size of specimen). Similar to Homan and Kasten (1980), the size-effect relationship for uniform uniaxial tensile specimens was not studied. It should be noted that large gross defects were often observed in the various billets. Figure 10 shows an acoustic scan of one end of a billet that had high variability. The scan shows flow lines of high-density material and the locations of large cracks. Density variations did not necessarily correlate with the loss of mechanical properties.

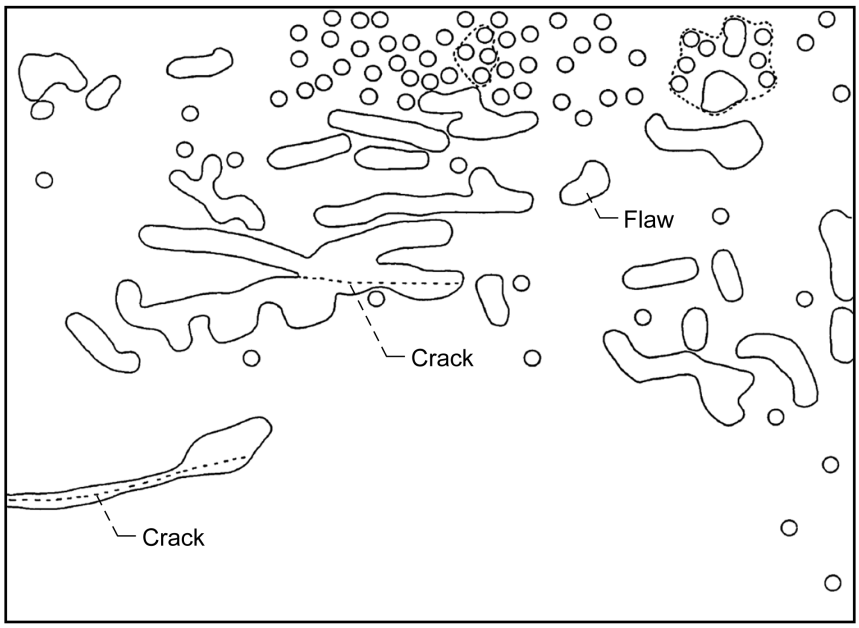

Figure 10.—Acoustic map of a section of graphite billet showing areas where no back-face signal was detected using a 2.25-MHz frequency probe. This corresponds to areas of high-density material. Reproduced from Kennedy (1987).

Kasten et al. (1989) give further (updated) results for Union Carbide's TS1792 with regard to size effect. Specimen types and testing protocols similar to Homan and Kasten (1980) were used. Size effect was examined relative to the location within the billet. Size effect consistent with the trends of the Weibull distribution was obtained, but the Weibull slope (the amount of average strength change with size) appeared to vary between the edge and center of the billet. Tensile strength also was correlated with density, with strength increasing with density. Size-effect testing of Stackpole 2020 over several orders of magnitude of stress volume and for various billets showed a consistent Weibull-like size effect between billets—where Weibull slope was little changed between billets, although mean fracture strength varied as much as 10 percent. Similar to Kennedy (1987), results for one size of tensile specimen were included with the other bending specimen results. Tensile strength results for two different specimen sizes (6.35 mm and 9.53 mm in diameter) were reported for H–451 and PGX grade materials. Although there was not a large volume difference between the two specimen sizes, the smaller diameter specimen had a lower average strength than the larger diameter specimen did, contrary to the trend expected from the Weibull distribution. These results may not have been statistically significant.

Strizak (1991) studied the effect of volume on the tensile strength of Great Lakes Carbon Corporation H–451 (ownership change) and Toyo Tanso Company IG–110. Specimens with gauge diameters of 6.35, 9.35, 15.88, and 25.4 mm, and gauge volumes of 1407, 3163, 12 577, and 51 482 mm^3, respectively, were tested. For both materials, the average strength measured for a given specimen volume increased with increasing gauge volume, contrary to the trend expected with the Weibull theory. The increases were relatively small and may not have been statistically significant. Strizak also considered an empirical conjecture by Ho (1979) that grain size affects strength negatively for specimens with diameters less than 10 to 15 times the grain size as well as the Burchell model (described in Sec. 2.1.6). Strizak concluded that the Weibull model correlated poorly for size effect and that Ho's modified Weibull model had mixed results, especially when it indicated that strength should decrease at the largest specimen sizes, contrary to the experimental results. Burchell's model showed correlation for the subset of data that was analyzed; however, correlating with the smallest specimen size required adjusting the fracture toughness (measured fracture toughness was reported to decrease with decreasing specimen diameter).

Mitchell et al. (2003) examined two billets of PPEA (UCAR International/GrafTech International) extruded medium-grained graphite for billet-to-billet, within billet, strength variation, and strength orientation anisotropy. Four-point-bending specimens and L-shaped specimens with various fillet radii were tested. Results from four-point testing indicated strength orientation anisotropy was small within the experimental margin of error but that strength varied as much as 12 percent within billets and mean strength between billets varied 7 percent. The Weibull modulus between individual tests varied between 8 and 22; however, because the number of specimens for each test was small, this variation was not necessarily statistically significant. The Weibull modulus for L-shaped specimens varied between 21 and 54, with the zero-fillet-radius specimens having the anomalously high Weibull modulus of 54.

The failure mode appeared to be different for the four-point and L-shaped specimens. Failure was abrupt and brittle-like for the four-point specimens where a single crack initiated and propagated through the specimen. For L-shaped specimens, failure was more gradual, with cracks starting at different locations (along the exposed face of the fillet) that joined to form a single crack that extended through the specimen. The time from the visible onset of cracking to when the crack extended across the face of the fillet varied according to the particular geometry of fillet radius and/or specimen thickness. Weibull predictions using the averaged properties of the four-point bend specimens and finite element analysis results from the L-shaped specimens did not correlate very well with the experimental data for the various fillet radii. A fracture mechanics analysis of the L-shaped specimen indicated that the stress intensity factor decreased with crack length, suggesting a stable crack growth failure mode (increasing load required to grow the crack), whereas analysis of the four-point specimen indicated that unstable crack growth would be the failure mode. It should be noted that Li and Fok (2009) reanalyzed these data by accounting for the nonlinear stress-strain response (see Sec. 2.1.5 for further discussion).

The authors herein speculate that the high Weibull modulus of 54 (corresponding to a relatively small coefficient of variation in fracture strength) for the zero-radius fillet of the L-shaped specimen in

Mitchell et al. (2003) was affected by the stress singularity at the fillet root. For example, in Choi and Salem (1992) scatter in strength of four-point-bending specimens decreased substantially when the specimens were indented. A consistently sized indentation flaw was introduced in each specimen, decreasing the average strength and decreasing the coefficient of variation from 13 to 5 percent. This lowered the effect of natural flaws on the specimen strength because any natural flaw existing near the crack tips of the introduced flaw was substantially shorter than the introduced flaw. The combined effect of a relatively short natural flaw near the crack tip of an introduced flaw would make the effective (equivalent) length of the introduced flaw only slightly longer; hence, the specimen would have only a slightly smaller fracture stress than if the natural flaw had not been in the vicinity of the introduced flaw crack tip. The net effect is that, if each specimen had an identical-sized indentation flaw, the fracture strength of the specimen would always be the same (deterministic with no scatter in strength), but the possibility that a natural flaw could exist near the crack tips of the introduced flaw would add a relatively small amount of variation to the observed fracture strength. The stress singularity induced by the zero radius of the fillet in the L-shaped specimen of Mitchell et al. (2003) had the same effect as introducing a large crack in the specimen and thereby decreasing the influence of the natural flaws in the specimen.

From the previous description, it can be seen that nuclear-grade graphite presents a more complicated, and perhaps somewhat chaotic, fracture behavior than that of classically brittle materials. Traditionally, the Weibull distribution has been used to describe the probability of failure of brittle materials under thermomechanical loading; however, Weibull analysis has not been uniformly successful in predicting graphite failure. Generally, it seems from the studies cited in this section that size effect exists for flexural specimens and is consistent with expected Weibull behavior. For uniform tensile loading, size effect is small or nonexistent—which is inconsistent with Weibull predictions. However, as noted by Ho (1979), grain-size effects complicate this problem. It is notoriously difficult to obtain uniform stresses through the cross section in tensile testing, and this introduces experimental biases. Smaller-than-expected size effect has been reported in the literature for other materials, for example by Lu et al. (2005) for zinc oxide electroceramics (containing significant porosity) and by Beyerlein and Phoenix (1996) for low-fiber-count "minicomposites."

In the large study done by Price (1976) (see also Nemeth et al. (2011)), the reported Weibull modulus for the graphite flexural specimens was consistently higher than that for the tensile specimens. This (if we assume that experimental errors were not to blame), along with Figure 7 showing different stress-strain responses for bending and tension, raises the possibility that bending involves different failure mechanisms (or modes) than those in uniform uniaxial tension. Li and Fok (2009) explained the difference in strength and Weibull modulus between tension and bending load as being due to the strain-softening behavior of quasi-brittle materials (also see Sec. 2.1.5). Also, as mentioned before, grain size negatively affects the strength of small-size specimens (Ho (1979)). Tucker et al. (1986) indicated that this is due to the presence of small-size cracks on the order of the grain size.

The potential for serious experimental errors, such as load eccentricities in tensile specimens, and consistency of approach, such as accounting for nonlinear stress-strain response in failure stress calculations makes drawing firm conclusions regarding graphite behavior problematic. An example of the difficulty of obtaining consistent estimates of Weibull parameters can be found in Tennery and Ferber (1989). In that international study, 21 laboratories measured four-point-bending fracture strengths and estimated Weibull parameters for two grades of silicon nitride and one grade of silicon carbide. A total of 2597 specimens were fractured, and individual data sets for each material from each laboratory ranged from 60 to 80 specimens. All specimens came from a single billet of each material, and Oak Ridge National Laboratory randomized (for each material) and distributed the specimens. Study participants used the same specimen and fixture dimensions and the same stressing rate.

Despite the large size of the data sets (60 to 80 specimens per data set), estimated Weibull parameters (using maximum likelihood analysis) showed scatter in values beyond what was expected from natural statistical variation. The Weibull modulus m for the SiC material varied from 4.9 to 8.3 for a range of 69 percent (based on the lowest value) among the 12 participating laboratories. For the ASEA-grade (ASEA Cerama AB) silicon nitride, m varied from 12.3 to 18.2, for a range of 48 percent, from the

13 laboratories. For the GTE Products Corporation (Wesgo Division) silicon nitride, *m* varied from 9.7 to 13.5, for a range of 39 percent from the 13 laboratories. The estimated characteristic strengths σ_θ showed less variation (as would be expected based on statistical uncertainty arguments). For the silicon carbide, σ_θ varied from 470 to 557 MPa (an 18-percent range); for the ASEA silicon nitride, σ_θ varied from 624 to 720 MPa (a 15-percent range); and for the GTE Wesgo silicon nitride, σ_θ varied from 611 to 714 MPa (a 17-percent range). The scatter in these values was beyond the ranges expected from natural statistical variation at the 95-percent confidence level.

Note that a discussion of expected confidence bounds on estimated parameters from natural statistical variation is beyond the scope of this report; however, these bounds are a function of sample size—meaning that, for smaller size data sets (which typically use about 30 specimens), the spread in these bounds would be even larger. The source of these unexpectedly large differences could not be identified. So despite the great care taken in this round-robin exercise and the large number of specimens fractured in each data set, large variation in estimated Weibull parameters—larger than would be expected based on statistics alone—still occurred.

Another interesting result of this study was that statistical tests performed to see if the data best fit the Weibull and other distributions indicated that generally the Weibull distribution was better except for the silicon carbide specimens, where Weibull or gaussian distributions fit the data equally well. This contrasts with Price (1976), where a best-fit distribution could not be identified with certainty. The Nemeth et al. (2011) reanalysis of Price (1976) was generally more favorable regarding the Weibull distribution. The specimens that were oriented radially to the material extrusion direction tended to better fit a two-parameter Weibull distribution, whereas the specimens oriented axially to the extrusion direction better fit to a three-parameter Weibull distribution or possibly some other distribution type (see Figure 9).

In the end, what can be concluded with certainty regarding graphite fracture behavior is that further experimental testing with the latest testing techniques using properly designed specimens and test matrices as well as reanalysis of historical data of good pedigree is needed to, hopefully, help clarify some of the apparent trends reported in the literature. In addition, identifying a best-fit distribution is problematic even for large-size data sets, and alternative tests, such as size-effect studies, are needed to help identify an appropriate distribution.

2.0 Statistical Models of Fracture

The question arises: Are design methodologies developed to describe classically brittle material failure suitable for graphite, or are alternative approaches needed? In the following sections, modeling approaches and simulation studies of brittle-constituent-controlled material failure are discussed to help clarify and (eventually) develop improved models describing the stochastic rupture of graphite. This report adds further background and updated information to reviews of graphite failure criteria by Tucker et al. (1986) and Tucker and McLachlan (1993).

The stochastic nature of fracture in engineered materials can be simulated by two distinct models: series systems and parallel systems. Series systems model the abrupt failure of brittle materials, such as glasses and ceramics, whereas parallel systems model the more gradual or graceful failure of fiber-reinforced composite materials. Series systems assume that material is composed of a set of *n* links connected in series such that the structure fails whenever any of the links fail. An electrical circuit analogy would be having *n* number of resistors or fuses connected in series so that, when a single fuse or resistor fails, electrical current can no longer flow. In the parallel system model, the *n* links are arranged in parallel. When one link fails, load is redistributed to the remaining $n-1$ links. The remaining $n-1$ links carry higher load, but the system (structure) may still survive. The structure does not fail until all *n* links fail. The electrical analog is a system of *n* resistors or fuses arranged in parallel. When electrical current flows such that one resistor or fuse element fails, the current is redistributed to the surviving elements. Only when all the resistors or fuses in the circuit fail will the flow of current cease. The electrical circuit analogy is useful for random fuse lattice models as described in Section 2.3.

Predictions from series system models tend to be more conservative than those from parallel system models. Series system models relevant to this report include the Weibull, Batdorf, and Burchell models. Relevant parallel system models include the uniform defect model, composite material models, and lattice system simulations. Overviews of these models are given in subsequent sections.

2.1 Series Systems—The Weakest Link

Series systems use the weakest-link theory (WLT) as originally proposed by Peirce (1926) to model failure in cotton yarns. The WLT model assumes that the structure is analogous to a chain with n links. Each link may have a different limiting strength. When a load is applied to the structure such that the weakest link fails, the structure fails. Peirce (1926) was the first to formulate the WLT model for fiber strength and was also the first to recognize the close relationship of this model to the asymptotic theory of extreme values in large samples of a statistical population.

Consider a chain containing many links, and assume that failure is due to any number of independent and mutually exclusive mechanisms. Each link involves an infinitesimal probability of failure P_f. Discretize the component into n incremental links. The probability of survival of the i^{th} link $(P_s)_i$ is related to the probability of failure of the i^{th} link $(P_f)_i$: $(P_s)_i = [1 - (P_f)_i]$. The resultant probability of survival of the whole structure is the product of the individual probabilities of survival:

$$P_s = \prod_{i=1}^{n} \left(P_s\right)_i = \prod_{i=1}^{n} \left[1 - \left(P_f\right)_i\right] \cong \prod_{i=1}^{n} \exp\left[-\left(P_f\right)_i\right] = \exp\left[-\sum_{i=1}^{n}\left(P_f\right)_i\right] \tag{1}$$

The approximation arises from truncation of the first two terms of a Taylor series expansion of the exponential function e^x. Equation (1) describes a series system where failure of any one element means failure of the whole system. This also leads to the prediction of a size effect. When more links are added to the chain, the probability of failure increases for a given load. The system is weaker because of the increased probability of having a weaker link present. For the same probability of failure to be maintained, the load would have to be decreased. The prediction of size effect is an important consideration when trying to determine an appropriate probabilistic distribution for modeling a material.

2.1.1 Extreme-Value and Weibull Distributions

Classically brittle materials such as ceramics and glasses have low fracture toughness and do not undergo significant plastic deformation prior to failure. Instead, when a load is applied, large stress concentrations occur at microscopic flaws. These flaws are unavoidable; they are the results of the manufacturing process or environmental factors. The microflaws or microcracks are numerous, are randomly located and oriented, and display a distribution of sizes. When a load acting on an individual microcrack reaches a critical level, catastrophic crack propagation ensues, causing the structure to fail. Therefore in a brittle material, fracture initiates from the combination of a tensile load and a weak flaw being unfavorably located and oriented. For a complex component, failure might not be initiated at the point of highest nominal stress. A particularly severe flaw may be located at a region of relatively low stress yet still be the cause of component failure. For this reason, the strength of a brittle material is statistical, and the entire field solution of the stresses should be considered when determining the potential for failure. From a statistical point of view, this problem leads to the distribution of the smallest value or largest value in large samples. Such distributions form the family of extreme-value distributions.

Extreme-value distributions are the limiting distributions for the minimum or the maximum of a very large collection of random observations from the same arbitrary distribution. The Weibull distribution (1951) is one of three extreme-value distributions discovered by Fisher and Tippet (1928) (the other two are known as the Frechet and Fisher-Tippett-Gumbel distributions).

- Fisher-Tippett-Gumbel, or type I, extreme-value distribution—

$$P\left(X \le x\right) = \exp\left[-\exp\left\{\frac{x - x_u}{x_o}\right\}\right] \tag{2}$$

- Frechet, or type II, extreme-value distribution—

$$P\left(X \le x\right) = \exp\left\{-\left(\frac{x - x_u}{x_o}\right)^{-m}\right\} \qquad x \ge x_u \tag{3}$$

- Reversed Weibull, or type III, extreme-value distribution—

$$P\left(X \le x\right) = \exp\left\{-\left(\frac{-\left(x - x_u\right)}{x_o}\right)^{m}\right\} \qquad x \le x_u \tag{4}$$

where P denotes probability, with parameters $x_u > 0$, $x_o > 0$, and $m > 0$. Equations (2) to (4) show the extreme-value distributions for maxima. By substituting $(-x)$ for x in the distribution function, one obtains the extreme-value distributions for minima (Wikipedia (2010) and Wapedia (2009)). Of these three distributions, Bazant and Planas (1998) and Bazant and Pang (2007) argue that only the Weibull distribution has a sound physical and conceptual basis for modeling structural strength, but Phoenix and Beyerlein (2000a) argue that the Weibull and Fisher-Tippett-Gumbel (henceforth, Gumbel) distributions are reasonable for modeling tensile strength. The Weibull distribution is obtained if the defect size distribution is described by a power law, and the Gumbel distribution is obtained if the defect size is exponentially distributed. Of further note, Bazant and Pang (2007) argue that neither gaussian nor lognormal distributions are appropriate for brittle structure strength statistics.

Weibull (1939a,b) arrived at the distribution function associated with his name by a heuristic argument unrelated to the asymptotic theory. He applied the WLT concept to a solid volume of a brittle material rather than to a fiber as was done by Peirce (1926). The Weibull equation assumes that catastrophic crack propagation initiates from a critically loaded flaw.

A flaw or microcrack of a specified size embedded in a material will require a critical level of applied stress before the crack will begin to extend. That critical level of stress is the critical strength of the given flaw. When there is a distribution of flaws of different sizes in a given volume, the flaws that are equal to or larger than a specified size (with an associated critical strength of σ) will fail at a strength σ or less. Weibull assumed the existence of a function $\eta_V(\sigma)$, referred to as the crack-density function, representing the number of flaws (or microcracks) per unit volume having a strength equal to or less than σ. Use of V as a subscript denotes a quantity that is a function of volume. Under a local tensile stress σ_i, the probability of failure of the i^{th} link, representing the incremental volume ΔV_i, is $(P_{fV})_i = [\eta_V(\sigma_i)\,\Delta V_i]$, where the incremental volume ΔV_i is arbitrarily small such that the value of the expression within the brackets is much less than one (and therefore represents the probability that a flaw of strength of σ_i or less exists within ΔV_i). If a uniform tensile stress σ is applied, such that $\sigma = \sigma_i$ for all incremental volumes ΔV_i, then from Equation (1) the resultant probability of survival for material volume V, where V is the sum of all ΔV_i, is

$$P_{sV} = 1 - P_{fV} = \exp\left[-\eta_V\left(\sigma\right)V\right] \tag{5}$$

where V is the total volume.

Note that the expression within the brackets can also be described as a function of the surface area of the component for flaws that reside on the material surface (e.g., flaws from machining damage). This subject is addressed further in Nemeth et al. (2003, 2005). For the sake of brevity, these relationships are not shown in this report. Equation (5) also can be obtained from the Poisson probability distribution

function, as shown in Section 2.1.7. If the magnitude of the stress is a function of the location within the component, then, again using Equation (1), the overall component failure probability becomes

$$P_{fV} = 1 - \exp\left[-\int_V \eta_V(\sigma)\, \mathrm{d}V \right] \tag{6}$$

This accounts for stress gradients in the component such as those experienced from flexure.

Weibull introduced a three-parameter power function for the crack-density function $\eta_V(\sigma)$,

$$\eta_V(\sigma) = \frac{1}{V_o}\left(\frac{\sigma - \sigma_{uV}}{\sigma_o} \right)^{m_V} = \left(\frac{\sigma - \sigma_{uV}}{\sigma_{oV}} \right)^{m_V} \tag{7}$$

where V_o represents a characteristic volume, which by convention is assumed to be a unit volume; σ_{uV} is the threshold stress parameter, which is the value of the applied stress below which the failure probability is zero. Note that from Equations (5) and (7), for a unit volume when $(\sigma - \sigma_{uV}) = \sigma_{oV}$, a value of 0.6321 is obtained for P_{fV}. When σ_{uV} is zero, the two-parameter Weibull model is obtained. The two-parameter Weibull distribution is widely preferred because of its simplicity (one less parameter to deal with) and its conservatism. With the two-parameter model, the scale parameter σ_o corresponds to the stress level where 63.21 percent of tensile specimens with unit volumes would fracture. The scale parameter σ_{oV} has dimensions of stress × (volume)$^{1/m_V}$, where m_V is the shape parameter (Weibull modulus)—a dimensionless parameter that measures the degree of strength variability. As m_V increases, the dispersion decreases. These three statistical parameters are considered to be material properties, and they are temperature and processing dependent.

Note that internal residual stresses and environment can affect the observed Weibull parameters obtained from experimental data. This includes the case of environmental effects from time-dependent subcritical crack growth. For example, Choi and Gyekenyesi (1999) showed that ultra-fast loading rates of 3.3×10^4 MPa/s were required to eliminate the effect of slow (subcritical) crack growth from strength measurements so that inert strengths of various ceramics could be determined at elevated temperatures. The Weibull parameters in Equation (7) represent inert (fast-fracture) strength parameters. The effect of time- or cycle-dependent subcritical crack growth should be modeled separately, as was done in Nemeth et al. (1993). The combination of Equations (6) and (7) define what is known as the Weibull stress-volume integral.

When Equations (6) and (7) are combined with a zero threshold stress, the two-parameter Weibull equation becomes

$$P_{fV} = 1 - \exp\left[-\int_V \left(\frac{\sigma(x,y,z)}{\sigma_{oV}} \right)^{m_V} \mathrm{d}V \right] \tag{8}$$

where x, y, z is the point location in the component. This equation can be reexpressed as

$$P_{fV} = 1 - \exp\left[-\left(\frac{\sigma_f}{\sigma_{oV}} \right)^{m_V} \left\{ \int_V \left(\frac{\sigma(x,y,z)}{\sigma_f} \right)^{m_V} \mathrm{d}V \right\} \right] \tag{9}$$

where σ_f is the maximum stress in the component and the term in braces { } is the effective volume V_e:

$$V_e = \int_V \left(\frac{\sigma(x,y,z)}{\sigma_f} \right)^{m_V} \mathrm{d}V \tag{10}$$

For two components of different sizes, but otherwise identical (except for the magnitude of loading), with identical stress distributions and identical survival probabilities, equating terms yields

$$P_{fV} = 1 - \exp\left[-\left(\frac{\sigma_{f1}}{\sigma_{oV}} \right)^{m_V} V_{e1} \right] = 1 - \exp\left[-\left(\frac{\sigma_{f2}}{\sigma_{oV}} \right)^{m_V} V_{e2} \right] \tag{11}$$

which simplifies to

$$\sigma_{f2} = \sigma_{f1} \left(\frac{V_{e1}}{V_{e2}} \right)^{1/m_V} \tag{12}$$

where subscripts 1 and 2 denote components with different sizes.

Equation (12) is the classic Weibull size-effect equation, which predicts that the strength of a component is a function of its size. As size increases, strength is predicted to decrease as a function of the Weibull modulus m_V. This is an important relationship because it provides a testable basis from which to infer the applicability of a probabilistic distribution for a particular material. As mentioned in Section 1.4, previous size effect studies of graphite have had mixed success correlating to the Weibull distribution. Size effect can have important implications in the design of safe graphite material. The graphite bricks used in a nuclear reactor tend to be quite large in relation to the specimens used to measure strength properties. For example, if specimens are 100 times smaller in effective volume than the component, then for Weibull moduli of 5, 10, and 15, the component strength would decrease by 0.40, 0.63, and, 0.74, respectively. If specimens are 1000 times smaller, these numbers decrease to 0.25, 0.50, and 0.63, respectively.

2.1.2 The Batdorf Model and Response to Multiaxial Stresses

2.1.2.1 Batdorf Multiaxial Strength Theory

The previous section described the Weibull distribution for predicting the likelihood that a component will fail from an applied uniaxial stress. This section describes the Batdorf theory for predicting brittle material failure from applied multiaxial stress states. The Batdorf methodology is typically used in conjunction with an underlying Weibull distribution. Similar multiaxial statistical failure theories such as the Evans elemental strength approach (Evans (1978)) and Matsuo (1981) have also been developed. The Evans approach (and likely Matsuo) has been shown to be equivalent to the Batdorf theory (Chao and Shetty (1990)), so these approaches are not described herein. The Batdorf theory is highlighted in this section because it successfully describes graphite's multiaxial strength and provides a plausible physical mechanism to explain this response.

Other deterministic global multiaxial failure criterion traditionally used for metals have been compared with graphite multiaxial rupture data (e.g., see Jortner (1972), Tang (1979), Taylor et al. (1967), Broutman et al. (1970), Babcock et al. (1972), Yahr et al. (1993), and Schmidt (2000)). Jayatilaka (1979) provides a good overview of these failure criterion as well as the fracture mechanics aspects of mixed-mode loading on flaws. In their general reference book, Munz and Fett (1999) provide an excellent treatment of global multiaxiality criteria for various defect geometries (cylindrical pore, spherical pore, ellipsoidal pore, and circular cracks. These failure criteria also consider the effect of compressive stresses.

The Weibull equation assumes that catastrophic crack propagation initiates from a critically loaded flaw; however, it does not describe the physical mechanism behind this phenomenon. Batdorf and Crose (1974) and Batdorf and Heinisch (1978) addressed this shortcoming by combining WLT with linear

elastic fracture mechanics (LEFM). Batdorf developed his theory primarily to account for the effect of multiaxial stress states for aerospace-grade graphite, which is a finer grained material. (Note that nuclear-grade graphite ranges from fine-grained to coarse-grained material.) Batdorf provided an improved physical basis for failure by incorporating an assumed crack geometry, mixed-mode fracture criterion, and a crack-orientation function. In addition to the previously cited Batdorf references, Nemeth et al. (2003, 2005) provide a full treatment of the Batdorf theory and extend the theory for time- and cycle-dependent subcritical crack growth and for the effect of transient stresses. The Batdorf theory has been developed for volume-residing flaws (failure probability as a function of material volume) as well as for surface-residing flaws (failure probability as a function of material surface area)—again, these are detailed in Nemeth et al. (2003, 2005). A brief summary of the development for volume-residing flaws follows.

In the Batdorf theory, the incremental failure probability at a given location in the component can be described as the product of two probabilities:

$$\Delta P_{fV} = \Delta P_{1V} \cdot P_{2V} \tag{13}$$

where ΔP_{1V} is the probability of the existence in ΔV of a crack having a critical strength between σ_{Ic} and $\sigma_{Ic} + \Delta\sigma_{Ic}$. Critical strength σ_{Ic} is defined as the remote, uniaxial fracture strength of a given crack in mode I loading. The second probability, P_{2V}, is the probability that a crack of critical strength σ_{Ic} will be oriented in a direction such that an effective stress σ_{Ieq} (which is a function of the fracture criterion, stress state, and crack configuration) satisfies the condition $\sigma_{Ieq} \geq \sigma_{Ic}$. The effective stress σ_{Ieq} is defined as the equivalent mode I stress that a flaw would experience when subjected to a multiaxial stress state that results in mode I, II, and III crack-surface displacements.

The strength of a component containing a flaw population is related to the critical flaw size, which is implicitly used in Batdorf's theory. Batdorf and Crose (1974) describe ΔP_{1V} as

$$\Delta P_{1V} = \Delta V \frac{\mathrm{d}\,\eta_V(\sigma_{Ic})}{\mathrm{d}\,\sigma_{Ic}} \mathrm{d}\,\sigma_{Ic} \tag{14}$$

and P_{2V} is expressed as

$$P_{2V} = \frac{\Omega(\Sigma, \sigma_{Ic})}{4\pi} \tag{15}$$

where $\eta_V(\sigma_{Ic})$ is the Batdorf crack-density function and $\Omega(\Sigma, \sigma_{Ic})$ is the area of the solid angle projected onto the unit radius sphere in principal stress space (see Figure 11) containing all the crack orientations for which $\sigma_{Ieq} \geq \sigma_{Ic}$ for the applied far-field multiaxial stress state Σ. The infinitesimal area, dA, on the unit sphere represents a particular flaw orientation (a direction normal to the flaw plane), and σ_{Ieq} is an equivalent stress, which is a function of an assumed crack shape and multiaxial fracture criterion. The constant 4π is the surface area of a unit radius sphere and corresponds to a solid angle containing all possible flaw orientations.

The component probability of failure is

$$P_{fV} = 1 - \exp\left\{-\int_V \left[\int_0^{\sigma_{Ieq,\max}} \frac{\Omega(\Sigma, \sigma_{Ic})}{4\pi} \frac{\mathrm{d}\,\eta_V(\sigma_{Ic})}{\mathrm{d}\,\sigma_{Ic}} \mathrm{d}\,\sigma_{Ic}\right] \mathrm{d}V\right\} \tag{16}$$

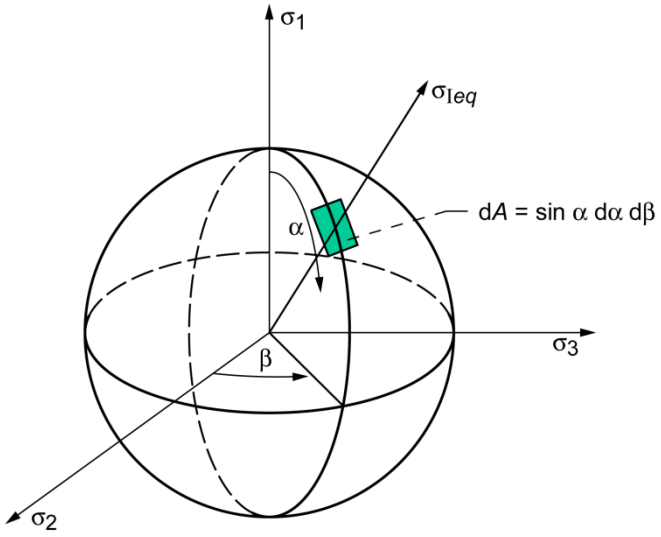

Figure 11.—Unit radius sphere representing all possible flaw orientations, where σ_1, σ_2, and σ_3 are the principal stresses and α and β are angular coordinates. An infinitesimal area, dA, on the unit sphere represents a particular flaw orientation (a direction normal to the flaw plane), and σ_{Ieq} is an equivalent stress that is a function of an assumed crack shape and a multiaxial fracture criterion.

where $\sigma_{Ieq,\max}$ is the maximum effective stress that a randomly oriented flaw could experience from the given stress state Σ. The crack-density function $\eta_V(\sigma_{Ic})$ is independent of stress state and has been approximated by a power function (Batdorf and Heinisch (1978)). This leads to the Batdorf crack-density function of the form

$$\eta_V\left(\sigma_{Ic}\right) = \frac{\bar{k}_{BV}\,\sigma_{Ic}^{m_V}\left(x,y,z,\alpha,\beta\right)}{\sigma_{oV}^{m_V}} \tag{17}$$

where x, y, z corresponds to the location and α and β are orientation angles. The normalized Batdorf crack-density coefficient $\bar{k}_{BV}$ is a function of the mixed-mode fracture criterion chosen. Equation (17) is similar to the Weibull power-law crack-density function of Equation (7) with a zero threshold stress. The exponent m_V is equivalent to the Weibull exponent in Equation (7). The value of the Batdorf crack-density coefficient $\bar{k}_{BV}$ normalizes Equation (16) to the Weibull equation (Eq. (8)) for a uniaxial stress state. It also means that Equation (16) takes on the characteristics of a Weibull distribution. The normalized Batdorf crack-density coefficient $\bar{k}_{BV}$ and the Weibull modulus m_V are evaluated from experimental inert strength fracture data.

Although the Weibull (Eq. (7) with zero threshold stress) and Batdorf (Eq. (17)) crack-density functions are similar in form, they are not the same. The Weibull function simply depends on the applied uniaxial stress distribution σ and is the only term other than the volume necessary to calculate P_{fV}. The Batdorf function depends on the mode I strength of the crack σ_{Ic}, which has an associated probabilistic distribution and must be integrated over a range of values for a given stress state. Furthermore, to obtain P_{fV}, a crack-orientation function, P_{2V}, must be considered in addition to the density function and the volume. Finally, the normalized Batdorf coefficient $\bar{k}_{BV}$ cannot be calculated from inert strength data until a fracture criterion and crack shape are chosen. To determine a component probability of failure, one must evaluate P_{2V} (Eq. (15)) for each elemental volume ΔV_i, within which a uniform multiaxial stress

state σ is assumed. The solid angle $\Omega(\Sigma, \sigma_{Ic})$ depends on the selected fracture criterion, the crack configuration, and the applied stress state. For multiaxial stress states, with few exceptions, $\Omega(\Sigma, \sigma_{Ic})$ must be determined numerically. For a sphere of unit radius (Figure 11), an elemental surface area of the sphere is $dA = \sin\alpha\, d\beta\, d\alpha$. If we project onto the spherical surface the equivalent (effective) stress $\sigma_{Ieq}(\Sigma,\alpha, \beta)$, the solid angle $\Omega(\Sigma, \sigma_{Ic})$ will be the area of the sphere containing all the projected equivalent stresses satisfying $\sigma_{Ieq} \geq \sigma_{Ic}$. Because of symmetry of stresses, this integration need only be performed over one-eighth of the unit sphere; therefore,

$$\Omega(\Sigma,\sigma_{Ic}) = \int_0^{\pi/2}\int_0^{\pi/2} H(\sigma_{Ieq},\sigma_{Ic}) \sin\alpha\, d\alpha\, d\beta \tag{18}$$

where

$$H(\sigma_{Ieq},\sigma_{Ic}) = 1 \qquad \sigma_{Ieq} \geq \sigma_{Ic}$$

$$H(\sigma_{Ieq},\sigma_{Ic}) = 0 \qquad \sigma_{Ieq} < \sigma_{Ic}$$

Substituting into Equation (16) and integrating with respect to σ_{Ic} changes the component failure probability to Batdorf (1978a,b) and Nemeth et al. (2003, 2005):

$$P_{fV} = 1 - \exp\left[-\frac{2}{\pi}\int_V\int_0^{\pi/2}\int_0^{\pi/2} \eta_V(\sigma_{Ieq}) \sin\alpha\, d\alpha\, d\beta\, dV\right] \tag{19}$$

where σ_{Ieq} replaces σ_{Ic} in Equations (17) and (19). For a given incremental volume, $\sigma_{Ieq}(x, y, z, \alpha, \beta)$ is the projected equivalent stress over the unit radius sphere in principal stress space as depicted in Figure 11. Using the power-law crack-density function η_V of Equation (17) will characterize the Batdorf model in Equation (19) as a form of the Weibull distribution. Equation (19) circumvents the more involved numerical integration of $\Omega(\Sigma, \sigma_{Ic})$.

Batdorf (1975, 1978a) gives an example of how the form of the crack-density function is related to the distribution of microcrack sizes and how this affects the statistics of fracture. Later She and Landes (1993) investigated the Batdorf relation for a normal distribution of crack sizes. Using the modeling framework of Equation (16), Batdorf (1975, 1978b) derived fracture statistics for intergranular cracks. This was based on work done by McClintock (1973). McClintock's model for crack-size distribution produced a probability-of-failure distribution that was not of the asymptotic forms of extreme-value theory. An interesting feature of this model is that scatter in strength, and therefore by analogy the Weibull modulus, is not constant as a function of volume.

McClintock's (limited) two-dimensional model assumes that each grain boundary has a small, but nonzero, probability q of being unbonded. Therefore, the probability that two connected grain boundaries are both unbonded and form a contiguous crack is q^2, the probability that three connected grain boundaries are unbonded is q^3, and so on. He showed that the probability of a crack (composed of connected unbonded grain boundaries) being longer than length a is $\exp(-a/a_\mu)$, where a_μ is the average crack length. From this, Batdorf (1975) derived a crack-density function of $\eta_V(\sigma_{Ic}) = N_o \exp\left(-1/\sigma_{Ic}^2\right)$, where N_o is the number of cracks per unit volume. Applying McClintock's conjecture for a penny-shaped crack gives a probability of a crack being larger than radius a of $\exp\{-\ln(q^{-1})\, \pi\, a^2/A_o\}$, where A_o is the area of a grain. The associated crack-density function is $\eta_V(\sigma_{Ic}) = N_o \exp\left(-1/\sigma_{Ic}^4\right)$. Both crack-density functions have a similar form. Using these functions with Equation (16) for a uniform, uniaxial applied stress resulted in the relative dispersion of strength decreasing as volume decreased. Fitting a three-parameter Weibull distribution to the predicted failure probabilities from the intergranular crack model yielded a

surprisingly good fit over a large range of volume. In the case of the penny-shaped crack, the Weibull modulus as a function of volume was approximated by $m_V = 1.7 \log_{10}(N_o V)$. For example, when the volume increased by a factor of 20, the Weibull modulus would increase by 2.2. Therefore, this theory indicates that Weibull modulus was not constant with volume. The degree of size effect likely also decreased with volume, indicating a possible relationship of low strength scatter with small-size effect (which was visually inferred from the figures presented in the Batdorf (1975) reference).

The Weibull modulus is notoriously difficult to measure consistently (e.g., see Tennery and Ferber (1989)), and the ceramics community usually does not assume that the Weibull modulus varies with volume because of the lack of consistent evidence. However, Batdorf's treatment of the McClintock model is an interesting exercise and shows that the Weibull modulus is not necessarily a true material constant. In the ceramics design community, the power-law crack-density function with the Weibull distribution is almost universally used (with no known exceptions to the best knowledge of the authors). The Batdorf model is usually used or described with a power-law crack-density function since it then becomes a form of the Weibull distribution (with all the inherent advantages of the extensive knowledge base and techniques that have been developed) and it has been incorporated in reliability analysis software such as Ceramics Analysis and Reliability Evaluation of Structures/Life (CARES/Life) (Nemeth et al. (2003, 2005)).

2.1.2.2 Multiaxial Strength Response of the Batdorf Model

All results shown subsequently in this section use the power-law crack-density function of Equation (17), which characterizes the Batdorf model as a form of the Weibull distribution. The effective stress σ_{1eq} represents an equivalent normal stress on the crack face from the combined action of the normal stress σ_n and the shear stress τ on the crack face. The microcrack orientation is defined by the angular coordinates of α and β, where the direction normal to the plane of the microcrack is specified by the radial line defined by α and β (see Figure 11). For the sake of brevity, the development of the effective stress equations is not shown (for details, see Nemeth et al. (2003, 2005)). For a penny-shaped crack with the Shetty mixed-mode fracture criterion (Shetty (1987)), the effective stress becomes

$$\sigma_{\mathrm{I}eq} = \frac{1}{2}\left\{\sigma_n + \sqrt{\sigma_n^2 + \left[\frac{4\tau}{\bar{C}(2-\nu)}\right]^2}\right\} \tag{20}$$

where ν is Poisson's ratio and $\bar{C}$ is the Shetty shear-sensitivity coefficient, with values typically in the range $0.80 \le \bar{C} \le 2.0$. As $\bar{C}$ increases, the response becomes progressively more shear insensitive. Shear increases the equivalent stress as shown in Equation (20), and this has a deleterious effect on the predicted material strength. For a penny-shaped crack with a material having a Poisson's ratio of about 0.22 and $\bar{C} = 0.80$, 0.85, 1.05, and 1.10, Equation (20) models, respectively, the following criteria: Ichikawa's maximum energy-release-rate approximation (Ichikawa (1991)), the maximum tangential stress (Erdogan and Sih (1963)), Hellen and Blackburn's maximum strain-energy-release-rate formulation (Hellen and Blackburn (1975)), and colinear crack extension. The value of $\bar{C}$ also can fit empirically to experimental data—either on introduced cracks (as was done in Shetty (1987)) or on specimens being tested multiaxially.

The following example illustrates the multiaxial response of nuclear-grade graphite. Sookdeo et al. (2008) performed CARES/Life reliability analysis using the Batdorf method on graphite multiaxial tube specimens previously tested at Oak Ridge National Laboratory. The tubes consisted of near-isotropic grade IG–110 graphite material (Toyo Tanso, Inc., reference) manufactured in a tubular configuration whereby combined axial force and internal pressurization could be imposed. In this way, the multiaxial strength response was measured in the tension-tension and tension-compression quadrant of stress-space. CARES/Life (Nemeth et al. (1993, 2003, 2005)) in conjunction with the ANSYS finite element analysis program was used to predict the failure response of the specimens for the Principle of Independent Action

(PIA)[1] and Batdorf multiaxial failure criterion. The PIA criterion (Barnett, et al. (1967) and Freudenthal (1968)) assumes that the principal stresses (σ_1, σ_2, and σ_3) act independently, where the product of the reliability for each principal stress component, calculated using the Weibull equation, determines the reliability of the component. The PIA criterion is expressed as

$$P_{fV} = 1 - \exp\left[-\frac{1}{\sigma_{oV}^{m_V}} \int_V \left(\sigma_1^{m_V} + \sigma_2^{m_V} + \sigma_3^{m_V} \right) \mathrm{d}V \right] \tag{21}$$

where the effect of compressive principal stresses is ignored in the equation.

For the Batdorf criterion, a penny-shaped crack was chosen with Shetty shear-sensitivity coefficients $\bar{C}$ of 0.82 and 1.20. The results are shown in Figure 12 at 10-, 50-, and 90-percent probability of failure levels. The figures clearly show that, although the PIA and Batdorf theories yield similar results in the tension-tension quadrant, the results diverge in the tension-compression quadrant. These figures show that the PIA criterion is nonconservative when compressive stresses are present, whereas the Batdorf criterion can be tuned for shear sensitivity such that good correlation to the data can be achieved. Figure 12(b) shows the results for $\bar{C}$ = 0.82, which is the case where the flaws are highly shear sensitive. Conversely, Figure 12(a), which shows the PIA criterion, is essentially identical to the graph of the Batdorf criterion with shear insensitive flaws ($\bar{C}$ is a large value such that the shear stress contribution is negligible in Eq. (20)). Figure 12(c) shows $\bar{C}$ = 1.20, which correlates well with the data. Uchimura et al. (1992) also showed good correlation with silicon nitride by using a Batdorf-style fracture-mechanics-based fracture criteria.

Graphite bricks are stacked in a reactor core, and compressive stress can be significant at the bottom of the stack. Therefore, the effect of compressive stresses should also be considered in a statistical failure criterion. Alpa (1984) extended the Batdorf theory to consider compressive stresses. In Alpa's model, compressive stress on the crack face results in friction and interlocking such that the effect of shear stresses on the crack face is effectively reduced. In Alpa's model, compressive failure stems from the same flaw population as tensile failure, and it uses the same crack-density function. Hence in Alpa's model, failure is WLT controlled and has the same Weibull modulus and, therefore, the same size effect as the tensile failure mode. Nemeth (1989) considered compressive failure as a separate and independent failure mode from tensile failure (also see Appendix A for an alternative failure criterion mechanism using the uniform defect model described in Sec. 2.1.7). The reliability (survival probability) of the multiaxial stress state was the product of the reliability of the compressive failure mode and the tensile failure mode.

$$P_s = P_{s,\text{tensile}} \cdot P_{s,\text{compressive}} \tag{22}$$

where P_s is the survival probability. Nemeth used Batdorf's methodology of random flaw orientation (the unit sphere of Figure 11) and the critical stress criterion to construct a simple effective stress relationship:

$$\sigma_{\mathrm{I}eq} = 2\tau \tag{23}$$

of which the value of 2 conveniently made the maximum value of effective stress $\sigma_{\mathrm{I}eq}$ in uniaxial compression equal to the value of $\sigma_{\mathrm{I}eq}$ in uniaxial tension on the unit sphere. This allowed the failure criterion to be easily normalized to the strength of uniaxial compression experimental rupture data. The compressive multiaxial failure response was assumed to be only a function of shear stress on the crack plane. This failure criterion also assumed the Weibull WLT mechanism; however, it allowed the Weibull modulus in compression to be independent of the Weibull modulus in tension. As indicated in Section 2.2.7 and in Bazant and Pang (2007), the Weibull modulus may be a function of mixed series-parallel system modeling, and thus compressive failure is possibly still amenable to Weibull distribution

[1]A commonly used Weibull-based multiaxial failure criterion based on principal stresses acting independently. A description is provided in Nemeth et al. (2003, 2005).

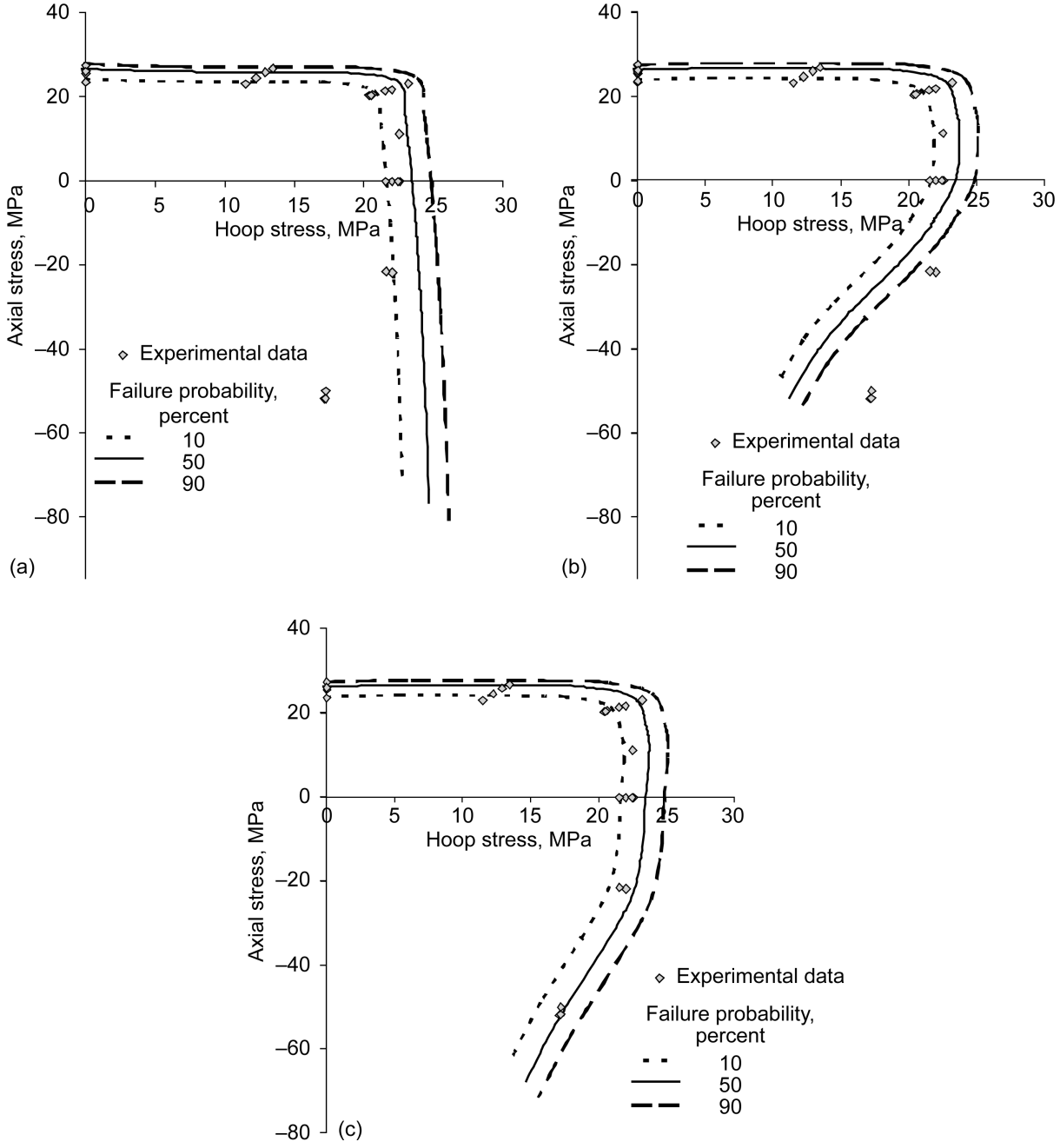

Figure 12.—Multiaxial failure probability predictions at 10-, 50-, and 90-percent levels for IG–110 grade graphite. (a) Principle of Independent Action (PIA) theory and Batdorf theory for shear-insensitive cracks (lines are coincident). (b) Batdorf theory for penny-shaped cracks with a Shetty shear-sensitivity coefficient of $\overline{C}$ = 0.82. (c) Batdorf theory for penny-shaped cracks with a Shetty shear-sensitivity coefficient of $\overline{C}$ = 1.20.

modeling. A size effect is still predicted in compression, but it is a function of the Weibull modulus for compression. Figure 13 shows an example of a failure envelope generated with a tensile and compressive failure criterion. In this example, the Weibull modulus for both tension and compression is assumed to be 10 and the material is assumed to be 5 times stronger in uniaxial compression than in uniaxial tension.

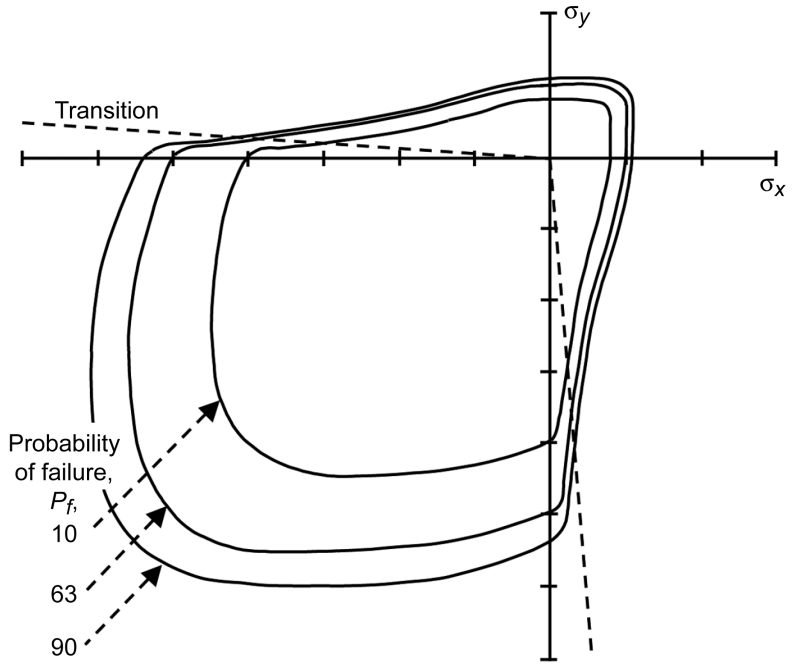

Figure 13.—Example of a failure envelope where compressive failure is treated as a separate and independent failure mode from the tensile failure mode. The overall reliability is a product of the tensile mode and compressive mode reliabilities. The compressive mode is a function of mode II (shear) stress only on the flaw. In this example, the tensile and compressive mode have the same Weibull modulus, but in the methodology they can be independent. The dotted lines denote the transition between the tensile-dominated and compression-dominated failure; σ_x and σ_y are the orthogonally applied uniaxial stresses.

2.1.3 Strength Anisotropy and Multiaxial Stresses

Graphite strength is mildly anisotropic relative to its extrusion axis. Extrusion and molding preferentially orient the graphite grains such that, for a graphite (cylinder-shaped) log, the strength response is transversely isotropic, with the strength stronger in the axial direction than in the radial direction (typically between 10 and 25 percent). Modern grades of graphite tend to be more isotropic in strength response (10 percent or better), and therefore, strength anisotropy becomes a less critical design issue. Nevertheless, strength anisotropy is a physical phenomenon that should not be ignored in a general failure theory for graphite. A brief discussion follows regarding work done using the Weibull distribution to model strength anisotropy for multiaxial stress states.

Margetson (1976) used a PIA approach to model strength anisotropy, which was validated against graphite and against rocket motor components in Cooper (1988). In Margetson's approach, the Weibull parameters for the uniaxial strength relative to three material axes normalize the model. A strength ellipsoid is constructed from the three material axes, and a transformation law converts the scale parameters for the three material axes into three equivalent scale parameters—$\sigma_{o,1}$, $\sigma_{o,2}$, and $\sigma_{o,3}$—corresponding to the principal stress directions from the applied multiaxial stress (see Figure 14). A PIA-type criterion is then constructed:

$$P_{fV} = 1 - \exp\left[-\left\{ \int_V \left(\frac{\sigma_1}{\sigma_{o,1}} \right)^{m_V} \mathrm{d}V + \int_V \left(\frac{\sigma_2}{\sigma_{o,2}} \right)^{m_V} \mathrm{d}V + \int_V \left(\frac{\sigma_3}{\sigma_{o,3}} \right)^{m_V} \mathrm{d}V \right\} \right] \tag{24}$$

where the effect of compressive principal stresses is ignored in the equation.

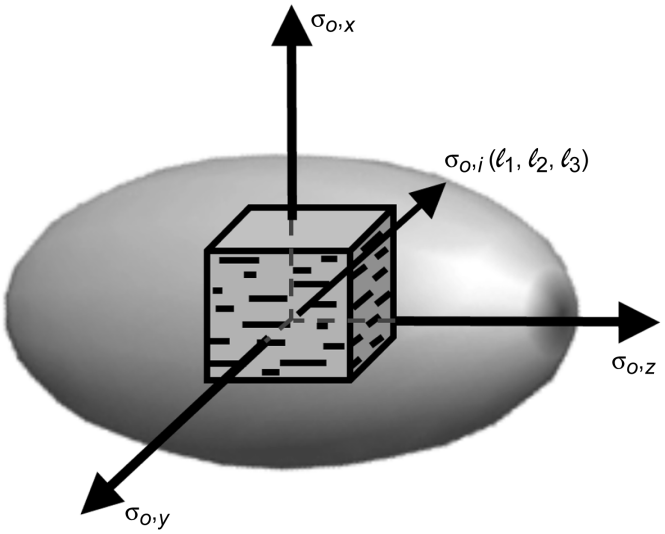

Figure 14.—Margetson strength ellipsoid. Weibull scale parameters ($\sigma_{o,x}$, $\sigma_{o,y}$, and $\sigma_{o,z}$) associated with the material axes are transformed into Weibull scale parameters ($\sigma_{o,1}$, $\sigma_{o,2}$, and $\sigma_{o,3}$) relative to the three principal stress axes for an applied multiaxial stress state. The parameter $\sigma_{o,i}$ arbitrarily denotes one of the transformed Weibull scale parameters for a given principal stress direction denoted with direction cosines ℓ_1, ℓ_2, and ℓ_3.

Batdorf (1973) extended the Batdorf and Crose (1974) unit sphere approach for anisotropic multiaxial strength (of graphite) by assuming that flaws were randomly oriented but that critical strength σ_{1c} was directionally dependent relative to a material coordinate system. Rather than the unit radius sphere (Figure 11), a critical strength ellipse was developed where σ_{1c} became a function of angles α and β, and P_{2V} in Equation (14) involved the integration of a normal stress (mode I stress on a flaw plane) σ_n, for the condition where $\sigma_n \geq \sigma_{1c}$, over the surface of the strength ellipse (equivalent to all possible flaw orientations) divided by the total surface area of the ellipse as shown in Figure 15.

Buch et al. (1977) assumed that flaws were not uniformly randomly oriented but had preferential orientation. They used the Batdorf and Crose (1974) unit sphere approach but superimposed a cosine power-law flaw orientation anisotropy probability distribution function on the orientation angle α. This meant that a flaw was more likely to be oriented in one direction than another. In this manner they accounted for a transversely isotropic strength response where the exponent of the cosine function determined the degree of strength anisotropy. Buch et al. (1977) only considered the normal component of stress σ_n on a flaw.

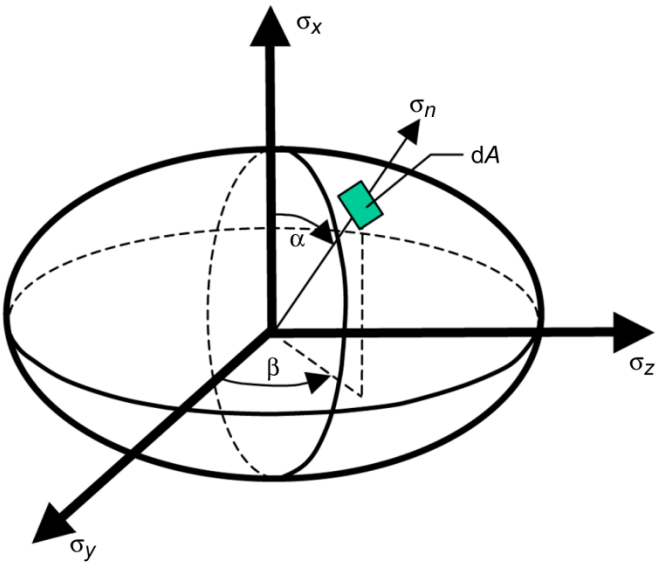

Figure 15.—The critical strength ellipsoid of Batdorf, where σ_x, σ_y, and σ_z are oriented relative to the material axes, σ_n is the normal stress, dA is an infinitesimal area, and α and β are angular coordinates.

Nemeth (1989) extended the Buch et al. (1977) approach for transversely isotropic brittle materials to include shear sensitivity on a flaw (e.g., see Eq. (20)) as well as the anisotropic stress intensity factor K_{Ic} versus the orientation of a flaw (more details are provided in Appendix B). Anisotropic K_{Ic} results in strength anisotropy modeling analogous to the Batdorf (1973) approach (and would also correspond to flaws being larger in one direction than another), but in this case a cosine power-law function was used as was done in Buch et al. (1977). This approach would allow K_{Ic} to be mapped from, for example, indentation testing with the indenter oriented at various angles to the extrusion direction (shown in Figure 16). Note that a more recent journal article by Quinn and Bradt (2007) recommends that indentation testing no longer be used for fracture toughness testing. However, in this case, only the relative difference in K_{Ic} from one orientation to another is required rather than an accurate value for K_{Ic}, so perhaps indentation testing results could still be used, although further research is needed. The determined functional relationship in conjunction with the unit sphere approach enables the stochastic strength response to be predicted from the multiaxial stresses. Alternatively, specimens could be excised at various angles to the extrusion direction and strength properties obtained similar to that done by Margetson (1976). From that information, the necessary functional relationship of strength with angle would also be obtained to calibrate the model.

Finally, Tang (1979) performed a literature survey of triaxial failure theories for anisotropic brittle materials (not considering the work already mentioned) and concluded that the strength tensor theory of Tsai and Wu (1971) could be appropriate for graphite. A reduction of the model for transversely isotropic materials was provided. This was a survey of deterministic failure criteria.

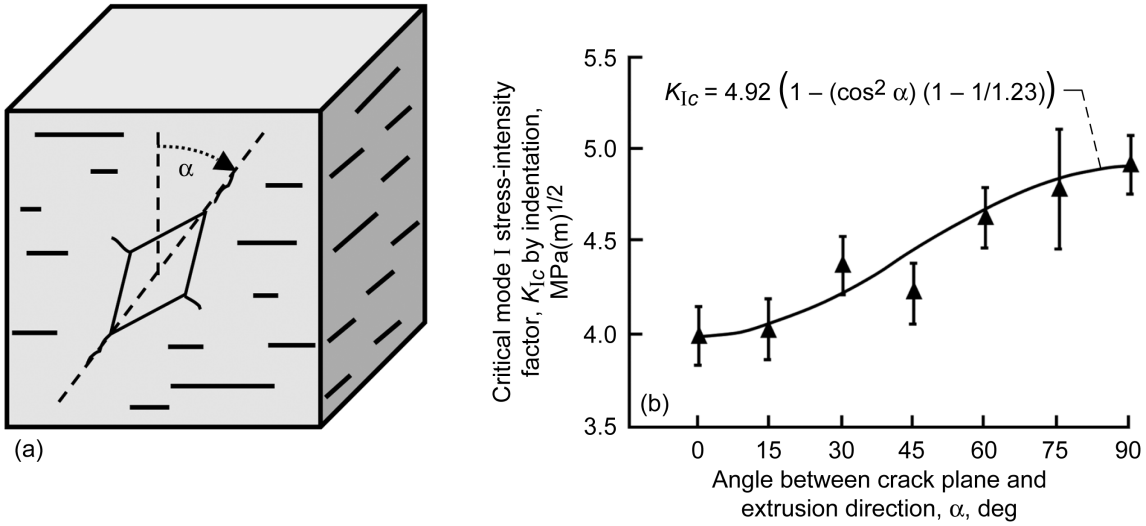

Figure 16.—Indentation testing used to determine the relationship between K_{Ic} and the extrusion direction. Experimental results from Corbin et al. (1988).

2.1.4 R-Curve Effect on the Weibull Distribution

The point of discussing R-curve is twofold. First, rising R-curve behavior tends to increase the apparent (experimentally observed) Weibull modulus. This decreases the scatter in measured strengths. Second, the subcritical (stable) crack growth that occurs prior to crack instability would cause acoustic emission (as the crack grows through individual grains). The implication is that a weakest-link failure mechanism may still be appropriate for graphite since R-curve behavior can hypothetically account for at least some of the acoustic emission observed prior to rupture as well as some level of distributed damage (more than one crack may be growing simultaneously before a single crack becomes critically unstable). This argument would certainly imply a Kaiser effect (1950), but how much of the acoustic emission profile and nonlinear stress-strain behavior can be attributed to R-curve behavior is a question that will have to be explored further. R-curve behavior also has potential ramifications on the deviation from the Weibull distribution, scatter in strength versus the amount of material under tension, and size effect. Note that the Burchell model, discussed in Section 2.1.6, implies an R-curve behavior in graphite.

The failure criterion in the Batdorf methodology is the simple LEFM criterion for mode I loading on a crack

$$K_I \geq K_{Ic} \tag{25}$$

which states that unstable catastrophic crack propagation occurs when the stress intensity K_I on a crack equals or exceeds the critical stress intensity K_{Ic} of the material. Equation (25) directly correlates the size distribution of flaws in the material to the observed scatter in strength. When there is mixed-mode loading on a crack, an equivalent stress intensity factor K_{Ieq} replaces K_I in Equation (25). If one assumes that material property K_{Ic} is constant with crack size, Equation (25) describes what is known as a flat R-curve material. This means that there is no stable subcritical crack growth or damage accumulation at all prior to catastrophic rupture. Hence, there would be no acoustic emission in the material, indicating crack growth, prior to failure. This is not consistent with what is observed with many grades of graphite.

A rising R-curve occurs when fracture toughness or fracture resistance K_R increases with crack size a. If the R-curve is steep enough, the crack extension is at first stable, satisfying $\partial K_I/\partial a < \partial K_R/\partial a$, and becomes unstable when $\partial K_I/\partial a \geq \partial K_R/\partial a$. Therefore, when a load is applied, a crack may extend some increment but arrest, and only if the load is increased will the crack either (1) further extend in a stable manner and arrest or (2) propagate uncontrollably, depending on the previously cited condition regarding

the stability of the crack. This is explained further in fracture mechanics textbooks such as Broek (1982). The implication for fracture statistics is that the observed scatter in strength becomes not only a function of the size distribution of the flaws in the material but also of the particular R-curve behavior.

Kendall et al. (1986) and Cook and Clarke (1988) experimentally demonstrated and theoretically showed that the strength scatter decreases, which affects the apparent Weibull modulus (observed from rupture experiments of specimens). Shetty and Wang (1989) and Munz and Fett (1999) pointed out that, for R-curve behavior modeled with a power law, the Weibull distribution for measured strengths is different from the hypothetical strength distribution based on the fracture toughness K_R treated as a constant with crack size (a flat R-curve). Therefore, the apparent Weibull modulus is not only controlled by the statistical distribution of the sizes of flaws, but it is influenced by the physics of crack growth (fracture toughness K_R changing with crack size). This applies for transformation-toughened ceramics and for ceramics that have elongated interlocking grains such that crack growth at the crack tip is impeded. Danzer et al. (2007) demonstrates how R-curve behavior affects the strength distribution as a function of volume under stress and shows that non-Weibull strength distributions can be obtained for an R-curve that follows an exponential law. The example provided in Danzer et al. (2007) also shows that Weibull behavior is asymptotically approached at low and high stress extremes and at low and high volume extremes. In a review of R-curve research, Munz (2007) shows how different R-curve relations affect the strength response and how crack-bridging parameters can be obtained from scatter in strength. Munz (2007) notes that extrapolation of experimental strength data to low probabilities of failure potentially leads to an overestimation of strength.

A statistical mechanism for R-curve development was explored by Planas (1995), and it was summarized in Bazant and Planas (1998) for transgranular fracture (fracture traveling through the grain of the material). Note that, for intergranular fracture, the crack front travels along the grain boundary. For a large crack growing under mode I, assume that the material ahead of the crack tip is divided into small cells (corresponding to individual material grains) with crack growth resistances uniform within each cell but varying randomly from cell to cell. Bazant and Planas (1998) showed that, as the crack grows through the individual grains, the likelihood of encountering a grain with a higher K_R increases. This gives rise to a statistical R-curve which Bazant and Planas modeled with a Frechet distribution. From their distribution, the slope of the R-curve is steepest at the smallest crack length increments Δa. Therefore, for an initial flaw or microcrack, if flaw size and grain size are not greatly different, one would expect that the effect of the R-curve on the Weibull modulus would be greater than if the inherent flaw was much larger than the grain size. In another study, Ramachandran et al. (1993) showed that, for a transformation-toughened zirconia, the scatter in strength was caused by variability in the R-curve and the instability crack lengths. Crack lengths at instability were much greater than the initial flaw size; thus, fracture strengths were insensitive to the initial flaw-size distribution. The implication for graphite is that R-curve behavior may make material insensitive to the size distribution of the crack-growth-initiating flaws. It is unclear what effect this type of behavior would have on size effect—whether extreme-value statistics would operate for R-curve variability and instability crack lengths or not.

From a practical point of view, it could be asserted that the Weibull distribution is still useful for modeling graphite strength, even when R-curve behavior is present. However, the experimentally observed scatter in strength represents an interplay of the distribution of the flaw sizes in the material and the factors related to the physics of crack instability. Danzer et al. (2007) showed that, when one starts with a Weibull strength distribution for a flat R-curve material, the strength distribution can become non-Weibull when a rising R-curve behavior is imposed. However, WLT behavior will still be operative in that model. For practical purposes, if the range of scaling of material volume (between the specimen and component) is only a few orders of magnitude, the Weibull distribution probably gives a reasonably accurate approximation of the strength response. However, Munz (2007) notes that extrapolating experimental strength data to low probabilities of failure may lead to an overestimation of strength.

Finally Jayatilaka and Trustrum (1977), Rickerby (1980), and Diaz et al. (1999) performed work relating Weibull modulus, an empirical material constant, to the properties of the flaw-size distribution of a material. This would be for flat R-curve materials. Therefore, how the crack-density function was

functionally related to the size distribution of flaws within the material distribution was shown. In those approaches, the flaw-size distribution was inferred from the measured strengths. However, Chao and Shetty (1992) and Burchell (1986, 1996), developed the opposite approach whereby they physically measured flaw sizes from micrographs, established an appropriate flaw-size distribution function that fit the data, and then predicted the strength distribution of components. Chao and Shetty's model was developed for a porous silicon nitride and is not described herein. The Burchell model was developed specifically for graphite and is described in Section 2.1.6.

2.1.5 Ho's Modified Weibull Distribution, Schmidt's Rule, and Strain-Softening Regarding the Size Effect

Ho (1979) introduced a correction factor to the Weibull scale parameter to empirically account for the effect of grain size relative to tensile specimen dimension for nuclear-grade graphite. In Ho's relation, specimen dimensions on the order of the grain size weaken the specimen. The correction factor was introduced because small-size tensile specimens were often observed to be weaker than larger-size specimens—contrary to the expectation based on the Weibull theory (see Strizak (1991) and Brocklehurst (1977), e.g., Figure 8). For instance, H–451 grade graphite has a mean grain size of 1.6 mm, so a 16-mm-diameter tensile specimen is only 10 times this size. In Strizak (1991), tensile specimen diameters between 6 and 25 mm were studied, raising concern about the effectiveness of the study regarding comparison to the expected Weibull size effect. In Ho's relation the Weibull scale parameter is modified by

$$P_{fV} = 1 - \exp\left[-V \left(\frac{\sigma}{\sigma_{oV} f\left(h_o, d\right)} \right)^{m_V} \right]$$

$$f\left(h_o, d\right) = \frac{2}{\pi} \cos^{-1}\left(\frac{h_o}{d} \right) \tag{26}$$

where h_o is the characteristic grain size and d is the diameter of the specimen. Tucker et al. (1986) explained that strength falls off with small diameter because the characteristic flaw size (related to grain size) penetrates a greater fraction of the specimen diameter.

In Schmidt (2000, 2003) the Weibull distribution was modified to eliminate the size-effect scaling of the specimen size but preserve the scaling effects of the stress gradient. This was developed to empirically fit to data from graphite-rupture experiments that did not correlate well to the traditional Weibull distribution. The equation is expressed as

$$P_f = 1 - \exp\left\{ -\left(\frac{\sigma_{e,f}}{\sigma_{\theta(\text{tensile specimen})}} \right)^m \left[\int_V \left(\frac{\sigma_e(x,y,z)}{\sigma_{e,f}} \right)^m \frac{dV}{V_{\text{tot}}} \right] \right\} \tag{27}$$

where $\sigma_{\theta(\text{tensile specimen})}$ is the characteristic strength of a reference tensile specimen (the strength of the specimen at $P_f = 0.6321$—not normalized to the volume), V_{tot} is the total volume of the component for which failure probability is to be predicted, σ_e is an effective stress for multiaxial stresses, $\sigma_{e,f}$ is the peak effective stress in the component, and $\sigma(x, y, z)$ is the stress at location x, y, z in the component. The effective stress is computed from the maximum deformation theory (MDE), which is based on the hypothesis that the elastic energy per unit volume that is stored in a given material element at the moment of fracture is equal to the energy that is stored in the uniaxial loaded test specimen at fracture as described in Schmidt (2000).

Schmidt (2000) contends that multiaxial experiments on graphite show that the criterion of the maximum strain energy (of which MDE is a variant) does not describe the experimental results exactly

but is better than other traditional criteria and has sufficient accuracy. The MDE criterion is not descriptive of the physical processes of converting elastic energy to microcrack progression and coalescence. Then again, none of the multiaxial theories described herein can describe the unique qualities of graphite damage accumulation and failure completely, although the Batdorf theory probably comes the closest.

The Schmidt modified Weibull methodology works for uniform uniaxial tensile specimens and flexure specimens. The effective volume (the term in square brackets […] in Equation (27)) is normalized by the volume of the component V_{tot} such that proportionally scaling the component dimension does not change the value in the square brackets, thereby leaving failure probability constant with specimen size. However, failure probability will differ depending on if the component is under uniform uniaxial tension or loaded such that a stress gradient exists. A scenario where Equation (27) fails, for example, is with a notched tensile rod (that has a finite fillet radius at the notch tip to avoid a stress singularity condition yet still be a region of high stress concentration). If the specimen diameter and notch geometry are kept constant, but the length of the specimen changes, then the probability of failure changes according to Equation (27). That result is not consistent since failure will be controlled only by the stress concentration at the notch root, and the length of the specimen is irrelevant. Nevertheless, Equation (27) is a useful attempt to preserve the strength size effect for the stress gradient while eliminating it for size scaling—and it works at least for certain controlled situations.

Li and Fok (2009) modeled nonlinear stress-strain behavior in graphite and posit that the difference in strength and Weibull modulus between tension and bending load is due to the strain-softening behavior of quasi-brittle materials. Their model offers an alternative to the Schmidt model to account for the difference in strength between bending and tension while also eliminating size effect with increasing specimen size. Li and Fok (2009) cite work from previous authors who modeled strain-softening and predicted a nonstochastic difference in strength between flexural loading (a situation where a stress gradient is present) and tensile loading but they base their approach on the work of Bazant and Li (1995). Nonlinear stress-strain behavior is modeled as a combination of linear increase of stress with increasing strain up to a critical strain threshold, and beyond that threshold, the stress decreases with increasing strain until the ultimate strain at failure is reached. The effect of this behavior is that the strain-softening (attributed to damage accumulation) requires higher load to fail a beam in bending than would be required with a purely linear-elastic material response. If the quasi-brittle material were analyzed as though it was linear elastic in behavior, it would appear that the material in bending was stronger than the material in pure tension.

In the Li and Fok model, the critical strain is modeled with a Weibull distribution with the additional result that the Weibull modulus in bending would appear to be higher than the Weibull modulus in tension. Their model highlights the need to properly account for nonlinear stress-strain behavior in any analysis. It should be noted that the Li and Fok model did not indicate a size effect for increasingly larger specimens because the Weibull distribution for critical strain was not made a function of material volume. Note that there is evidence in the literature, at least for flexural loading, that strength does decrease with increasing specimen size (e.g., see Figure 8(a)).

A further item worth noting regarding the Li and Fok model is that, for the limiting case of a linear-elastic brittle material, there is no difference in strength between flexure and tension since the failure criterion is simply a deterministic value of ultimate strain. For classically brittle materials like ceramics, where the size of preexisting critical flaws controls the strength response, there is clearly a difference in strength between flexural and tensile loading as explained through the Weibull distribution. The Li and Fok model assumes that graphite has no sensitivity to preexisting flaws. If larger sized preexisting flaws are present in the material, then the strength response will be governed by the size distribution of the critical flaws and not solely by a critical strain. Their model also did not consider that graphite has bimodulus behavior—where the stress-strain behavior is different in tension and compression. In their model, the material response is initially linear elastic until the critical strain threshold is reached (somewhere in the neighborhood of the value of the ultimate failure strain).

For graphite the stress-strain response may be nonlinear from the very onset of loading or at relatively low loading levels (e.g., see Figure 5). The Li and Fok model predicts that the ratio of flexural strength to tensile strength increases as the ratio of ultimate strain to critical strain increases. With regard to the assumption that failure strain is a material constant that does not change in flexure or tension, Figure 7 shows that the failure strains in four-point flexure and tension are within about 10 percent of one another, although it is not clear if this difference is statistically significant. Figure 7 also shows that the scatter in the failure strain may also need to be accounted for in modeling. Lastly, a failure criterion based on a critical strain criterion will give significantly different results in comparison to stress-based failure criteria for multiaxial loading. For example, equibiaxial loading strength will be predicted to be higher for strain-based criteria than for stress-based criteria because of the Poisson effect.

2.1.6 Graphite Microstructure Specific—The Burchell Model

The Burchell model (Burchell 1986, 1996, 1999; Burchell et al. 2006), which was developed specifically for graphite, combines fracture mechanics with a physics-based microstructural description of graphite failure. It directly incorporates specific graphite features such as the grain size, pore size, pore distribution, particle fracture toughness, graphite density, and specimen size (size effect) into the model. Tucker and McLachlan (1993) further refined this model primarily to account for strain hysteresis and acoustic emission. However, the Tucker and McLachlan model, though it may provide an improved physical basis, requires data for 14 different input parameters, which makes its use cumbersome. Although these parameters were initially based on measured parameters, they were subsequently altered to best fit the experimental results presented in their journal article. The Tucker-McLachlan model appears to be best suited for explaining the mechanisms of fracture in graphite; it is not necessarily well suited as an engineering tool for designing a structure. In this section, the discussion focuses on the Burchell model and its description of fracture.

The Burchell model is a refinement or variant of the Rose-Tucker model (Rose and Tucker (1982) and Tucker et al. (1986)), which itself is a refinement of a model proposed by Buch (1976). In the Rose-Tucker model, individual graphite grains are assumed to be cubes of the dimension of the average particle size. The structure is composed of these grain-cubes stacked together with the layers perpendicular to the local stress field (see Figure 17(c)). Each grain in the structure has a randomly oriented cleavage plane as shown in Figure 17(a). Failure in a grain is assumed to have occurred when the tensile stress component (from the far-field applied stress) normal to the crystallite cleavage plane exceeds a critical value (assumed to be a deterministic value). The probability of failure of each grain under the applied stress is equal to the fraction of possible orientations for which cleavage would occur. Note that this is equivalent to calculating P_2 in Equations (15) and (18) in the Batdorf methodology. Porosity is considered by making an appropriate fraction of grains have zero strength; however, the stress-raising properties of pores on the grains in the immediate vicinity of pores is not considered. The probability of specimen failure is the probability of a layer having sufficient contiguous failed grains equivalent in size to a single crack whose stress intensity factor exceeds the material K_{Ic} (shown in Figure 17 parts (b) and (c)).

In the Burchell model, fracture is assumed to initiate at or very near pores—which are stress concentrators. The distribution of pore sizes is modeled as a lognormal distribution (measured from micrographs). Crack growth extends from the pores through individual particulates. Similar to Rose-Tucker, the particulates are modeled as an array of cubic particles of size equal to the mean filler particle size. Each particulate cube has a random crystalline orientation. Figure 18 is a schematic of this idealization. Fracture initiates at or very near pores, and crack growth proceeds through the individual particulates along their cleavage planes when stress in the particulate exceeds a critical value (the fracture strength of the cleavage plane). Crack growth proceeds through each row of particulate blocks as shown in Figure 19 until overall crack length equals or exceeds K_{Ic}. Therefore, in the Burchell model two stochastic quantities are involved: the distribution of pore sizes and the random orientation of cleavage planes in individual particulates. Further details regarding the development of the Burchell model follow.

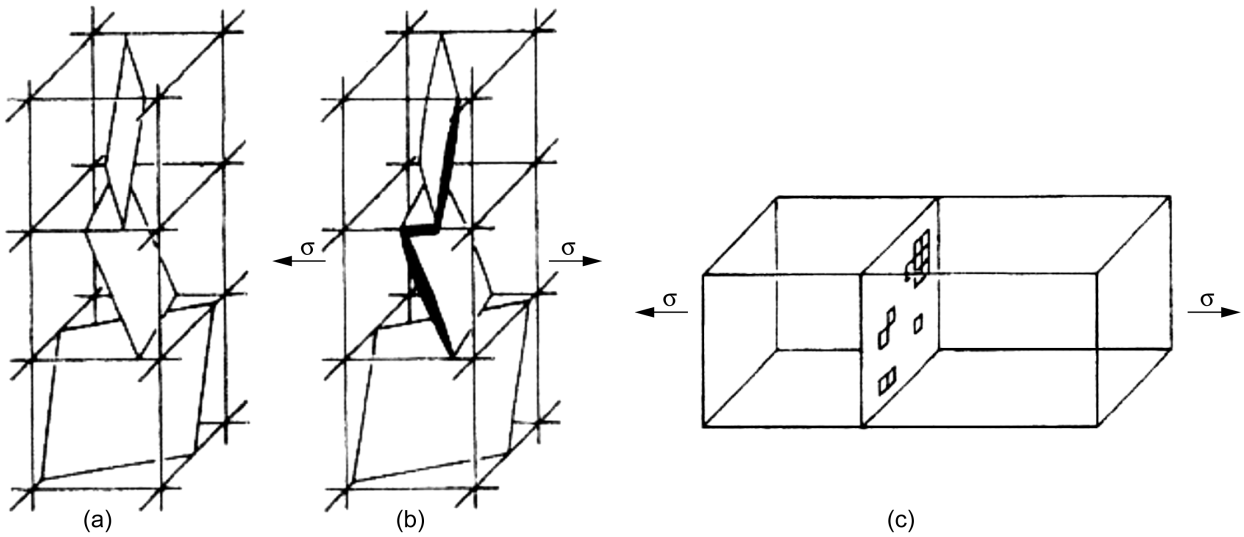

Figure 17.—Failure in graphite assumed cube-shaped grains, where σ is the critical strength. (a) Cleavage planes randomly oriented for each grain. (b) Adjacent failed grains forming a contiguous crack. (c) Cross section of failed grains normal to the applied stress. Reproduced from Tucker et al. (1986). Copyright Elsevier; used with permission.

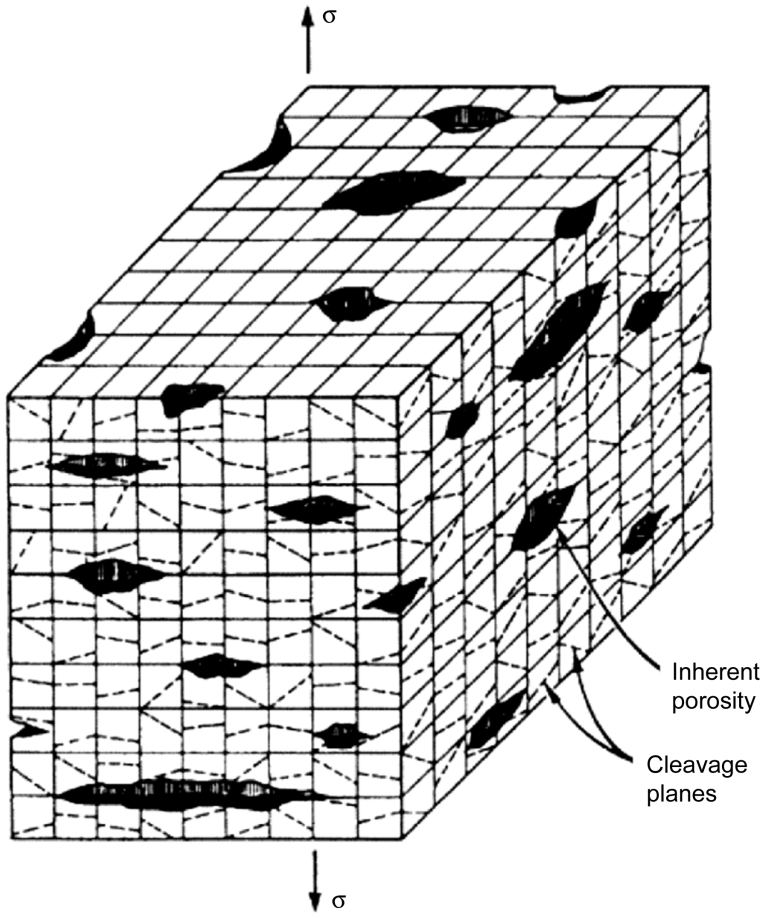

Figure 18.—Burchell's idealized model of graphite, where σ is the applied stress. Reproduced from Burchell (1996). Copyright Elsevier; used with permission.

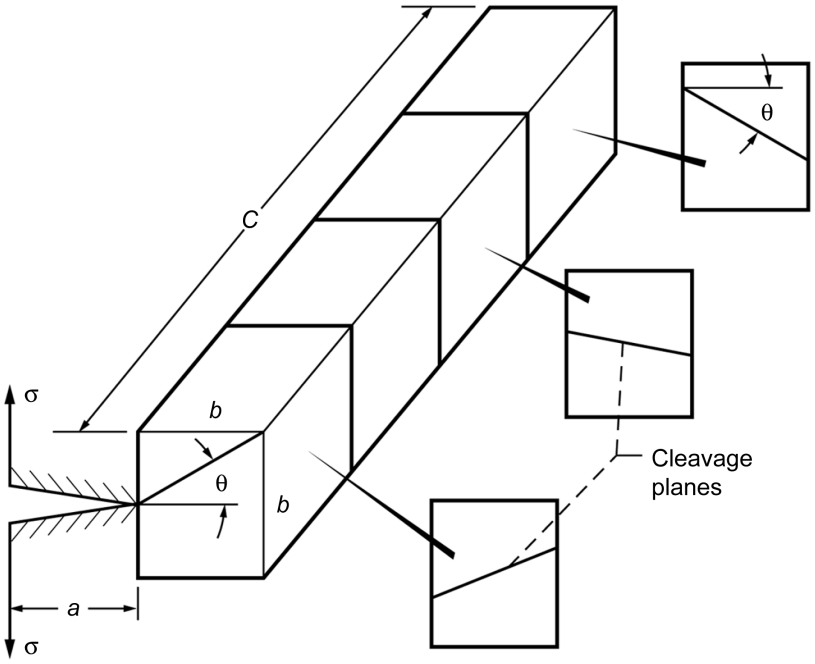

Figure 19.—Crack front originating from a pore proceeds through a row of particulates—adding the particulate width to the overall length of the crack, where σ is the applied stress. Reproduced from Burchell (1996). Copyright Elsevier; used with permission.

The graphite grain consists of parallel hexagonal planes with weak van der Waals bonding between the planes and strong covalent bonding within planes (as described in Greenstreet (1968)). Because of this granular anisotropy, fracture within the grain is preferentially oriented along the c-axial direction. If one assumes that fracture is transgranular, the probability of failure of an individual graphite grain *i* ahead of a crack tip and oriented at an angle θ to it is given by

$$P_{fi}(\sigma,a)=\frac{4}{\pi}\cos^{-1}\left(\frac{K_{Ic}}{\sigma\sqrt{\pi a}}\right)^{1/3} \tag{28}$$

where K_{Ic} is the grain fracture toughness, a is the crack size, and σ is the remote applied tensile stress. If there are n_g grains in an entire row ahead of the crack tip, the probability that they will all fail is

$$P_{fn_g}(\sigma,a)=\left[\frac{4}{\pi}\cos^{-1}\left(\frac{K_{Ic}}{\sigma\sqrt{\pi a}}\right)^{1/3}\right]^{n_g} \tag{29}$$

Equation (29) assumes that the crack will extend from length a to $a + b$, where b is the average graphite grain size. The probability that the crack will extend from a to $a + jb$, fracturing j rows of grains, may be approximated by

$$\ln\left[P_{fn_g}(\sigma,a)\right]=n_g\int_0^j\ln\left[\frac{4}{\pi}\cos^{-1}\left(\frac{K_{Ic}}{\sigma\sqrt{\pi(a+jb)}}\right)^{1/3}\right]dj \tag{30}$$

If one assumes that the graphite microstructure contains a lognormal distribution of pores, then the probability that the length of a specific defect will fall between a and $(a + d)$ is $S(a)\,da$, with $S(a)$ defined as

$$S(a) = \mathrm{c}\left\{\exp\left[-\frac{1}{2}\left(\frac{\ln 2a - \ln S_{\mu}}{\ln S_d}\right)^2\right]\right\} \tag{31}$$

where c is a constant, S_{μ} is the mean pore size, and S_d describes the scatter in the pore distribution (similar to standard deviation). When N is the number of pores per unit volume, and V is the specimen volume under uniform tensile stress σ and the number of crack tips under stress is $2NV$, then the probability of failure for the entire specimen is given by

$$P_f = 1 - \left[1 - \int_0^{\infty} S(a)\; P_{fn_g}\left(\sigma, a\right) da\right]^{2NV} \tag{32}$$

As can be seen, Equation (32) is derived to describe P_f for specimens subjected to uniaxial, uniform tensile stress state due to volume-residing defects.

Equation (32) is a WLT model. This can be shown by analogy from Chao and Shetty (1992), Epstein (1948), and Shih (1980). For a uniformly stressed body that contains N flaws per unit volume, fracture will occur within that unit volume at a stress level corresponding to the weakest strength among those N flaws. Thus, the cumulative failure probability distribution for N flaws, where each flaw is exposed to a tensile stress of magnitude σ, is

$$P_f = 1 - \left[1 - P\left(\sigma_{\mathrm{I}c} \le \sigma\right)\right]^{NV} \tag{33}$$

where $P(\sigma_{\mathrm{I}c} \le \sigma)$ is the probability that a given flaw will fail at a stress level of σ or less than σ, or the probability that the strength of the flaw, denoted by $\sigma_{\mathrm{I}c}$, is at a stress level of σ or less than σ. For large values of N, this equation is approximated by

$$P_f \approx 1 - \exp\left[-NV\,P\left(\sigma_{\mathrm{I}c} \le \sigma\right)\right] \tag{34}$$

When comparing Equation (32) for the Burchell model and Equation (33)—a WLT model of individual flaws—it is clear that they have the same functional form. Analogous to Equation (34), the Burchell model, therefore, could also be expressed as

$$P_f \approx 1 - \exp\left[-2NV \int_0^{\infty} S(a)\; P_{fn_g}\left(\sigma, a\right) da\right] \tag{35}$$

and would show a size effect consistent with the WLT model.

An interesting feature of the Burchell model is that transgranular fracture is modeled somewhat similar as by Planas (1995) and Bazant and Planas (1998), who describe the statistical R-curve. Indeed in Burchell (1996) and Burchell et al. (2006), the R-curve effect can be seen for initial versus final critical crack size for H–451 graphite (Figure 20). Therefore, the Burchell model explicitly models a statistical R-curve and consequently predicts acoustic emission prior to catastrophic failure.

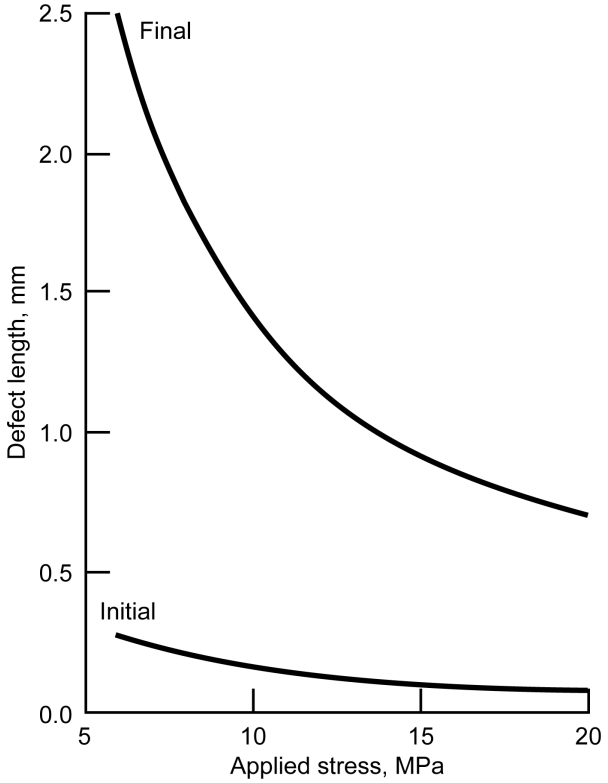

Figure 20.—Initial defect length and final crack length at failure calculated with the Burchell model for H–451 graphite. Reproduced from Burchell (1996). Copyright Elsevier; used with permission.

Ishihara et al. (2001) used Burchell's model to account for stress gradients by assuming small uniformly stressed incremental volumes, which is the WLT assumption of Equation (1). Predictions made using the Burchell and Weibull models showed only minor differences when they were compared with experimental results for H–451 graphite data. The effect of multiaxial stresses and anisotropic strength also was considered in Burchell et al. (2006), who used a PIA-style approach, and more recently by Battiste et al. (2010), who used the Shetty (1987) mixed-mode interaction equation.

2.1.7 The Uniform Defect Model

The uniform defect model is interesting because a probabilistic relation is developed for a critical density of number of defects as a failure criterion. Since load redistribution is not involved, this model is not a parallel model. The WLT analogy is the occurrence of a critical density of defects under a specified load causing catastrophic rupture. Freudenthal (1968) assumed that inhomogeneities are uniformly distributed over the volume of a material body and developed a fracture model where the occurrence of a critical number of defects within a confined volume gives rise to a statistical aspect of fracture as well as a size effect.

Freudenthal assumed that a Poisson process governed the general equation for the probability of occurrence of k inhomogeneities in the volume V. The Poisson density function is described by (e.g., see Hoel et al. (1971))

$$P(X=x)=f(x)=\begin{cases}\dfrac{\lambda^{x}\exp(-\lambda)}{x!} & x=0,1,2,\ldots\\ 0 & \text{elsewhere}\end{cases} \tag{36}$$

where λ is a positive number. The real-valued function $f(x)$ is the discrete density function of random variable X where $P(X = x)$ is the probability that a discrete real-valued random variable X equals a possible value x. The Poisson distribution approximates the binomial distribution for large values of n, where n is the number of Bernoulli trials with success probability $P_{event} = \lambda/n$ at each trial. When $P(X = 0)$ is computed for $n = V$ and $P_{event} = c_\mu$, then

$$P(X=0)=\frac{\lambda^0 \exp(-\lambda)}{0!}=\exp(-\lambda)=\exp\left[-c_\mu V\right] \tag{37}$$

where c_μ, which has dimension of V^{-1}, denotes the mean concentration of inhomogeneities. When $c_\mu = \eta_V(\sigma)$ is substituted from Equation (7), the Weibull equation is obtained in Equation (37). This represents the probability of zero defects occurring within volume V, which also represents the survival probability of the material under WLT. For the probability of occurrence of k inhomogeneities in the volume V,

$$P(X=k)=\frac{1}{k!}\left(c_\mu V\right)^k \exp\left[-c_\mu V\right] \tag{38}$$

If the probability of fracture is identified with the probability of occurrence of at least n inhomogeneities, then the probability of survival is the probability of occurrence of less than n inhomogeneities, which is identical to the sum of the probabilities of occurrence of from zero to $(n - 1)$ inhomogeneities

$$P_{sV}=\exp\left[-c_\mu V\right]\sum_{k=0}^{n-1}\frac{c_\mu V^k}{k!} \tag{39}$$

and therefore

$$P_{fV}=\exp\left[-c_\mu V\right]\sum_{n}^{\infty}\frac{c_\mu V^k}{k!} \tag{40}$$

The probability density function of Equation (40) is a gamma distribution. Freudenthal further shows that

$$P_{fV}=1-\frac{\left[\Gamma(n+1)-\Gamma(c_\mu V,n+1)\right]}{\Gamma(n+1)} \tag{41}$$

Since c_μ is the mean concentration of inhomogeneities per a specified volume, the effect of the volume ratio $c_\mu V$ can be examined. As Freudenthal reports for $c_\mu V = 1, 10, 100$, the values of P_{fV} are 0.190, 0.990, and 1.000 for $n = 3$, and 0.000, 0.411, and 1.000 for $n = 10$, respectively. Clearly a size effect is predicted with this model. Freudenthal further notes that the effect of stress could be introduced by assuming that the critical number of inhomogeneities required for fracture increases as the applied stress decreases. For example $n = n_o\sigma_{con}/\sigma$, where n_o and σ_{con} are material constants. Appendix A shows an argument that the uniform defect model can be approximated with a Weibull distribution, which might be appropriate to describe the strength distribution for compressive stress states.

2.2 Parallel Systems

Nuclear graphite exhibits distributed and accumulated damage (as indicated by acoustic emission) and nonlinear stress-strain response. As previously described, under the action of a monotonically

increasing progressive load, microcracks form and arrest, leading to load redistribution and the formation of new microcracks. Eventually, a local concentration of microcracks develops and coalesces to form an unstable macrocrack of critical size. The Burchell model and the Weibull model with R-curve behavior (e.g., Danzer et al. (2007) and Munz (2007)) do not account for these interactive effects of microcracking. They are weakest-link series-system models, whereby the material is assumed to be composed of a set of n links connected in series in such a manner that the structure fails whenever any of the links fail.

Because of the interactive nature of microcrack formation, load redistribution, and microcrack coalescence, it may be more appropriate to consider graphite material failure in terms of a parallel-system analog. Recall that in the parallel-system model, the n links are arranged in parallel. When one link fails, load is redistributed to the remaining $n - 1$ links. The remaining $n - 1$ links carry higher load, but the system (structure) may still survive. The structure does not fail until all n links fail. This line of inquiry leads to consideration of models that describe the failure of other quasi-brittle materials, such as fiber-reinforced composite materials and lattice system models, which describe the process of material break-down in terms of connected beams, springs, bonds, or fuses. Fiber-bundle models and lattice models study the process of damage initiation, damage accumulation, damage clustering, and system instability leading to ultimate failure relative to the initial state of disorder within the material. Lattice models more closely approximate the structural features of graphite.

Fiber-reinforced composite materials and graphite bear no outward resemblance to one another; however, their processes of progressive damage leading to failure do resemble each other—at least at a generalized mathematical level. Phoenix and Beyerlein (2000b) have commented on the similarity between composite fiber-bundle models and lattice models, and an extensive body of knowledge has been developed regarding modeling the failure strength distribution of fiber-reinforced composite materials. The authors of this report believe that this body of work has relevance and is worth reviewing. Graphite failure behavior likely ranges between that of classically brittle materials and the damage-tolerant behavior of composite materials. Therefore, exploring the implications of the behaviors displayed between classically brittle materials and quasi-brittle materials, such as fiber-reinforced composites, should provide useful perspective with regard to further development of appropriate graphite failure strength models.

Fiber-reinforced composite materials are typically engineered to fail in a damage-tolerant manner. That is, the material system is designed so that failure in a single fiber will redistribute the load such that the remaining fibers will not (in most cases) fail unless the load is sufficiently increased. Therefore, a composite will have significant damage accumulation and a nonlinear stress-strain response prior to ultimate structural failure. Similar to graphite, localized failure is arrested and (both local and global) stresses can redistribute. Subsequent material failure would involve accumulated damage either over the entire material cross section or localized material damage that reaches a critical size or density within a critical volume. The strength distribution of the individual fibers and the load transfer that takes place both locally and globally at the site of broken fibers influences the damage accumulation and ultimate fracture behavior of the composite; thus, fracture behavior can range from brittle (with little distributed damage) to quasi-brittle (with significant distributed damage).

Lattice models are a closer analog to graphite. In a lattice model a material such as graphite is represented as a network of elastic beams, springs, bonds, or electrical fuses with individual random failure thresholds. The individual discrete elements of the lattice simulate local inhomogeneities of mechanical properties, such as strength, within the material. Depending on the strength distribution of the individual elements, brittle fracture behavior or quasi-brittle distributed damage behavior can be simulated.

Sections 2.2.1 to 2.3.3 provide an overview of some of the work that has been done modeling and simulating the failure of unidirectional continuous-fiber-reinforced composites and lattice models under progressive uniaxial tensile loading. These models predict the consequences of distributed damage, load redistribution, and damage coalescence on the strength of a structure. Fiber-reinforced composite models are shown because the mathematical framework is more developed than for the lattice models of homo-geneous materials. As pointed out in Phoenix and Beyerlein (2000b), the severe computational demands

have limited the network sizes that can be investigated with lattice simulations, whereas composite fiber-bundle models in one dimension can be solved exactly or asymptotically for increasing size scale. Emphasis is placed on describing the consequences of these models on the distribution of strength, the size effect, and the role of system disorder on the brittle-to-ductile (ductile-like) transition.

Sections 2.2.1 to 2.3.3 highlight the implications of local versus global load sharing, a WLT mechanism for composite materials, asymptotic Weibull behavior for composite materials, the Watson-Smith modified Weibull relation, extreme-value implications from the presence of large flaws in lattice models, and the implications of the brittle-to-ductile-like transition for both composite and lattice models. Unidirectional fiber-reinforced composite models are described first, followed by lattice models. In these sections, the evidence or the basis for using WLT and the Weibull distribution is presented. It is also noteworthy that other researchers such as Wetherhold (1983) and Duffy et al. (1993) have advocated the use of the Weibull distribution for the design of polymer matrix and ceramic matrix composite structures.

Phoenix and Beyerlein (2000a) give an authoritative overview of statistical strength theories for unidirectional fiber-reinforced composite materials under tension. Alava et al. (2006) also provide an excellent summary of statistical strength theories for material systems (homogeneous and heterogeneous) but are focused more toward lattice models. Mahesh and Phoenix (2004) and Phoenix and Beyerlein (2000b) provide useful perspective and further details. The following overview only touches upon the extensive body of work that has been performed regarding parallel system modeling.

2.2.1 Two Composite Material Failure Modes

The continuous-fiber-reinforced composite described here is a heterogeneous material consisting of unidirectional fibers embedded in a matrix material. The matrix usually does not carry load but does transfer load to the fiber. Failure of the composite involves reaching a critical level of damage accumulation of broken fiber segments.

The failure of composite materials falls between two distinct extremes: dispersed failure and localized failure. In dispersed failure, the fibers fail in a dispersed manner until the load exceeds the material's capacity to support load. The fracture surface of the composite appears to be brushlike. This failure mode is associated with things like a weak interface between the fiber and matrix, a matrix with a low yield strength compared with stiffness, or fibers with a large variability in strength. In localized failure, fracture initiates and coalesces around local clusters of fibers. This is due to the stress concentration in the immediate vicinity of fiber breaks. In this failure mode, the fiber-matrix interface is usually strong, the matrix less plastic, and/or there is lower variability in fiber strength. See Phoenix and Beyerlein (2000a) for further details.

2.2.2 Equal-Load-Sharing and Local-Load-Sharing Fiber-Bundle Models

Fiber-bundle models fall into two classes: equal load sharing (ELS) and local load sharing (LLS). In the ELS model, the fiber bundles do not interact with one another (whether they are loose or embedded in a matrix material). When a fiber fails, the load is equally distributed to all the remaining fibers. In the LLS model, the fibers are embedded in a matrix and do interact with one another. If a fiber fails, adjacent local fibers will carry an increased load and have an increased risk of failure. Breaking of a critical number of local fibers causes an instability point to be reached, resulting in a cascade of fiber failures until the whole composite catastrophically fails. Consequently, LLS shows more localized breakdown and flaw sensitivity, whereas ELS has a more dispersed fiber-failure character. ELS and LLS models predict different consequences with regard to strength distribution and size effect, which are discussed next. ELS and LLS models are complex and not easily amenable to closed-form solutions. Typically, they are studied through computer simulations or determination of asymptotic behaviors (e.g., for large numbers of fibers or for low probabilities of failure). Also LLS models can have many variations depending on load-sharing rules, two-dimensional versus three-dimensional analysis, and fiber-packing arrangement. Although composite modeling and simulation is complex, important insights and generalizations have been achieved. Sections 2.2.3 to 2.2.6 describe some of this work.

2.2.3 Daniels's Equal-Load-Sharing Bundle Model

Peirce (1926) and Daniels (1945) were the first to model the failure of fiber bundles. In the bundle model, a structure is viewed as a bundle of parallel fibers of equal length and cross section. Each fiber is assumed to be governed by weakest-link strength (typically the Weibull distribution). Under a uniform load, failure of a single fiber redistributes load in the remaining fibers, which does not necessarily lead to structural failure (i.e., failure of all the fibers). The fracture strength of the "dry" bundle model (where the bundle is a loose collection of fibers) is determined by the forces under which a "chain reaction" process of consecutive filament failures occurs from the progressive overload carried by the surviving filaments. This ultimately leads to the final failure of all filaments. The fracture process starts at the weakest point in the bundle, but contrary to the WLT model, the bundle does not fail unless the load is increased sufficiently. A single fiber can cause the bundle to fail if the filaments are arranged in the order of their consecutive failure, which is unlikely.

The fiber-bundle model, which was derived in Daniels's (1945) classical paper, assumed an ELS rule, whereby the surviving fibers share the applied load equally. For a bundle of n_f filaments, where n_f is large, Daniels showed that the probability distribution of strength tends to a normal distribution, the average strength is independent of n_f, and the variance is an inverse function of n_f and thus tends toward zero for very large n_f. There is no size effect for this model of asymptotic behavior.

For fiber strength (load per fiber) distributed according to $P(x)$ such that $\lim_{x\to\infty} x[1 - P(x)] = 0$, then the strength of the fiber bundle (expressed as load per fiber) is normal with a mean of

$$\sigma_\mu = x^*\left[1 - P\left(x^*\right)\right] \tag{42}$$

and a standard deviation of

$$\sigma_{sd} = \frac{\sqrt{P\left(x^*\right)\left[1 - P\left(x^*\right)\right]}}{\sqrt{n_f}} \tag{43}$$

where x^* is the point where the function $x^*[1 - P(x^*)]$ is maximum. For Weibull-behaved fibers, the Daniels model shows that the bundle ultimate strength is

$$\sigma_\mu = \sigma_o \left(\frac{1}{m}\right)^{1/m} \exp\left(-\frac{1}{m}\right) \tag{44}$$

and the standard deviation is

$$\sigma_{sd} = \frac{\sigma_o \left(\frac{1}{m}\right)^{1/m} \sqrt{\left[\exp\left(-\frac{1}{m}\right) - \exp\left(-\frac{2}{m}\right)\right]}}{\sqrt{n_f}} \tag{45}$$

2.2.4 Chain of Equal-Load-Sharing Bundles

Gücer and Gurland (1962) (see also Smith and Phoenix (1981) and Coleman (1957)) proposed the chain of ELS bundles model, and Rosen (1964) and Scop and Argon (1967) applied it to fibrous composites. "Chain of bundles" refers to the fact that a broken fiber in a matrix will carry load a certain distance away from the break—the "ineffective length," or "stress transfer length"—and the composite is treated as a serial arrangement of independent bundles, each of length 2δ (usually a few fiber diameters), which is shown schematically in Figure 21.

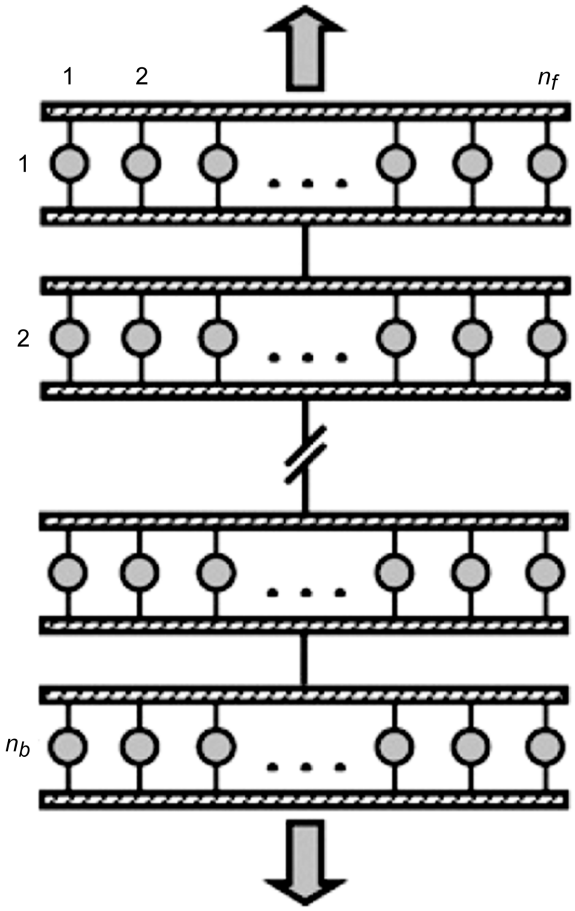

Figure 21.—Schematic of chain of bundles, where n_f is the number of fibers and n_b is the number of bundles. Reproduced from Bazant and Pang (2007). Copyright Elsevier; used with permission.

Therefore, a composite of length L composed of n_f fibers can be represented as a chain (a series) of $n_b = L/(2\delta)$ mutually exclusive, but linked, bundles. The chain of bundles has a WLT failure mechanism controlled by the weakest bundle, but each fiber bundle behaves as an independent ELS (or LLS) system; that is,

$$H_{n_f,n_b}(x) = 1 - \left[1 - G_{n_f}(x)\right]^{n_b} \tag{46}$$

where $H_{n_f,n_b}(x)$ is the composite strength distribution, $G_{n_f}(x)$ is the bundle strength distribution, and x is the load per fiber. Equation (46) implies that composite strength is determined solely from the statistical mechanics of the individual bundle: that is, from the load-sharing scheme and the strength distribution for individual fibers. Smith (1982) improved the accuracy of the model for smaller n_f and

showed that, when n_f is small and n_b is large, asymptotic Weibull behavior is obtained. For the strength distribution for moderate to large n_f and n_b, Smith (1982) showed that the Gumbel extreme-value distribution (based on a normal distribution for link strength) is obtained. For ELS bundles with small n_f, a size effect is present (Smith and Phoenix (1981) and Phoenix et al. (1997)), but this decreases with increasing n_f since strength dispersion decreases as $1/\sqrt{n_f}$. This is true regardless of fiber length L.

2.2.5 Local-Load-Sharing Modeling

Bundle models have been proposed with LLS rules whereby stress is concentrated in the immediate vicinity of failed fibers. Several variations of LLS modeling for two- and three-dimensional unidirectional composites are summarized in Phoenix and Beyerlein (2000a) along with appropriate references. In LLS models the fibers are embedded in a matrix. The fibers interact, and a critical number of breaks in a localized region induce a catastrophic cascade of fiber failure across the bundle, resulting in total failure. Many factors can influence LLS modeling, including the variability of fiber strength, the yield strength of the matrix in shear, the friction at the fiber-matrix interface after debonding, the geometrical distribution of fibers, and the rules used to define material failure. These factors make the modeling algorithms and analytical effort difficult.

A size effect exists for LLS, but it is always less pronounced than for a single fiber that is modeled with the Weibull distribution. Zweben and Rosen's (1970) model prescribed composite failure as the occurrence of at least one cluster of failed fibers of a specified size. Harlow and Phoenix (1978a,b; 1981a,b), Batdorf and Ghaffarian (1982), and Smith et al. (1983) extended the failure criterion to consider the probabilities of growing clusters up to instability. Smith (1979, 1980) indicated that, for a chain of bundles where k consecutive (adjacent) fiber failures within a single bundle defines failure, the composite strength for large system size n_{sys} is proportional to $\sigma_f \propto c \cdot n_{sys}^{-1/km}$, where σ_f is the failure stress, n_{sys} is the product of n_f and n_b, m is the fiber Weibull modulus, c is a constant, and k is a constant argued to be between 2 and 4. The system size n_{sys} is proportional to volume and, therefore, follows the size-effect relation described in Equation (12) but with the modified Weibull modulus of km instead of m for the uniformly stressed volumes V_1 and V_2. This indicates that the composite size effect is less than that for the single fibers under LLS. Smith (1980) conjectured that the standard deviation of strength was $\sigma_{sd} = c/\ln(n_{sys})$. This compares with Daniels (1945), where ELS indicated that the standard deviation is related by $n_f^{-1/2}$. Therefore as the system size increases, the standard deviation decreases under both ELS and LLS. In their analysis, Harlow and Phoenix (1978a,b; 1981a,b) indicated that scatter in strength decreases with volume.

Batdorf (1982) and Batdorf and Ghaffarian (1982, 1984) simplified concepts from Harlow and Phoenix (1978a,b; 1981a,b) and modeled the formation and growth of multiple fiber fractures as the basis of their failure criterion. In their model the Weibull relation for single fiber strength is used to determine the number of critical fiber fractures (singlets), double adjacent fractures (doublets), triple adjacent fractures (triplets), and so on as a function of stress and volume. They constructed a failure envelope of "multiplets" consisting of line segments with slope $1/(im)$ where i is an integer multiple of the fiber Weibull modulus corresponding to the i^{th} multiplet where i fibers form a critical cluster of failed fibers. This analysis was based on a Griffith-type instability showing an inverse relationship between crack size (number of adjacent fiber breaks) and failure stress. In Batdorf and Ghaffarian's theory of multiplets, the size effect is the same as in Equation (12) except with a modified Weibull slope of $1/m^*$, where $1/m^*$ is the local slope of the failure line as shown in Figure 22. As seen in the figure, the size effect is no longer linear with the log of σ_f (it is piece-wise Weibull, but overall it is non-Weibull), and it decreases with increasing volume.

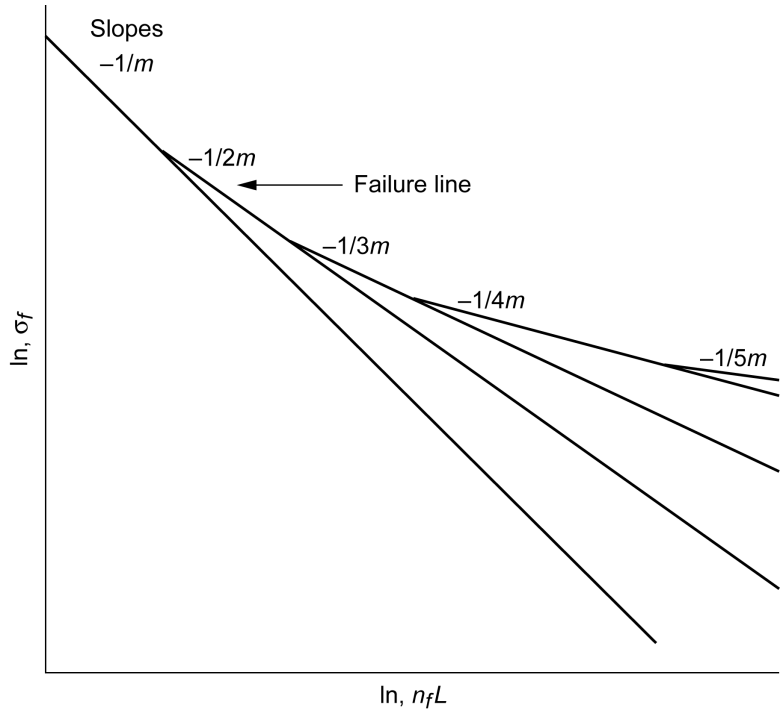

Figure 22.—Failure envelope for composite strength versus volume, where m is the Weibull modulus, σ_f is the failure stress, and n_f is the number of fibers of length L in the composite. Note that the product of $n_f L$ is proportional to the composite volume. Reproduced from Batdorf, S.B.; and Ghaffarian, Reza; 1984: Size effect and Strength Variability of Unidirectional Composites. Int. J. Fracture, vol. 26, no. 2, Fig. 1, p. 115. Copyright Springer Publishing Company; used with kind permission from Springer Science + Business Media B.V.

2.2.6 Weakest-Link Relation for Composite Materials

Harlow and Phoenix (1978b) found that an LLS fiber bundle follows the WLT scaling law for number of fibers n_f under certain conditions. This was proved rigorously by Kuo and Phoenix (1987) and other authors have contributed to this development (see Mahesh and Phoenix (2004)). The Harlow and Phoenix (1978b) model was for a two-dimensional arrangement of fibers assuming simplified load-sharing rules. For $G_{n_f}(x)$, the probability strength distribution for a fiber bundle of size n_f, they found asymptotically that there is a WLT characteristic probability distribution $W(x)$ independent of n_f such that

$$G_{n_f}(x) \cong 1 - \left[1 - W(x)\right]^{n_f} \quad \text{as} \quad n_f \to \infty \tag{47}$$

Equations (46) and (47) can be combined to express the composite strength distribution as a WLT relation:

$$H_{n_f, n_b}(x) = 1 - \left[1 - W(x)\right]^{n_f n_b} \cong 1 - \exp\left\{-n_f n_b W(x)\right\} \tag{48}$$

Hence a fiber-reinforced composite is predicted to fail, under assumed LLS rules, in a brittle-like manner. Exact analytical forms for $W(x)$ have not been determined. Harlow and Phoenix (1978b) determined that $W(x)$ is independent of n_{sys} for $n_{sys} \geq 9$ and $m \geq 5$. They also found that ELS bundles do not follow this WLT scaling. The function $W(x)$ is not a power law of x, so $H_{n_f, n_b}(x)$ is non-Weibull.

Mahesh et al. (1999, 2002) and Landis et al. (2000) performed Monte-Carlo simulations on the fracture process that examined the validity of Equation (48) for various values of fiber Weibull modulus and system sizes. Mahesh et al. (1999) used the Hedgepeth and Van Dyke (1967) (HVDP, with P for periodic) LLS model for a cross section of a three-dimensional composite (square-packed and hexagonal-packed fiber arrangements) for various m. They show that $m \geq 3$ was required for $W(x)$ to be independent of n_{sys} for the limited system sizes in their analysis. Mahesh et al. (2002) show that $m \geq 2$ and $m \geq 1$ were required for $W(x)$ to be independent of n_{sys} for three-dimensional and two-dimensional bundles, respectively, using HVPD. Their results indicate that the strength distribution was neither normal nor Weibull distributed although it was perhaps closer to a Weibull form (Mahesh and Phoenix (2004)).

Landis et al. (2000) performed full three-dimensional simulations of composite failure and tested the WLT scaling law using the relation

$$P_{f,V_2}(\sigma) = 1 - \left[1 - P_{f,V_1}(\sigma)\right]^{V_2/V_1} \tag{49}$$

where the probability of failure of a composite P_{f,V_2} with volume V_2 loaded to stress σ is related to probability of failure of a composite P_{f,V_1} with volume V_1 under identical loading. Note that Equation (49) is a reexpression of Equation (48) using volume instead of system size $n_{sys} = n_b n_f$ (system size is proportional to volume). Landis et al. (2000) found good correlation for this relation for larger system sizes (volumes)—larger than a 25 by 25 array. This suggested that there was a minimum bundle size (number of fibers) for this relationship to be valid.

The Mahesh et al. (1999) simulations showed a common trend for both the particular LLS and ELS models and for the values of fiber Weibull moduli studied: the mean strength and standard deviation decreased with increasing composite size. Landis (2000) also showed similar results for their full three-dimensional simulations with their LLS model. The ELS bundles closely approached Daniels's asymptotic results as size increased. The strength distributions from the LLS simulations were not consistently Weibull or normal, but the ELS simulations were normally distributed. Landis et al. (2000) also found that the stress- (concentration-) driven failure process followed a WLT scaling, whereas the fiber-strength-dominated mode did not.

Watson and Smith (1985) suggested a modification to the Weibull distribution to account for a smaller-than-expected size effect of the form

$$P_f(\sigma) = 1 - \exp\left(-\left(\frac{L}{L_o}\right)^{\varphi^*}\left(\frac{\sigma}{\sigma_o}\right)^{m^*}\right) \tag{50}$$

where L is the length of the fiber, L_o is a characteristic length, and φ^* is a constant between 0 and 1. This form is applicable both to the individual fiber and the composite if the appropriate values of φ and m are used for φ^* and m^*, respectively, depending on the material system. When $\varphi^* = 1$, the usual Weibull size-effect relation with exponent $1/m^*$ is obtained (see Eq. (12)). When $0 < \varphi^* < 1$, the size effect is appropriately diminished by the exponent φ^*/m^*. This factor is said to account for variations in fiber diameter and material changes from fiber to fiber in a yarn. Beyerlein and Phoenix (1996) (and Otani et al. (1991)) applied the Weibull distribution modified by Watson and Smith (1985) to account for the size effect of microcomposites (composites consisting of only a few fibers embedded in a matrix). Beyerlein and Phoenix (1996) required $\varphi^* = 0.6$ in order to achieve good correlation to experimental results. They used Weibull approximations from lower-tail (asymptotic) analysis to construct a failure envelope for a four-fiber microcomposite as shown in Figure 23.

Each line ($k = 1, 2, 3, 4$) represents the failure probability for k critical number of failure breaks approximated by a Weibull distribution of the form

$$H_{k,n_b}(\sigma) = 1 - \exp\left\{-(n_b)^{\varphi} n_f \left(\frac{\sigma}{\sigma_{\delta,k}}\right)^{km}\right\} \tag{51}$$

where $\sigma_{\delta,k}$ is a Weibull scale parameter appropriate for the k^{th} Weibull line, as explained in Beyerlein and Phoenix (1996). What is interesting about Figure 23 is that it shows the failure envelope having Weibull-like failure behavior at low probability-of-failure regimes but with a modified size-effect relation. This approach seems to bear at least some outward similarities to the Batdorf (1982) and Batdorf and Ghaffarian (1984) approach. Note that for fiber-controlled failure with a Weibull-style failure distribution, using either the fiber stress or the composite stress will not affect the results. See Appendix C for a simple explanation.

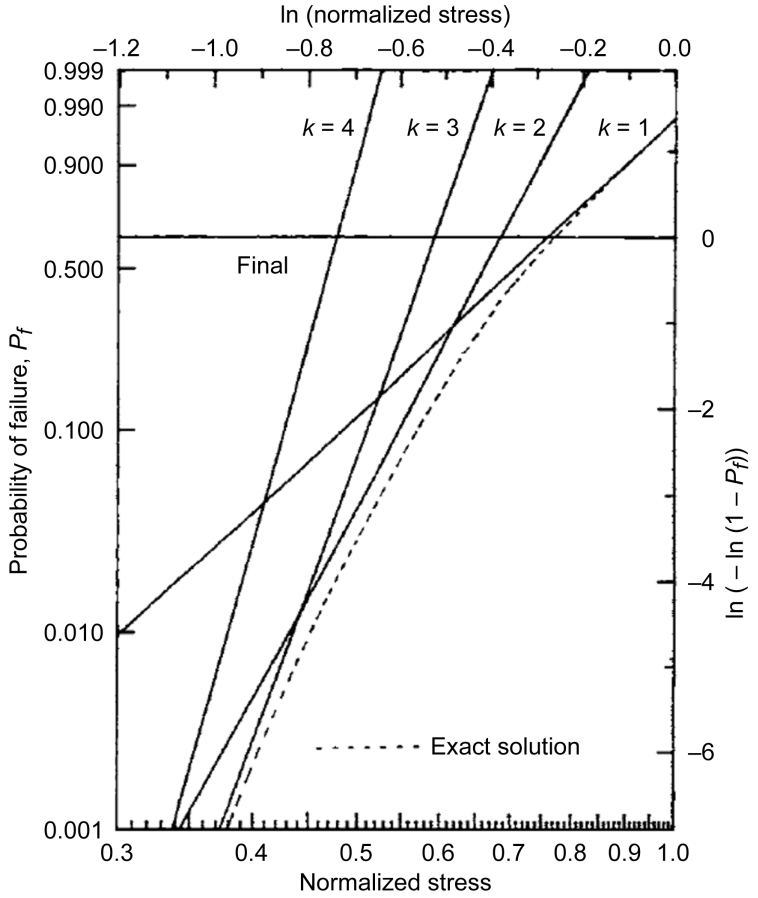

Figure 23.—Weibull line failure envelope construction compared with equal load sharing (ELS) exact solution ($G_4(\sigma)$) from Harlow and Phoenix (1978a) for a four-fiber microcomposite. Each line (k = 1,2,3,4) represents the failure probability for k critical number of failure breaks. Reproduced from Beyerlein and Phoenix (1996). Copyright Elsevier; used with permission.

Bazant and Pang (2007) developed a multiscale model composed of mixed series and parallel systems that they argue provides a physical underpinning to the Weibull distribution. In their model, quasi-brittle materials (including fiber composites, polygranular graphite, and concrete) will have a two-parameter Weibull distribution at the lower probabilities of failure—the lower tail of the strength distribution—which is the region of highest interest to the design engineer. In their approach, a material is modeled with a representative volume element (RVE) subunit. The structure (of positive geometry[2]) is modeled as a weakest-link-series system of RVEs, but each RVE is modeled as a parallel coupling of only two long subchains, each consisting of subbundles of two or three long sub-subchains of sub-subbundles, and so forth, until the nanoscale of the atomic lattice is reached. This is shown schematically in Figure 24.

The RVE is taken as the size of the fracture process zone (FPZ), which is roughly 3 times the size of the maximum inhomogeneity size (grain size for ceramics and graphite). Medium-grained graphites can, therefore, have FPZs that are several millimeters long. Therefore, structures with cross sections much larger than the FPZ are brittle, and smaller structures are quasi-brittle.

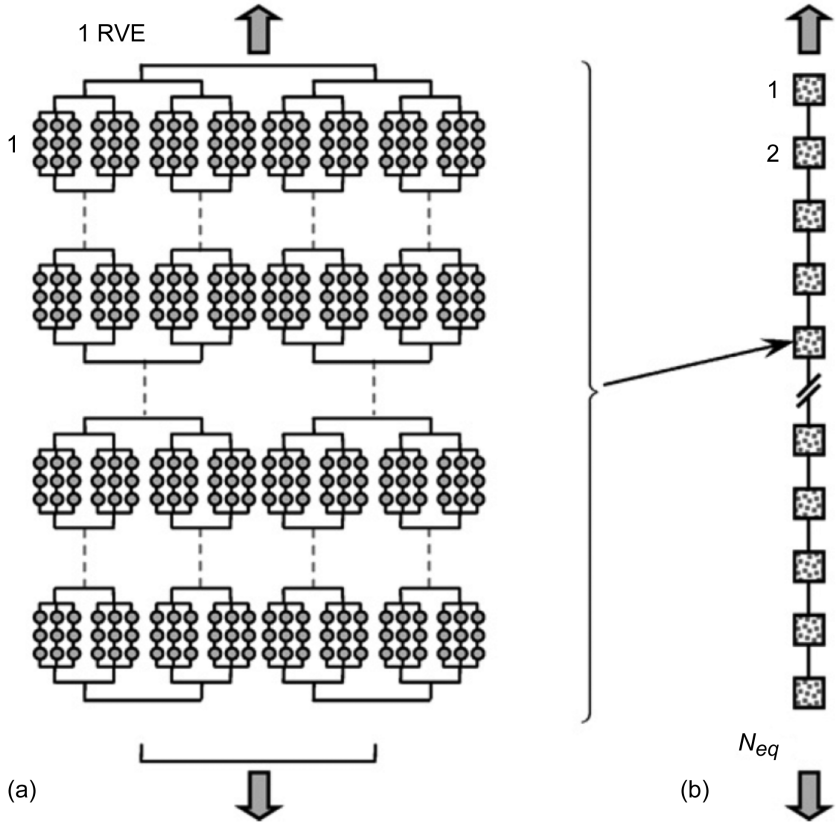

Figure 24.—Model of quasi-brittle structure, where N_{eq} is the equivalent number of links in a series. (a) Hierarchical model of representative volume element (RVE) consisting of subchains and subbundles. (b) Weakest-link series system of RVEs representing the structure. Reproduced from Bazant and Pang (2007). Copyright Elsevier; used with permission.

[2]Positive geometry means that the stress intensity factor at constant load increases with the crack length.

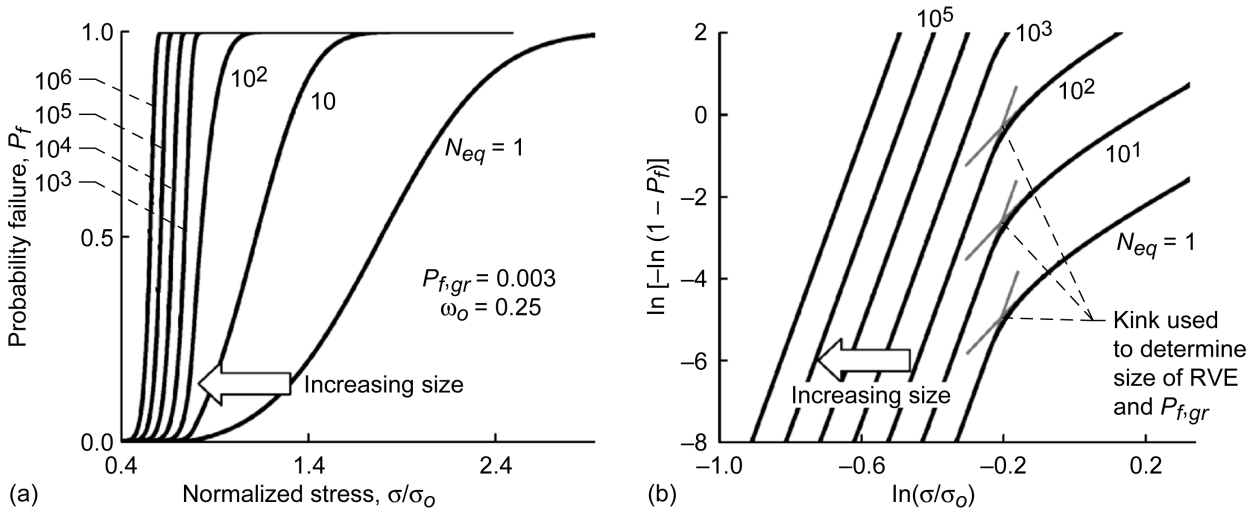

Figure 25.—Size effect on the cumulative distribution function of structural strength with the grafting probability of failure $P_{f,gr}$ = 0.003; N_{eq} is the number of identical links or subunits of volume of identical size, ω_o is the coefficient of variation, and RVE is the representative volume element. (a) Linear scale. (b) Weibull scale. Reproduced from Bazant and Pang (2007). Copyright Elsevier; used with permission.

At the atomic scale, the Bazant and Pang (2007) model has a power-law tail of exponent 1 of the cumulative distribution function of strength based on the Maxwell-Boltzmann distribution of the thermal energies of atoms. Bazant and Pang argue that the threshold of the power-law tail must be zero. In the model, the power-law tail exponent of a chain represents the lowest exponent of its individual links, and the power-law tail of a bundle is equal to the sum of the power-law tail exponents of all the parallel fibers in the bundle. Scaling this behavior up through series couplings in chains and parallel couplings in bundles raises this exponent to the value of the Weibull modulus observed at the level of the structure and is interpreted as being equal to the number of dominant cracks needed to break the RVE. At the RVE level, the model has a gaussian distribution (between the tails) with a power-law-tail exponent corresponding to the Weibull modulus grafted at failure probabilities in the neighborhood of 0.0001 to 0.01. This gives rise to a kink in the distribution. This "grafting point" moves to higher failure probabilities as the structure size increases and can be used to determine the size of the RVE as indicated in Figure 25. Size effect is also indicated in the figure.

The model indicates that, on the scale of at least 500 RVEs and larger, the structure follows a Weibull distribution with zero threshold (a two-parameter Weibull distribution). Bazant and Pang posit that three-parameter Weibull distributions (indicating a nonzero threshold), which are often empirically fitted to experimental rupture data, are actually misinterpretations of the kink produced by the grafted two-parameter Weibull distribution on the core gaussian distribution of the structure. The Bazant and Pang model is an interesting reinterpretation of the Weibull model.

2.2.7 Bundle Model Ductile-Like to Brittle-Like Transition

Mahesh et al. (1999) compared ELS modeling with the HVDP LLS model for fiber system sizes ranging from 15 by 15 to 50 by 50 arrays and fiber Weibull moduli ranging from m = 1/2 to 10. Their simulations showed that, for low Weibull moduli ($m \leq 1$), the ELS and LLS models correlated closely. The particular LLS model indicated that low-Weibull-modulus fibers fail in a more dispersed manner and that stress concentration from load sharing is not dominant. That trend was opposite for higher Weibull-modulus fibers, where fiber failures clustered and damage accumulation was driven by stress concentration. This seems to imply that two competing failure modes exist and that the magnitude of the Weibull

modulus of the fiber controls the failure behavior of the composite—ranging between the ELS fiber-strength-dominated failure mode and the LLS fiber-strength-concentration-driven failure mode.

On the other hand, Mahesh and Phoenix (2004) indicate analytically that idealized LLS bundles behave in a WLT manner driven by extreme-value statistics regardless of the strength variability of the individual fibers and that critical defects form, although very large samples may be required—much larger than that used in Mahesh et al. (1999). Their result implies that there is no disorder-induced transition from brittle failure to a more gradual dispersed failure regime. Phoenix (2007) says that for practical purposes there is an LLS-like to ELS-like transition. For idealized LLS, it is $m = 1$; for a planar model, it is approximately $m = 2$; and for the hexagonal packing model, it is $m = 4$. So above these fiber Weibull moduli values, LLS-like behavior is predicted; and below these values, ELS-like behavior is expected.

To study failure behavior, Hidalgo et al. (2002) used a load-transfer function that decays as $1/r_d^{\kappa}$, where r_d is the distance from a broken fiber. When κ was close to zero, they obtained ELS behavior, and for large κ, they obtained LLS expected behavior with $\kappa \cong 2$ at the transition region. Alava (2006) notes the similarity of this result with the two-dimensional random fuse (lattice) model where load (current) is transferred in a nonlocal, but geometrically dependent, fashion with the redistribution decaying as $1/r_d^2$ —which they state is the crossover point between local and global behavior.

Another aspect of failure behavior worth considering is that the variability of fiber strength affects the toughness of the composite. This was shown by Beyerlein and Phoenix (1997), who investigated the effect of a transverse notch of broken fibers on the fracture process, fracture resistance, and overall strength distribution for an elastic composite lamina. They showed, that for low-Weibull-modulus fibers, the composite becomes tougher as crack growth proceeds—that is, R-curve rises, with consequently stable crack growth. However, high-Weibull-modulus fibers resulted in a flat R-curve and, thus, unstable crack growth. This interesting observation seems to fall in line with Planas (1995) and Bazant and Planas (1998), as discussed in Section 2.1.4.

2.3 Lattice Models

Brittle materials such as monolithic ceramics and graphites appear to be homogeneous at the macroscale but are heterogeneous at the microscale. They consist of nonuniform distributions of the grain shapes, (possibly) multiple material grain phases, grain boundary, and flaws such as voids, inclusions, and microcracks. This represents a level of disorder that can be described as a characteristic of the material. In a material with broad disorder (quasi-brittle materials), fracture is not influenced exclusively by the weakest flaw in isolation but also by the proximity and local interaction of defects, including stress concentration and shielding effects around defects. As the material reacts to increasing load, defect clusters can develop, evolve, and coalesce, leading to the final breakdown of the material.

Since the 1980s, various types of discrete element models, called lattice models, have been developed to investigate the fracture characteristics of quasi-brittle materials. As mentioned in Nukala and Simunovic (2004) and Phoenix and Beyerlein (2000b), there are electrical fuse (conductivity breakdown) models (de Arcangelis and Redner (1985), de Arcangelis et al. (1986), Duxbury et al. (1986, 1987), Duxbury and Leath (1987), Li and Duxbury (1987, 1989), de Arcangelis and Herrmann (1989), Kahng et al. (1988), and Roux et al. (1988, 1991)); central-force (spring) models (Sahimi and Goddard (1986), Beal and Srolovitz (1988), Feng and Sen (1984), and Hansen et al. (1989)); bond-bending models (Kantor and Webman (1984), and Sahimi and Arbabi (1993)); and beam category models (Herrmann and Roux (1990), and Herrmann et al. (1989)). Alava et al. (2006) provide an excellent review of this work, and Nukala and Simunovic (2004) mention other comprehensive references: Hansen and Roux (2000), Herrmann and Roux (1990), Sahimi (1998), and Chakrabarti and Benguigui (1997). Additional useful references used here include Nukala et al. (2006), Zapperi and Nukala (2006), and Nukala and Simunovic (2004).

The following short summary highlights important results regarding failure mode, strength distribution, and size effect. However, stress-strain response, acoustic emission, toughening, and fracture

morphology are not discussed herein. The interested reader should begin with the previously mentioned review articles for an overview of the various material breakdown phenomena that have been investigated.

Lattice models are used to simulate the state of initial material disorder and the subsequent material breakdown process from progressive loading. Interesting questions can be investigated with these models, including size scaling, strength distribution, nonlinear elastic response as it relates to damage, the role of disorder (as well as the relation to percolation), avalanches—or bursts of microfailures (which can be related to acoustic emission), and weakest flaw versus crack clustering. Lattice models are arrangements of discrete springs, beams, or electrical fuses linked together in an ordered cubic, triangular, or diamond lattice. Over the last 25 years, the majority of lattice model research has been with random fuse models (RFMs), introduced by de Arcangelis et al. (1985). These are electrical analogs to a loaded structure where the link is a fuse and the electrical current, voltage, and conductance are analogous to stress, strain, and Young's modulus, respectively. This simplifies the model by substituting a scalar field for vectorial elasticity, decreasing the degrees of freedom of the system and therefore allowing larger system sizes to be solved for the available computational resources. Figure 26 shows a schematic of the RFM.

Nukala et al. (2005) compared the RFM with the random spring model (RSM) for a triangular lattice with a uniform distribution of failure threshold and found that the two models gave qualitatively similar results for fracture strength distribution, size effect, and damage characteristics. They concluded that the simplified scalar model of the RFM could be used to investigate the statistical properties of fracture in disordered media.

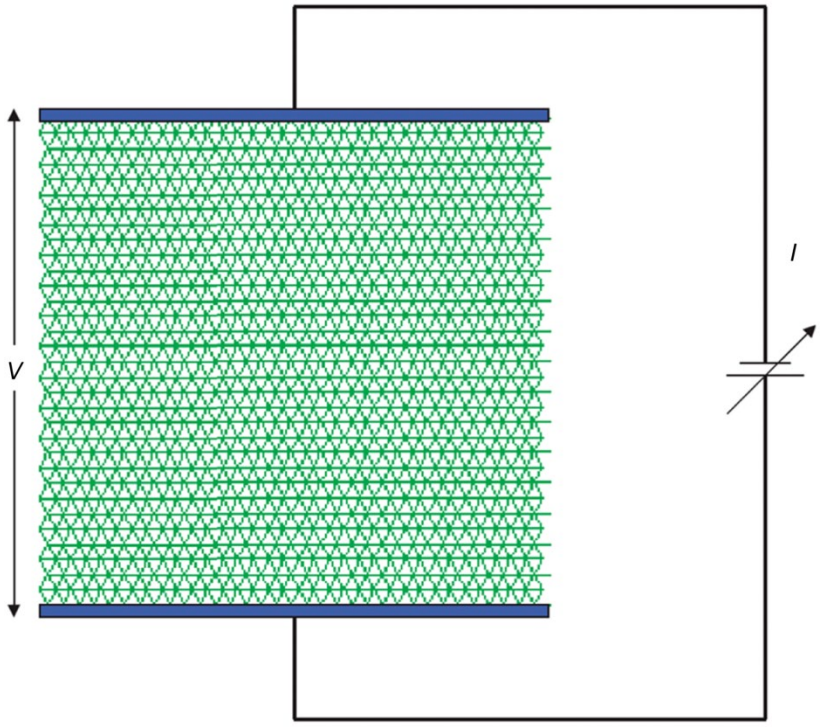

Figure 26.—Random fuse model (RFM). A triangular lattice is shown where each bond has a random breaking threshold, where *V* is the voltage and *I* is the current. Reproduced from Alava et al. (2006). Copyright Taylor & Francis Group; used with permission.

2.3.1 Disorder and System Breakdown

Modeling disorder in a material is related to the concept of percolation. A lattice that has a randomly selected fraction of bonds allowing a transport process (diffusion, conduction, flow, and force) while the rest of the bonds are insulating (nonactive) is defined as a bond percolation network. Work on percolation theory is extensive and has been applied to many areas including flow phenomena in porous media, transport, mechanical and rheological properties of disordered materials, diffusion, and precipitation. Percolation is mentioned here because much of the literature regarding lattice modeling refers to this body of work. However, although fractured media are similar to the concept of percolation, there are distinct differences. Crack coalescence and macrocrack propagation is one difference, and randomly distributed microcracking is one similarity. Sahimi (1998) provides a good review of this body of work.

Disorder is introduced in a lattice by assigning the individual elements or links (springs, beams, or fuses) random values of a property, such as failure threshold, according to a prescribed statistical distribution. In this manner the level of disorder input into the system can be quantified. In its initial state, the lattice may be complete or have some fraction of the links removed. Applying a progressively increasing load or displacement causes individual bonds to break (or be diluted as in Zapperi et al. (1997)) and causes the internal resistance load to redistribute until a critical instability is reached and the lattice system breaks down. In other words, the bonds break one by one until a path of broken bonds is created that prevents any load (or current) from being transmitted from one end of the lattice, where load or displacement (or voltage) is prescribed, to the other end. One can readily visualize that there are certain similarities between lattice models and the fiber breakage models described in Sections 2.2.2 to 2.2.6. This is a "quenched" disorder problem, where the disorder is introduced prior to the breakdown process (the breaking threshold of each bond is assigned before loading and held constant as loading progresses). In contrast, an "annealed" disorder problem is where disorder is introduced stochastically as loading (and breakdown) progresses.

Weak disorder systems (where the variation in bond strength is small) are dominated by stress concentrated around the crack tips and the early onset of unstable crack growth because of the lower probability of encountering strong bonds that will arrest crack growth. Consequently, WLT behavior would be expected in a weak disorder system. Conversely, in strong disorder systems (where variation in bond strength is large), a "cloud" of microcracks (blown fuses) form and eventually coalesce into a structure-spanning crack. Here, both the weakest and strongest bonds have important roles in the breakdown process. The stronger bonds arrest or redirect developing cracks. The weaker bonds initiate microcracks or allow existing cracks to propagate. The strong bonds, by arresting cracks, enable further microcrack nucleation at new sites. In this manner, distributed damage can develop in strong disorder systems. Figure 27 demonstrates the development of distributed damage and crack coalescence in an RFM for a strong disorder system. Figure 28 shows damage progression from an initial notch in an RFM with strong disorder. Note that in Figure 28 diffuse damage still occurs (shown as specks in the figure) despite the presence of a large, centrally located macrocrack.

A basic assumption in RFM is rapid current redistribution upon bond breakage (current redistributes before another bond breaks), whereby equilibration occurs before load can increase—simultaneous bond breakage is not allowed. Multiple bond breakage has been studied little. Duxbury et al. (1986, 1987) argue that, for weak disorder systems, the largest crack (connection of broken bonds) controls the breaking process and has current flow enhancement (stress enhancement) of a factor proportional to the square root of the crack length. Sahimi (1998) mentions that three-dimensional stress enhancement is much weaker than two-dimensional enhancement, so even a modest amount of disorder can result in distributed microcracking.

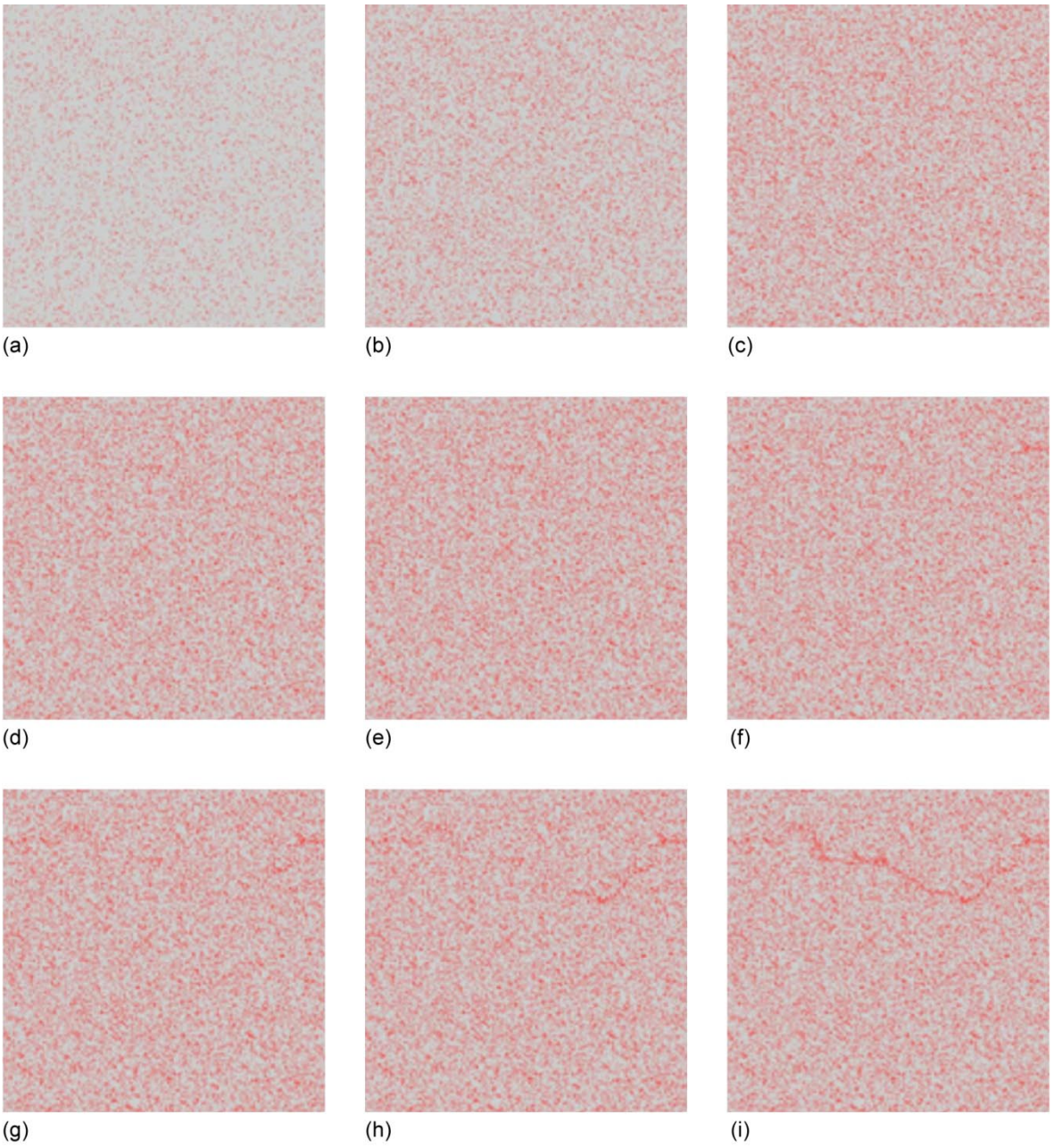

Figure 27.—Snapshots of damage in a two-dimensional triangular lattice of size $L = 512$. Number of broken bonds n_{br} at the peak load and at failure are 83 995 and 89 100, respectively. Parts (a) to (i) show snapshots of damage after breaking n_{br} bonds. (a) $n_{br} = 25\,000$. (b) $n_{br} = 50\,000$. (c) $n_{br} = 75\,000$. (d) $n_{br} = 80\,000$. (e) $n_{br} = 83\,995$. (f) $n_{br} = 86\,000$. (g) $n_{br} = 87\,000$. (h) $n_{br} = 88\,000$. (i) $n_{br} = 89\,100$ at failure. Reproduced from Nukala and Simunovic (2004) and Alava et al. (2006). Copyright Springer Publishing Company and Taylor & Francis Group; used with kind permission of Springer Science+Business Media and Taylor & Francis Group.

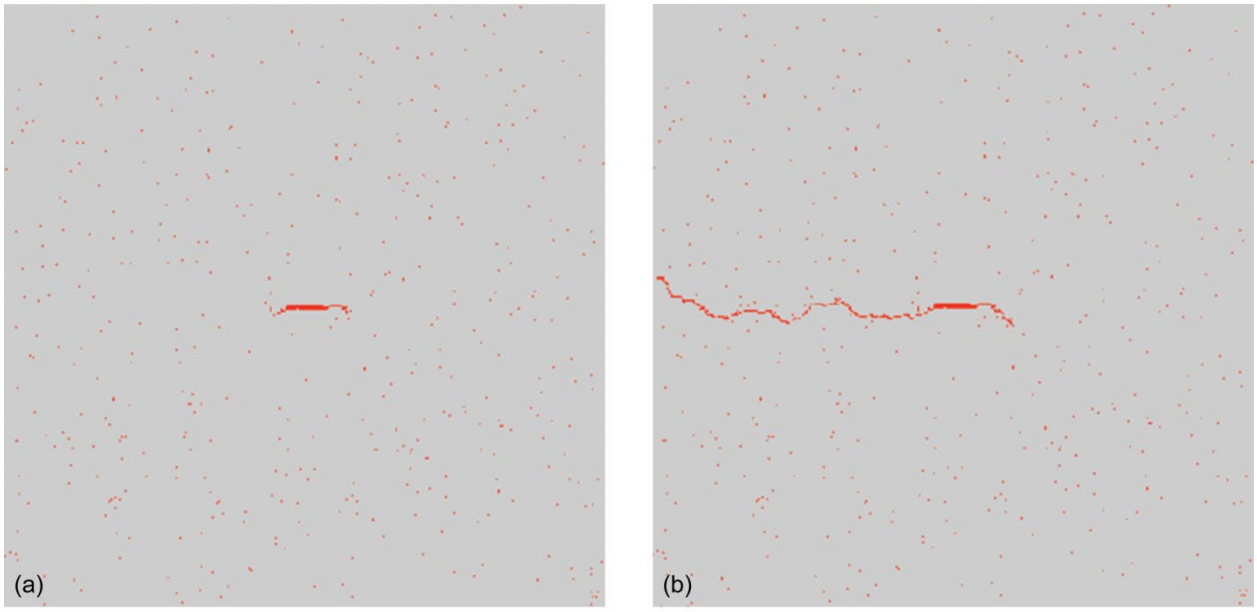

Figure 28.—Damage and crack formation from an initially notched random fuse model (RFM). (a) Damage propagation. (b) Although diffuse damage occurs, a spanning crack eventually forms from the notch. Reproduced from Alava et al. (2006). Copyright Taylor & Francis Group; used with permission.

2.3.2 Lattice Brittle-to-Ductile-Like Transition

Kahng et al. (1988) investigated the role that disorder plays in the transition between brittle and quasi-brittle, or ductile-like, failure and showed a relationship between this transition and system size L (number of fuses along the busbar) in their model. Figure 29 is reproduced from this reference.

In their probabilistic modeling and RFM simulations, Kahng et al. (1988) assumed that each bond had unit conductance and that the bonds had a uniformly distributed voltage threshold between $1 - w/2$ and $1 + w/2$, so that the average threshold voltage was unity and the width of the bond-breaking distribution w was between 0 and 2. Upon breaking the first (the weakest) bond in the system, the vertical bonds horizontally adjacent to the broken bond have the largest local change in voltage. Those bonds are the ones most likely to break next without any additional increase in the externally applied voltage potential. For sufficiently small w, less than the threshold w_o, the initial failure of this weakest bond is always unstable to further cracking. This regime is the "trivial" region bounded by $w = w_o$ in Figure 29 and is trivially governed by extreme-value statistics. Kahng et al. (1988) argues that $w_o \cong 0.24$ is the lower bound for the true value of w_o. For $w > w_o$, there is a nonzero probability that the initial crack is stable without further increase of the external potential. In this region, shown in Figure 29 as the "brittle" region, failure occurs after one of the first few bonds broken nucleates a crack that catastrophically propagates across the system. Therefore, fracture is controlled by the weakest, or one of the weakest, bonds in the system.

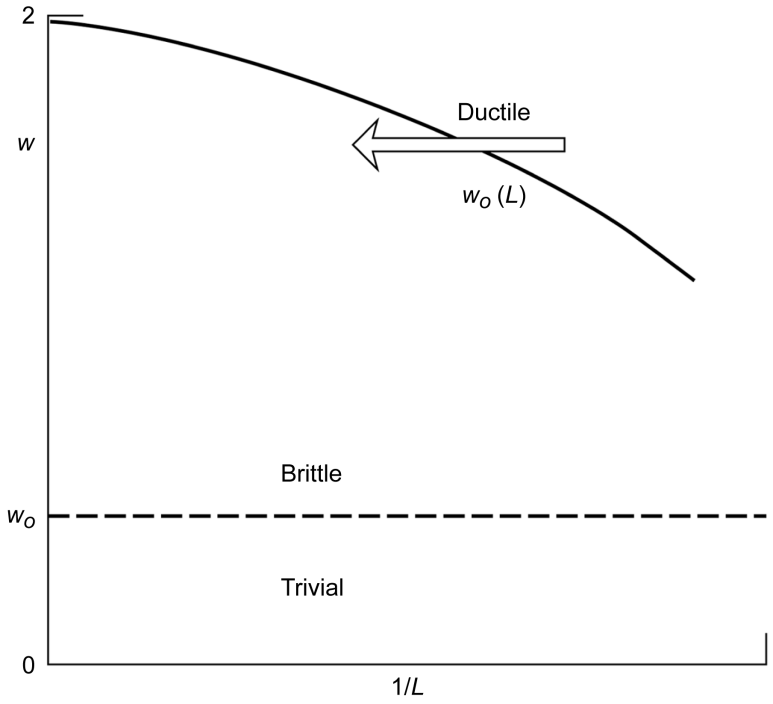

Figure 29.—Random fuse model (RFM) showing a brittle-to-ductile-like transition region as a function of system size L. The term w is the span over which a uniform distribution of fuse breaking threshold occurs. The average threshold is assumed to be 1, the uniform distribution is applied between 1 – w/2 and 1 + w/2, $w_c(L)$ is the critical transition of w between brittle-like and ductile-like behavior as a function of L, and w_o is the threshold of w where single-bond breakage causes system failure. Reprinted Figure 1 with permission from Kahng, B.; Batrouni, G.G.; Redner, S.; de Arcangelis, L.; and Herrmann, H.J.: Phys. Rev. B, vol. 37, no. 13, 1988, p. 7626 (Kahng et al., 1988, http://link.aps.org/abstract/PRB/v37/p7625). Copyright (1988) by the American Physical Society.

In the so-called ductile (ductile-like) regime, breakdown of the network is more gradual: individual bonds break over a large range of monotonically increasing voltage potential (monotonically increasing load). The boundary between brittle and ductile-like failure, denoted by the curve labeled $w_c(L)$ in Figure 29, is defined by Kahng et al. (1988) as the equality of likelihood of the unstable growth of an existing crack versus the forming of a new crack, which occurs after n_c bond breaks, and the likelihood that the n^{th} weakest vertical bond is spatially independent of all other cracks already in the system (related to the problem of "birthday coincidences"). If n_{indep} is the maximum number of n where spatial independence is maintained, then if $n_{indep} > n_c$ the system is brittle. Conversely, if $n_{indep} < n_c$, then crack growth is as likely to occur as new crack initiation when the external potential is increased, and failure of the network will then be more gradual than brittle fracture. Since this is a probabilistic argument, it does not represent an abrupt transition between brittle and ductile-like behavior. Kahng et al. (1988) indicate that w_c is a function of system size L (proportional to volume). It is significant to note that as volume increases brittle behavior is expected to predominate even in high-disorder systems. In the limit of infinite system size, the RFM is brittle except in the special case of $w = 2$, which implies that the distribution of fuse threshold has to include the zero value for quasi-brittle behavior to exist at this limit.

Sahimi and Goddard (1986) used Hooke-type spring lattice models to investigate the role of disorder in brittle versus distributed damage (ductile-like) behavior. They used three basic models involving the

stochastic spring constant k_s and the critical strain ε_c with various probability distributions. Model I assigned the same spring constant $k_s = 1$ to some fraction p of randomly chosen springs; the remaining $p - 1$ fraction had $k_s = 0$, and critical strain was constant at ε_c. Model I simulated the initial state of microporosity in the material. Model II maintained ε_c as constant, but k_s was randomly distributed to a prescribed distribution function. In model II, heterogeneous constituents had varying elastic response, although they had the same strain-to-failure threshold. Model III maintained constant $k_s = 1$ but assumed that ε_c was the distributed quantity. In other words, in model III the bonds represented individual grains with different strain-to-failure thresholds, or perhaps they represented small regions of material with stochastic strength response. Regions of varying residual stress were not considered in these models although this was considered by Curtin and Scher (1990a,b).

For Model I for $p \cong 1$, brittle failure was observed where a broken spring caused adjacent springs to fail in a cascade. However, for $p \cong p_{ce}$ (elastic response threshold where removed members affect the elastic response of the system) cracks were generated at several locations and propagate. This behavior differentiates intrinsically flawed systems from damaged systems.

For Model II for a uniform distribution of k_s between 0 and 1, brittle behavior was maintained unless a large fraction of springs had $k_s = 0$ as in Model I. Quasi-brittle behavior of microcrack formation and propagation was observed for a power-law type distribution of k_s:

$$f\left(k_s\right) = \left(1-\phi\right) k_s^{-\phi} \quad 0 < \phi < 1 \tag{52}$$

when ϕ became larger (the distribution became broader). For $\phi \cong 0$, brittle behavior was observed because the distribution was very narrow.

For Model III, assuming a uniform or power-law distribution for ε_c (similar to Eq. (52)) showed behavior similar to Model II. For the uniform distribution, behavior was brittle-like with a single crack forming and subsequently spanning the entire lattice. Using Equation (52) caused microcracks to initiate at numerous distributed locations before ultimate breakdown. Sahimi and Goddard (1986) noted that sometimes crack growth was arrested when a relatively strong region was encountered. They proposed that the macroscopic response of the system depends on the form of the probability distribution functions (PDFs) for k_s and ε_c, whereby if the first inverse moment of the PDF is finite, a brittle failure mode occurs, but if the first inverse moment of the PDF is infinite, distributed damage is the dominant mechanism leading to failure. That is, if f_{-1} is finite,

$$f_{-1} = \int_0^\infty \frac{f(y)}{y} \mathrm{d}y \tag{53}$$

and the probability density function $f(y)$ of either k_s or ε_c is finite, then brittle fracture behavior is expected. However, if f_{-1} is divergent, then quasi-brittle behavior is expected.

Hansen et al. (1991) and Batrouni and Hansen (1998) used RFM with breaking thresholds uniformly distributed between 0 and 1, but raised to an exponent. The cumulative probability distribution was $P(\sigma) = \sigma^{1/|\phi|}$ when $\phi > 0$ and was $P(\sigma) = 1 - \sigma^{1/|\phi|}$ when $\phi < 0$. The smaller the value of $|\phi|$, the smaller that the amount of disorder in the system was. When $\phi > 0$, the power-law tail extended toward the weak bonds, and when $\phi < 0$, the tail extended toward the strong bonds. For small values of $|\phi|$, brittle behavior was observed where a macroscopic crack developed early in the fracture process. For large values of $|\phi|$, quasi-brittle behavior occurred where a cloud of disconnected microcracks developed before the cracks coalesced into the final macroscopic crack.

Although beyond the scope of this article, microfracturing has an obvious relationship to acoustic emission observed in real materials prior to fracturing. Strong disorder will cause significant microfracturing events prior to final breakdown. Quasi-static lattice models qualitatively indicate a power-law distribution of avalanche events (not including the last avalanche event), where more activity occurs as

the peak failure load is approached. The aforementioned review articles are a good starting point for exploring this subject further.

2.3.3 Strength Distribution and Size Effect in Lattice Models

In section 6.3.1 of their journal article, Alava et al. (2006) note several studies (references not reproduced here) that showed in randomly diluted disorder problems (where some fraction of the links were randomly removed prior to loading) the defect-cluster-size distribution was exponential far away from the percolation threshold (the threshold where long-range connectivity first appears) but followed a power law close to the percolation threshold. The implication is that a Gumbel distribution more appropriately describes the fracture strength distribution far away from the percolation threshold, and a Weibull distribution is more appropriate close to the percolation threshold. However, Sahimi (1998), in section 7.2.1.1 of his journal article, cites work indicating that Weibull and Gumbel worked equally well away from the percolation threshold but that neither distribution performed very well near the percolation threshold. For RFM models with weak disorder, the failure is dominated by the stress concentration near the crack tip, implying that WLT behavior should dominate and that fracture strength should follow the Weibull or Gumbel extreme-value distributions (Alava et al. (2006)). For strong disorder, a different situation arises because of the distributed damage, which is discussed later in this section.

The Gumbel distribution—as determined from Duxbury and Leath (1987) and Duxbury et al. (1986, 1987) for randomly diluted RFM and subsequently used in an elastic spring model of fracture by Beale and Srolovitz (1988)—expresses the failure threshold stress (stress required to break the first bond in the system) probability distribution as

$$P_f(\sigma) = 1 - \exp\left\{-c_G L^D \exp\left[-\frac{k_G}{\sigma^u}\right]\right\} \tag{54}$$

where c_G and k_G are constants characteristic of microscopic properties of the system, D is the number of dimensions of the system ($D = 2$ for a two-dimensional network {$\propto$ area}, $D = 3$ for a three-dimensional network {$\propto$ volume}), and $1 < u < 2$. The defect cluster size distribution is exponential, and a size-effect relation is obtained by equating failure probability for different system sizes L_1 and L_2:

$$\sigma_2 = \left[\frac{1}{\frac{1}{\sigma_1^u} + \ln\left\{\left(\frac{L_2{}^D}{L_1{}^D}\right)^{1/k_G}\right\}}\right]^{1/u} \tag{55}$$

In contrast, the Weibull distribution has the form

$$P_f(\sigma) = 1 - \exp\left\{-c_G L^D \sigma^m\right\} \tag{56}$$

where the defect cluster size has a power-law distribution. The size-effect relation (also see Eq. (12)) is

$$\sigma_2 = \sigma_1 \left(\frac{L_1{}^D}{L_2{}^D}\right)^{1/m} \tag{57}$$

It is not completely established which distribution (Weibull or modified Gumbel) is most appropriate for lattice models with weakly disordered bonds.

For a strong disorder system, damage is distributed, rather than localized, and the largest defect cluster at peak load may not be responsible for the final material breakdown cascade. For two- and three-dimensional lattice architectures, respectively, Nukala and Simunovic (2004) and Zapperi and Nukala (2006) investigated the effects of strong disorder on large lattice size (in comparison to previous studies) RFM. For the two-dimensional case, L was as large as 512, and for the three-dimensional case, it was as large as 64. Their systems were initially intact, with each bond being linear elastic until fracture, and they assumed a uniform distribution of fracture thresholds between 0 and 1. This approach differs from many earlier studies, where a random fraction of the links was removed prior to loading (percolation disorder). Nukala and Simunovic (2004) state that the defect cluster distribution evolves differently for the two approaches. In the initially intact RFM, the defect clusters evolve not only from the weakest bonds but from the stress concentration effects around the defect clusters. The simulation results show broadly distributed damage (see Figure 27) and indicate that the fracture strength (the stress at peak load) was neither Weibull nor Gumbell distributed but rather best fit to the lognormal distribution. Nukala and Simunovic (2004) argue that this arises by way of the central limit theorem: "the product of a large number of independent factors, none of which dominates the product, will tend to the lognormal distribution regardless of the distribution of the individual factors involved in the product." This contrasts with weak disorder (narrowly distributed breaking thresholds), where the breaking of a bond significantly influences the further breakdown of the material and leads to WLT behavior and extreme-value theory.

It is interesting that, for the size effect, Nukala and Simunovic (2004) and Zapperi and Nukala (2006) found that the Gumbel distribution form of Equation (55) worked well but that the Weibull size-effect scaling did not. Specifically they found that

$$\sigma_\mu = c_1 L^{\Phi - D + 1} + \frac{c_2}{L^{D-1}} \tag{58}$$

where mean fracture strength σ_μ = peak force/L^{D-1}, c_1 and c_2 are constants, and $D = 2$ for the two-dimensional mode and $D = 3$ for the three-dimensional mode. The exponent Φ is 0.96 for RSM, 0.97 for RFM for both diamond and triangular lattice networks in two-dimensional models, and 1.95 for three-dimensional RFM. For $(D - 1 - \Phi) << 1$, Equation (58) could be approximated as

$$\sigma_\mu = \frac{c_3}{(\ln L)^\psi} + \frac{c_2}{L^{D-1}} \tag{59}$$

where c_3 is also a constant and ψ has a value of approximately 0.15. This suggests that for large lattice systems the mean fracture strength decreases very slowly, scaling proportional to $1/(\ln L)^\psi$. However, a word of caution has been sounded by Phoenix and Beyerlein (2000b). They note that the limited simulation system sizes L reported in the literature are often much too small to reveal the ultimate large-scale behaviors. They recommend more studies on a larger scale of several orders of magnitude and analytical asymptotic studies, if possible. They state

> "…regardless of their points of view, many investigators have turned to rigorous study of idealized, one-dimensional models of failure in an attempt to put approximate analysis and interpretations from simulations of more complex networks on firmer ground. Such models, which are often variations on the LLS models of Harlow and Phoenix, are analytically solvable, rich in behavior, and qualitatively show many features seen in simulations. In most cases, results in LLS fiber-bundle models support the logarithmic size scaling, but more generally, such results depend on the load-sharing scheme (LLS vs ELS) and on the assumed form of the distribution for element failure."

Alava et al. (2006) state that for strong disorder the lognormal strength distribution is observed, but they concede that "whether this is a general result valid at all scales or the signature of a crossover behavior to Gumbel or Weibull scalings, still remains to be explored." They argue that models such as RFM may lie "exactly at the boundary between LLS and ELS and the lognormal distribution could then arise from the competition between local and global effects in a strongly disordered environment."

Another interesting result comes from Nukala et al. (2006) regarding crack-cluster distribution for broad (strong) disorder systems using RFM (with an initially intact lattice with a uniform distribution of fracture thresholds). They found in their two- and three-dimensional models that the largest crack-cluster size distribution at peak load fitted a lognormal distribution rather than a power-law or exponential distribution, as previously indicated for randomly diluted networks (percolation disorder). They also found that the final spanning crack was often formed from the coalescence of smaller cracks rather than from the propagation of the largest crack at peak load; therefore, the largest crack at peak load and the fracture strength (at peak load) were not correlated (or were weakly correlated at best).

Alava et al. (2006) discussed notch sensitivity where an initial notch is introduced into a two-dimensional RFM lattice with uniform threshold distribution bond strength. Figure 28 shows an example where the role of disorder can be seen in the wandering crack path as well as in the diffuse distributed damage that also developed. This illustrates the interplay between an existing crack of size a_0 relative to the system size L and the level of disorder in the system. Figure 28 is also interesting in that it shows a preexisting crack dominating the fracture response but that distributed damage also occurs—indicating that, in a real material, independent randomly distributed microfracturing events (evidenced by acoustic emission) could occur even if a preexisting crack was dominating the fracture behavior.

A weak disorder leads to LEFM behavior and extreme-value statistics for heterogeneous materials with a population of preexisting cracklike flaws of variable (stochastic) severity. That is, the extreme-value statistics of the flaw population drive the material strength response. Strong material disorder is a more complicated situation, where the crack size of the preexisting flaw relative to the size of material microstructural heterogeneities can affect the size-effect response—giving intermediate behaviors.

Alava (2006) investigated the interplay between a_0/L, disorder, and L on size effect. Results from simulations of fracture strength for various a_0/L ratios versus system size L were fitted with a power law where fracture strength was proportional to L^{-c}, where c is a constant best fit for a given a_0/L ratio. For a small a_0/L, c is small and equivalent to the logarithmic relation described previously, but for a larger a_0/L, c approaches one-half as predicted from LEFM. In other words, the presence of large intrinsic flaws in the strong disorder heterogeneous material will also lead to LEFM behavior and fracture strength governed by extreme-value statistics. Alava et al. (2006) also mention that the FPZ is typically rather small for RFM and decreases in relative size as a_0/L increases. Curtin (1997) investigated the toughening effect that disorder plays in the RSM with an introduced notch. Curtin concluded that the difference in toughening between weak and strong disorder was only about 10 percent in the model and that, in real materials, other effects such as grain bridging could play a larger role.

3.0 Discussion and Summary

> "… as we know, there are known knowns; there are things we know we know. We also know there are known unknowns; that is to say we know there are some things we do not know. But there are also unknown unknowns—the ones we don't know we don't know."
> (D.H. Rumsfeld, former Department of Defense secretary, February 12, 2002, Department of Defense news briefing)

The fracture of nuclear-grade graphite is a function of the distribution, interaction, and growth kinetics of flaws of various forms and size scales. Graphite fracture strength is stochastic: Nominally identical tensile and flexural specimens show large specimen-to-specimen variation in strength. Average strength has been shown to vary within billet, between billets, and with the orientation relative to the billet (strength anisotropy relative to processing direction). Different grades of graphite can have very

different morphologies and, it would be expected, different fracture behaviors ranging from classically brittle to quasi-brittle. Add to this the fact that the stress-strain response is nonlinear and involves irreversible accumulation of damage, and it becomes clear that the fracture behavior of graphite is complex, falling somewhere between brittle monolithic ceramics and damage-tolerant composite materials. Therefore, models that access the failure potential of graphite structures will need to consider this rich behavior as well as account for the statistical nature of graphite failure. An ultimate goal would be to develop statistical models of failure that can be employed with finite-element programs, such as CARES/Life (see Nemeth et al. (1993, 2003, 2005)), to predict the probability of failure of a generalized structure under thermomechanical loading.

In experimental studies of graphite, use of the Weibull model to predict failure has met with apparent mixed success, and others have criticized the applicability of its physical assumptions. This has led to the development of alternative models. This review article describes various statistical models of brittle-constituent-controlled material failure. Some of these models were developed specifically for graphite. All the models assume that material breakdown begins at inherent flaws or weak regions in the material. However, the models differ in how material breakdown proceeds. They are broadly categorized into series-system or parallel-system models. Table I summarizes the models that are discussed in this report. From the survey of literature that was performed herein, the following four overarching observations can be made:

(1) WLT modeling applies over a broad range of material systems ranging from the classically brittle to distributed damage (bundle and lattice) models, and at low probabilities of failure this behavior may be approximated by a Weibull distribution. The implication is that WLT models may be appropriate for graphite despite the fact that the material displays distributed damage.

(2) There may be a transition where material behavior (fiber composite or monolithic) goes from classically brittle to quasi-brittle, which is apparently a function of the level of disorder in the material system. For graphite, this means that the inhomogeneity of local properties has been identified as a means with which to explore and possibly engineer the failure behavior of the material.

(3) For high-disorder (highly quasi-brittle) material systems, the process of microcracking leading to crack coalescence may not be governed by extreme-value statistics: that is, Weibull or Gumbel. The Weibull distribution may work empirically to approximate the distribution of strength, but for those grades of graphite that display a large amount of distributed damage, the actual failure mechanism may not necessarily be driven by WLT extreme-value statistics. This may need further investigation.

(4) However, for high-disorder material systems, intrinsic flaws, starting at some size threshold, behave according to LEFM; therefore, the material strength should follow an extreme-value distribution like a Weibull distribution. The implication is that larger sized flaws (significantly larger than the individual grains in the microstructure) will control the strength response of graphite and that the distribution of the sizes of these flaws requires that the strength response be an extreme-value distribution such as a Weibull distribution.

Some of the important points that will be discussed in subsequent sections follow:

(5) The Weibull distribution is argued to be the most appropriate probability distribution for fitting to experimental rupture data and extrapolating to low probabilities of failure. This is true for brittle and quasi-brittle materials including graphite.

(6) Size effect and strength dispersion are functionally related in WLT. This is true for any material whose strength response is governed by the WLT mechanism.

(7) A Watson-Smith-style modified Weibull formulation is proposed for graphite to reduce the size effect and better correlate with experimental data.

In addition, miscellaneous issues including the physical interpretation of the Weibull modulus, the stress gradient, scaling problems, multiaxial stresses, microstructural models such as Burchell's, and probabilistic design are discussed and summarized.

3.1 Uncertainty in Experimental Data and the Weibull Distribution

For fitting a probability distribution to experimental rupture strength data, including extrapolation to low probabilities of failure, the Weibull distribution is the most appropriate choice. Although the use of the Weibull stress-volume integral (Eq. (8)) has detractors as well as proponents, the Weibull distribution (expressed independently of volume; see Eq. (4) and Weibull (1951)) fits the available experimental data as well as or better than other commonly used distributions. For design purposes, the trends of experimental data must be extrapolated to very small probabilities of failure. The Weibull two-parameter distributions tend to be more conservative (or pessimistic) than, for example, gaussian or lognormal distributions. Liu (1997) systematically studied data sets of finite size (up to 100 samples per data set) generated from the two-parameter Weibull and lognormal distributions where distribution parameters for one distribution type were erroneously estimated from data generated from the other (true) distribution type. Liu concluded, "erroneously classifying data and using one or the other model is less damaging if the Weibull model is chosen than if the lognormal model is used." In other words, the bias of the Weibull distribution tended to be conservative, whereas the bias from the lognormal distribution tended to be nonconservative.

This level of bias increased at lower probabilities of failure. For example, if the sample is from the Weibull distribution but is erroneously fitted to a lognormal curve, the extrapolated failure probability at low levels of probability of failure (the lower tail of the distribution) will be too low and, therefore, nonconservative. If the sample is from the lognormal distribution but is erroneously fitted to a two-parameter Weibull curve, the extrapolated failure probability will tend to be lower and, therefore, more conservative.

> "For 20 or less failures (in data), always use the two-parameter Weibull distribution even if you know the underlying failure mechanism demonstrates a different distribution—the reason for selecting the two-parameter Weibull is both a more stable predictor and a more conservative predictor" (interpretation of Liu's results by Abernethy (2008) of Weibull Analysis Handbook fame (Abernethy et al., 1983)).

Therefore it seems clear that, based on the uncertainties of using experimental data and/or whenever there is doubt as to the true source of the data, the Weibull distribution should always be assumed. A mild caveat to this statement is that, for this report, the authors could not find a study of all possible distribution types—either pro or con—for this position. The Burchell model was a lognormal distribution of pore sizes estimated from material micrographs. In this case, extrapolation to low probabilities of failure means extrapolating the lognormal distribution to larger sizes of pores. It is not clear how the uncertainties related to this extrapolation would compare with the Weibull distribution of strength.

Another important factor to consider is that flaw populations may not be detected when specimens are tested. A low-Weibull-modulus flaw population is a scarce flaw population. Testing of small-size specimens (or measuring pore-size distributions in micrographs to characterize microstructural models such as the Burchell model) may not sample enough material volume to detect these larger and weaker flaws (which are distinct from background defects). Therefore, extrapolating results from specimen testing to lower probabilities of failure for structures with larger volumes could result in a nonconservative estimation of structural strength if a more severe flaw population was not detected during specimen testing and was not accounted for. This is true regardless of the probability distribution used for the extrapolation. From Figure 10 it is readily apparent that large gross flaws may exist in graphite blocks, but specimen testing may miss these flaws (specimens that contain these gross flaws might even be rejected before fracture testing by "quality control").

When the parameters of a probability distribution are estimated from a set of experimental data, there is an inherent uncertainty as to what the values of the true parameters of the underlying distribution are. The smaller the number of samples there are within a data set, the larger the range of uncertainty is for both the true values of the underlying distribution and the failure stress for a given probability of failure. This leads to the question of confidence bounds on parameters and confidence bands on distributions. Basically, the values of these intervals can be specified with a given level of statistical certainty. For example, the Weibull modulus can be predicted to lie within a certain range of values with a 90-percent level of confidence for a given number of samples in a data set. A discussion of the methodology for determining confidence intervals, confidence bands, estimated parameters, and other statistical metrics is beyond the scope of this report; however, some useful references regarding the Weibull distribution include Thoman et al. (1969), Abernethy et al. (1983, and later revised editions), Pai and Gyekenyesi (1988), and Danzer et al. (2008). Meeker and Escobar (1998) provide a more generalized and comprehensive textbook regarding these subject areas. In addition, Weibull plotting software programs such as WeibPar (Connecticut Reserve Technologies, Inc., 2009) and SuperSMITH (Barringer & Associates, Inc., 2009) are available for estimating Weibull parameters and determining confidence intervals and confidence bands.

For materials that behave consistent with the Weibull distribution, data from separate data sets of various sized specimens are commonly pooled (combined) to estimate Weibull parameters instead of obtaining these parameters from a data set of a single specimen size. This technique offers advantages in using information efficiently (decreasing uncertainty) and in model validation (e.g., Johnson and Tucker (1994)). However, for graphite these techniques must be considered carefully (or modified appropriately) since the Weibull modulus observed from the size effect of the different specimen sizes may not correlate effectively with the Weibull modulus observed from the scatter in strength data. Nevertheless, having rupture strength data available from two or more (significantly) different sizes of specimens is important for exploring the relationship between the size effect and the scatter in strength. Note that WeibPar (Connecticut Reserve Technologies, Inc., 2009) can estimate Weibull parameters from pooled data of various specimen sizes.

3.2 Large Intrinsic Flaws and Extreme-Value Statistics

The existence of gross flaws may be an important issue from another respect. As mentioned in Section 2.3.3, Alava et al. (2006) showed that, when embedded cracks were significantly larger than the background defects (the individual lattice elements), the large defect behaved according to classical LEFM. This suggests that a population of large, relatively isolated defects should behave according to extreme-value statistics; that is, Weibull or Gumbel distributions. Recall that Pears and Sanders (1970) (see Sec. 1.2) describe graphite as consisting of background and disparate defects such that the disparate defects are large in comparison to the background defects. If some of the disparate defects are sufficiently large, they will likely produce a classical WLT brittle-failure mode. Therefore, for a small-size scale, where gross defects may not be present, graphite may be quasi-brittle with distributed microcracking, as lattice simulations and experimental observations suggest. However, for larger scale structures, the increased likelihood of a gross flaw being present shifts the failure mode toward being classically brittle.

The presence of gross flaws is undesirable, and nondestructive evaluation (NDE) techniques are often used to try to identify and remove components containing the worst-of-the-worst—that is, the largest—flaws. This truncates the flaw-size distribution and implies a threshold stress below which failure will not occur. Statistical techniques have been developed to determine the probability of detection, but this is beyond the scope of this report. Proof testing is also used to screen components and provide a minimum assured strength. Again a discussion of this subject is beyond the scope of this report; however, multiaxial proof testing reliability analysis is discussed in Nemeth et al. (2003, 2005).

3.3 Weakest-Link Theory and Asymptotic Weibull Behavior at Low Probability of Failure

By definition, the WLT applies to series-system models, but what is interesting is that WLT modeling also has been applied to fiber-bundle models, as described in Sections 2.2.4 and 2.2.6. However, WLT may not be applicable for very high disorder systems, as discussed in Sections 2.2.7 and 2.3.2. Bazant and Pang (2007) argue (see Sec. 2.1.1) that WLT is always applicable at the RVE size scale and larger for (essentially) all brittle constituent materials. Whether it is argued that graphite behaves more like a composite with distributed damage or more like a classically brittle material, it seems that WLT-series system modeling will probably be required to physically describe the structure beginning at some threshold size scale.

There are physical and mathematical arguments that can be cited to help bolster the case of using the Weibull distribution. Extreme-value statistics points to the Weibull distribution, with further justifications provided by Bazant and Planas (1998) and Bazant and Pang (2007) (see Sec. 2.1.1). The extreme-value argument is strongest for classically brittle materials. However, for parallel systems (or mixed series-parallel systems), the Weibull distribution also seems appropriate, asymptotically, at the lower tail of the distribution. This was illustrated in Section 2.2.6 for Bazant and Pang (2007) and Beyerlein and Phoenix (1996). It is also supported by Batdorf (1982) and Batdorf and Ghaffarian (1984). Bazant and Pang (2007) argue that, at the RVE level (about 3 times the size of the maximum inhomogeneity), strength is gaussian with a Weibull lower tail and that, at the size level of about 500 RVEs, the structure has a two-parameter Weibull distribution. Therefore, extreme-value WLT, chain-of-bundles, and (from Bazant and Pang (2007)) mixed series-parallel systems argue for Weibull-like behavior at the lower tail of the strength distribution. This applicability covers a broad range of material systems. Regardless if one asserts that graphite should be modeled as a series system, a parallel system, or a mixed series-parallel system, a justification can be given for using the Weibull distribution, at least at low probabilities of failure.

3.4 Non-Weibull-Distribution Models and the Role of the Brittle-to-Ductile-Like Transition

Some of the various models reviewed predicted non-Weibull behavior. For the series-system models in Section 2.1.2.1, the Batdorf model can be made non-Weibull depending on the form of the crack-density function. As discussed in Section 2.1.4, R-curve behavior can cause deviations from the Weibull distribution, although it is asymptotically Weibull at low probabilities of failure and for structures that have large volume. In Sections 2.1.6 and 2.1.7, the strength distributions are non-Weibull, but the uniform defect model has a strength distribution composed of Weibull-like elements. If graphite can be classified as a strongly disordered material system such that it is on the ductile-like end of the brittle-to-ductile-like spectrum of material behaviors (schematically shown in Figure 29), then the strength distribution may be non-Weibull. This was discussed in Sections 2.2.7 and 2.3.2.

3.4.1 Bundle Models and the Brittle-to-Ductile-Like Transition

In Section 2.2.3, with the Daniels (1945) ELS bundle model, strength is normally distributed. As discussed in Section 2.2.4, Smith (1982) argues that the strength distribution is Gumbel distributed, and as discussed in Section 2.2.6, Harlow and Phoenix (1978b) state that the strength distribution is non-Weibull and that ELS bundles do not follow WLT scaling. Mahesh et al. (2002) and Mahesh and Phoenix (2004) indicate that the strength distribution of LLS bundles is neither normal nor Weibull, although it is perhaps closer to Weibull in form, and Mahesh et al. (1999) and Landis et al. (2000) show that ELS bundles approach the Daniels asymptotic results as size increases. Section 2.2.7 shows that fiber composites with very low Weibull modulus fibers behave more like an ELS system. This would analogously correspond to individual ligaments of graphite (the spacing between cracks of pores) having high scatter in strength, where the ligaments act as fibers, or to distributed microcracking with crack arrest. For this material behavior, a Daniels ELS-style model controlled by a normal distribution may be more appropriate.

However, the asymptotic modeling of Mahesh and Phoenix (2004) indicates that at some specified size level extreme-value statistics should dominate—although that size may be very large.

3.4.2 Lattice Models and the Brittle-to-Ductile-Like Transition

In Section 2.3.2, lattice simulations indicate that weak disorder systems behave like a brittle material (governed by extremal statistics) and that moderate to strong disorder is required for the material to become ductile-like with distributed damage. This transition is probably not abrupt. In Section 2.3.3, weak disorder systems are said to follow either the Weibull or Gumbel extremal statistics. For strong disorder systems with distributed damage, the lattice simulations by Nukala and Simunovic (2004) indicate that fracture strength is neither Weibull nor Gumbel but fits the lognormal distribution best. In contrast, Alava et al. (2006) note that it remains to be explored if a crossover to Weibull or Gumbel occurred at larger size scales. Alava et al. (2006) also shows that, when embedded cracks were significantly larger than the background defects (the individual lattice elements), the large defect behaved according to classical LEFM and, therefore, populations of large relatively isolated defects should likely behave according to extremal statistics—that is, Weibull or Gumbel distributions. Finally, if Bazant and Pang (2007) are correct, the lower tail of the strength distribution should always be Weibull, and this is probably regardless of the level of disorder in the system.

3.5 The Physical Interpretation of the Weibull Modulus

The Weibull modulus m calculated from fracture experiment results represents strength response resulting from a variety of phenomena. For classically brittle materials, such as glasses and some ceramics, the Weibull modulus can be directly related to the size distribution of inherent flaws by the rules of LEFM. For polycrystalline materials where the presence of grains may provide additional resistance to fracture, the Weibull modulus becomes a function of the size distribution of inherent flaws and the physics of crack growth (rising R-curve). This is true when porosity may arrest crack growth as well. For composite materials, the presence of fibers and the fiber load-sharing rules modify the Weibull modulus of the individual constituents (the fibers).

Microcracking (distributed damage) also apparently affects the Weibull modulus. Afferrante et al. (2006) examined an idealized array of in-plane microcracks and concluded that the Weibull modulus is not solely related to the defect distribution, finding that Weibull modulus depends on both the distribution of crack sizes and the distribution of ligaments (spacing between cracks). Li and Fok (2009) and Nemeth et al. (2011) indicate that the observed Weibull modulus could be affected by the nonlinear stress-strain response. So although the Weibull modulus can be regarded as a characteristic of a material, it is not necessarily a function of a single physical quantity. This appears to be the case for graphite, where multiple mechanisms—such as the defect distribution, the R-curve, crack arrest from porosity, and microcracking—likely play a role. What is not clear is how strong a contribution each constituent plays in determining the overall stochastic strength response for graphite.

Bazant and Pang (2007) assert that the observed or macroscopic Weibull modulus is a result of the interplay of the Maxwell-Boltzmann distribution of thermal energies modeled as a power law of exponent 1 at the atomic level modified by the scaling up of the material system at various levels of series and parallel systems. In the end, the Weibull modulus observed from fracture experiments can arise from multiple and synergistic phenomena whose source and limitations must be considered carefully.

3.6 Strength Dispersion, Size Effect, and Material Volume

The Weibull modulus m is a measure of scatter in strength. An important question is whether m (or strength dispersion) can vary with volume and whether this is related to the size effect. It is the opinion of the authors that the experimental studies cited do not strongly support this assertion (that m changes with volume—except in the case of concurrent flaw populations), but it is worth considering since some models described here indicate that it may. The Weibull distribution (Eqs. (8) and (9)) implies that m is

constant with volume as well as independent of specific geometry provided that the material can be treated as a continuum. However, Batdorf (1975) shows that physically based criterion can be constructed where *m* changes with volume. The preponderance of literature regarding fracture experiments on brittle ceramics and glasses does not support a general trend of *m* changing with volume—except in the case where the flaw population is changing (i.e., multiple concurrent or partially concurrent populations). In materials with multiple concurrent (mutually exclusive but simultaneously occurring) flaw populations with different *m* values, the flaw population with the lower *m* will dominate in higher volume structures. This is because more material is present, increasing the likelihood that a scarcer flaw type will be present in the structure—akin to a spin of a roulette wheel, where the more times the wheel is spun, the greater the chance that a particular number will be selected at least once. In that situation, *m* will actually decrease with volume. An excellent discussion of multiple flaw populations and their effects on fracture statistics can be found in Johnson (1983).

The general situation that measuring *m* consistently from data sets can be problematic (e.g., Tennery and Ferber (1989)) plus the lack of forensic evidence from the fractography of graphite makes any assertion of Weibull modulus variability with volume more difficult to prove. Another potential problem arises if surface-residing defects affect the failure of the material differently than volume-residing defects do. If surface defects are a distinct population from volume defects, then bending tests could show a different *m* from tensile tests. Results from Price (1976) and the subsequent reanalysis of that data by Nemeth et al. (2011) show this possibility. In that case, Weibull reliability analysis has to be performed as a function of both the structure volume and the surface (see Nemeth et al. (2003, 2005) for a description of the methodology). This also accounts for the differences in stress distribution when the integration shown in Equation (6) is performed either over the volume of the structure or over the surface area of the structure. The reliability (or survival probability) of the structure is then the product of the reliability of each independent volume-flaw-controlled and surface-flaw-controlled failure mode. However, as previously indicated by Li and Fok (2009), the difference in Weibull moduli observed in flexural loading versus tensile loading could be attributed to a nonlinear stress-strain response.

The examined literature shows mixed results with regards to size effect (see Sec. 1.4). Weibull methodology (see Eqs. (8) to (12)) seems to apply for flexural specimens (i.e., four-point- and three-point-bending bar testing). For tensile specimens, the size effect is rather negligible—considerably less than that expected from Equation (12). If one assumes that the tensile testing was performed without systematic error, then this trend is not consistent with Weibull methodology. This has led some to criticize use of the Weibull methodology for graphite. Compounding the issue are fracture tests that show lower-than-expected strength (from Eq. (12)) for small specimens. The apparently different tensile and flexural failure behaviors raise the suspicion that they may have different failure modes.

Several of the models in this review predict a dimunition of size effect with increasing volume and a simultaneous decrease of strength scatter. Of the models cited herein for predicting size effect, the Batdorf model (see Sec. 2.1.2.1) behaves identical to the Weibull model (Eqs. (8) and (9)) when the crack-density function is a power law. Calculations made using the crack-density functions derived from the McClintock model of intergranular cracks showed that size effect and strength scatter decreased with increasing volume (*m* increased). For the Rose-Tucker, Burchell, and Tucker-McLachlan microstructural models (see Sec. 2.1.6), good qualitative and quantitative success in predicting size effect was reported (Tucker et al. (1986) and Tucker and McLachlan (1993)). This includes accounting for the dropoff in strength for small specimens (attributed to the fracture mechanics effects of a small crack on the order of grain size existing on the specimen surface). Relative scatter in strength versus volume was not reported in these references.

For the parallel-system models, it was shown that size effect and strength distribution generally decrease with increasing volume. This is true for ELS and LLS bundle models spanning the more brittle to more ductile-like range of rupture behaviors (see Sec. 2.2 to 2.3.3 for specific details). However, for LLS bundle models, it may be inferred that size effect and strength dispersion will asymptotically obey a Weibull distribution for increasingly larger volumes. This is argued because of the WLT assumption that the models are built on and the asymptotic Weibull behavior predicted at low probabilities of failure (also

see Sec. 3.6.1). The authors herein believe that, for the bundle models, the LLS model is more representative of the graphite failure process than are the ELS models because of the likely role that stress concentration would play near nucleating microcracks.

Somewhat similar to LLS model trends, Bazant and Pang (2007) indicate a bimodal behavior in a material where, at the RVE level, a Weibull distribution predominates over a normal distribution at low failure probabilities. As volume is increased, the Weibull distribution predominates at higher and higher failure probabilities, and a classic Weibull size effect occurs. For lattice models, the level of disorder in the system determines fracture behavior, strength dispersion, and size effect. For low to moderate disorder, size effect and strength dispersion behavior should follow extreme-value distributions like the Weibull. However, for strong disorder lattice models strength distribution appears to be lognormal and size effect decreases very slowly with system size. This is discussed in Section 2.3.3.

For the parallel-system models, the Daniels asymptotic model (see Sec. 2.2.3) has no size effect, the distribution is normal, and the standard deviation of strength varies as $1/\sqrt{n_f}$. In Section 2.2.4 it was indicated that ELS bundles have a WLT size effect related to the length of the bundle, but the size effect decreases with increasing n_f and this is true regardless of fiber length. In Section 2.2.5 a size effect was indicated, although always smaller than that for the individual (Weibull) fiber constituent. The size effect and standard deviation of strength decreased with system size—the standard deviation of strength being related by perhaps $1/\ln(n_f)$. Also Batdorf and Ghaffarian's theory of multiplets shown in Figure 22 related size effect to piece-wise Weibull segments, showing that size effect decreased (a function of the local Weibull modulus) as volume increased. As discussed in Section 2.2.6, Mahesh et al. (1999) and Landis et al. (2000) show in ELS simulations that mean strength and standard deviation decreased with increasing composite size and that stress concentration failure was driven by a process that followed WLT. ELS bundles approached Daniels's asymptotic results, implying that size effect would be nonexistent at large system sizes. Bazant and Pang (2007) indicate a bimodal behavior in a material where, at the RVE level, a Weibull distribution predominates over a normal distribution at low failure probabilities. As volume increases, the Weibull distribution predominates at higher and higher failure probabilities and a classic Weibull size effect occurs. However, the observed effect is that strength scatter and size effect decrease as volume increases unless the structure size is very large relative to the RVE (see Figure 25). As discussed in Section 2.3.3, Nukala and Simunovic and Zapperi and Nukala indicate that, for strong disorder and large system sizes, the size effect is small and the strength is decreasing very slowly in proportion to $1/(\ln L)^{0.15}$.

3.6.1 The Functional Relationship Between Size Effect and Strength Dispersion in Weakest-Link Theory

In fact, strength scatter and size effect are related for WLT-controlled failure-prediction methodologies (Weibull, Batdorf, Burchell, and chain of bundles). This is easily illustrated by taking the double logarithm of Equation (49) for two different volumes of material, V_1, and V_2, under tensile loads σ and expressing it as

$$\ln\ln\left(\frac{1}{1-P_{f,V_2}(\sigma)}\right)=\ln\left(\frac{V_2}{V_1}\right)+\ln\ln\left(\frac{1}{1-P_{f,V_1}(\sigma)}\right) \tag{60}$$

What this equation says is that, on a Weibull plot (i.e., $\ln\ln[1/(1-P_f)]$ versus $\ln\sigma$) where an arbitrary (Weibull or non-Weibull) WLT-based probability-of-failure function, $P_{f,V}(\sigma)$, is $P_{f,V_1}(\sigma)$ for volume V_1 and is $P_{f,V_2}(\sigma)$ for volume V_2, then for volume V_2, this function will displace vertically (i.e., along the $\ln\ln[1/(1-P_f)]$ coordinate axis) by a constant amount of $\ln(V_2/V_1)$ for any given value of stress σ. If $V_2 > V_1$, then the function will displace vertically upward on the graph.

If one looks at the local slope of a small segment of the curve $P_{f,V_1}(\sigma)$, which would be the local Weibull modulus m_{local} (between the increments σ and σ + Δσ), the vertically displaced portion of the curve will maintain the same local slope for $P_{f,V_2}(\sigma)$: that is,

$$m_{\text{local}} = \frac{\ln\ln\left(\frac{1}{1-P_{f,V_1}(\sigma+\Delta\sigma)}\right) - \ln\ln\left(\frac{1}{1-P_{f,V_1}(\sigma)}\right)}{\ln(\sigma+\Delta\sigma) - \ln(\sigma)} = \frac{\ln\ln\left(\frac{1}{1-P_{f,V_2}(\sigma+\Delta\sigma)}\right) - \ln\ln\left(\frac{1}{1-P_{f,V_2}(\sigma)}\right)}{\ln(\sigma+\Delta\sigma) - \ln(\sigma)} \tag{61}$$

which is easily shown from Equation (60). Provided that m_{local} is constant over a sufficient interval of failure probability, the local size effect will be $\Delta\ln\sigma_{\text{local}} = (1/m_{\text{local}})\ln(V_2/V_1)$, where a small m_{local} indicates a large-size effect and large m_{local} indicates a small-size effect (see Eq. (12)).

The visual effect of this relation can be seen in Figure 25(b), where the curve $P_{f,V}(\sigma)$ is displaced upward vertically as the volume (or system size) increases. For WLT models, the $P_{f,V}(\sigma)$ curve that characterizes the model should be normalized to the volume of the RVE as per Bazant and Pang (2007).

Consider that the curve $P_{f,V_o}(\sigma)$ for a characteristic volume V_o spans an entire range of values of ln ln[1(1 – P_f)] from negative infinity to positive infinity. On a Weibull plot, the shape of the curve for any other value of volume $P_{f,V}(\sigma)$ is identical to that of $P_{f,V_o}(\sigma)$ except that the curve is displaced vertically by $\ln(V/V_o)$. Therefore, the functional interpretation of Figure 25(a) and (b) appearing to show decreased strength scatter and size effect with increasing volume (or system size) is that it simply reflects the "master" curve $P_{f,V_o}(\sigma)$ being displaced vertically by $\ln(V/V_o)$. The appearance of change in size effect with increasing volume only means that a particular event that has a low probability of occurrence (a low probability of failure) within volume V_o has a higher probability of occurrence (a higher probability of failure) in a larger volume V. It also means that strength scatter and size effect are intimately related in WLT models: low scatter in strength translates to small-size effect and vice versa.

Another practical consideration concerns fracture specimen testing. A criticism of specimen testing is that it does not sample the probability-of-failure curve at low probabilities of failure, but Equation (60) clearly shows that this range can be sampled simply by increasing the (effective) volume of the specimens. Specimens with effective volume on the order (or larger if possible) of the effective volume of components will reduce the uncertainties associated with extrapolation to low probabilities of failure. In fact, pooling (combining) the data from a reasonable number of standard size samples with that of a smaller number of larger sized specimens can characterize the probability-of-failure distribution down to low failure probabilities (for a curve normalized to the small-size geometry). This is achieved by using Equation (60) to graft the large specimen data to the small specimen data. Unfortunately, specimens of an unreasonably large size are probably required in order to reach sufficiently low probabilities of failure.

3.6.2 Weibull Modulus, Size Effect, and Scaling Issues Versus Trends in Experimental Data

Specimen sizes tend to be small in comparison to a reactor brick—making the scaling issue an important consideration for a life-prediction methodology for graphite. Depending on the loading situation, the Weibull methodology may predict a large percentage decrease in the mean strength of a brick relative to measured mean specimen strength, which a designer may regard as overly conservative. Because the Weibull moduli measured from specimen data are notoriously variable (Tennery and Ferber (1989)), a common practice is to determine m from size-effect studies—correlating m with the observed decrease in strength as size is increased. However, the negligible size effect observed from some

experimental studies implies a much larger *m* (not considering small-specimen fracture effects) in comparison to *m* estimated from fracture experiments of fixed specimen size. As explained in Section 3.6.1, scatter in strength and size effect are functionally related for weakest-link-series systems. If we assume that the reported experimental data for tensile failure are not in error, then some correction to life-prediction methodology may be required (or one may need to test larger specimens to avoid orders of magnitude extrapolation). The Rose-Tucker, Burchell, and Tucker-McLachlan models have reported success at predicting diminution (decay) of size effect with specimen size, but as Equation (60) points out, this decrease should also correlate with decreased scatter in fracture strength. This trend has not been clearly and consistently observed in experimental data.

Fracture in flexure seems to obey Weibull methodology reasonably, but fracture in tension does not correlate as well with regard to size effect. This raises a question of whether flexural loading and tensile loading have different fracture behaviors. If so, are they competing failure modes, or are they a single failure mode that manifests itself differently with different loading? Further study of this question is needed. In addition, it would be interesting to know how sensitive bending stress is to surface finish (surface roughness). For ceramics, strength in flexure is quite sensitive to the surface finish. However, this effect may be negated for graphite when open porosity at the surface is larger than grinding-induced damage.

Microstructure-based models have to account for the physics taking place within the RVE. The size of the RVE may be relatively large. If the RVE is roughly three times the size of the maximum inhomogeneity, then the RVE of nuclear-grade graphite may be 12 mm or larger (recall that grain size in nuclear-grade graphite is defined as being less than 4 mm and greater than 100 μm). Therefore, typical specimen cross-section dimensions for tensile fracture testing could be sampling within the RVE level. It is unclear how this may have affected experimental studies. The Bazant-Pang model assumes mixed series-parallel systems with the observed Weibull modulus ultimately a function of atomic force interactions. Does this make sense for all material systems? For classically brittle ceramics, the Weibull methodology has been successful, and it seems that fracture mechanics and a prescribed distribution of intrinsic flaws provide an adequate explanation. However, for quasi-brittle materials, the Bazant-Pang modeling approach may be more appropriate and certainly some of the historical roots of this methodology go back to Harlow and Phoenix (1978a,b).

3.7 Watson-Smith-Style Modified Weibull Distribution

It is suggested herein that the Harlow and Phoenix (1978b) WLT chain-of-bundles model (Eq. (48)), along with the modified Weibull relation proposed by Watson and Smith (1985) (Eq. (51)), could be used to empirically model graphite strength and the smaller-than-expected size effect (as predicted by the Weibull distribution in Eq. (12)) observed in tensile loading. This would be in contrast to the modified Weibull model of Schmidt (2000) described in Section 2.1.5, which posits that there is no size effect with regard to the size of a specimen but that there is a size effect between tensile and flexural loadings. The proposed relation decouples the size effect from the strength scatter. On that basis, the following equation could be considered for uniform uniaxial tensile loading of a constant material cross section

$$P_f = 1 - \exp\left[-\left(\frac{V_\delta}{V_{\delta,o}} \right)^{\varphi_1} \left(\frac{n_\delta}{n_{\delta,o}} \right)^{\varphi_2} V_{\delta,o}\, n_{\delta,o}\, W(\sigma) \right] \tag{62}$$

where $W(\sigma)$ is some function of σ. For a power-law formulation of $W(\sigma)$, a modified Weibull equation is obtained

$$P_f = 1 - \exp\left[-\left(\frac{V_\delta}{V_{\delta,o}} \right)^{\varphi_1} \left(\frac{n_\delta}{n_{\delta,o}} \right)^{\varphi_2} V_{\delta,o}\, n_{\delta,o} \left(\frac{\sigma}{\sigma_{oV}} \right)^{m_V} \right] \tag{63}$$

It is assumed that a potential fracture path is a plane normal to the direction of loading with an associated thickness where microcracks may nucleate and coalesce into a macrocrack. In Equations (62) and (63), a cross section of a volume V_δ of height δ represents a potential fracture plane and n_δ chains of height δ make up the total volume $V = V_\delta n_\delta$. The terms $V_{\delta,o}$ and $n_{\delta,o}$ are characteristic values. The exponents φ_1 and φ_2 are constants between 0 and 1. The height δ represents the average grain height or some small multiple of the average grain height. The exponents φ_1 and φ_2 allow decoupling from the WLT argument. A Weibull relation is obtained as φ_1 and φ_2 approach 1. The assumption of Equation (62)—that there is a fracture plane which has a role in failure—is similar to that of Rose and Tucker (1982). Treating individual fracture planes as a weakest-link-series system yields $\varphi_2 = 1$ and

$$P_f = 1 - \exp\left[-\left(\frac{V_\delta}{V_{\delta,o}} \right)^{\varphi_1} V_{\delta,o}\, n_\delta \left(\frac{\sigma}{\sigma_{oV}} \right)^{m_V} \right] \tag{64}$$

If φ_1 and φ_2 are equal ($\varphi_1 = \varphi_2 = \varphi$) in Equation (63), then the modified size effect is only a function of volume and

$$P_f = 1 - \exp\left[-\left(\frac{V}{V_{ox}} \right)^{\varphi} V_{ox} \left(\frac{\sigma}{\sigma_{o_V}} \right)^{m_V} \right] \tag{65}$$

where V is volume, V_{ox} is some characteristic volume, and φ is a constant between 0 and 1. For a constant value of P_f, this equation linearizes to

$$\ln \sigma = -\frac{\varphi}{m_V} \ln V + c \tag{66}$$

where c is a constant and the Weibull slope is modified to φ/m_V.

Equations (63) to (65) would accommodate the relatively negligible size effect reported for tensile specimens while keeping the relative amount of strength scatter constant. Prudence would also dictate that Equations (62) to (65) not be applied over too many orders of magnitude of size scaling because of the potential inaccuracy of the scaling approximation or the possible presence of unaccounted-for flaw populations (e.g., the presence of gross flaws behaving in a classic Weibull manner). Equations (63) to (65) are only a starting point and further development to incorporate a methodology for the stress gradient and multiaxial stresses will be needed. However, the simpler route to account for flexural failure is to treat it as a separate competing failure mode (from tensile) that is a function of component surface area. This failure mode would have its own set of Weibull parameters. See Nemeth et al. (2003, 2005) for a further description of the methodology regarding treating volume flaws and surface flaws as separate and competing failure modes.

3.8 The Continuum Assumption and Stress Gradient

The Weibull methodology (as well as the Batdorf methodology) assumes that the material is a continuum and that flaws are small relative to any stress gradient. For the Batdorf methodology, which assumes that the flaws are microcracks, this means that flaws will see no stress gradient across the length of the crack. This is actually a conservative assumption if the highest gradient stress value is used. Bruckner-Foit (2000) considered the effect of stress gradient on volume-distributed flaws for the situation where the stress gradient was so high (such as in thermal shock) that intrinsic microcracks would themselves experience a significant stress gradient. Their simulation showed that the Weibull stress-volume integral (see Eqs. (8) and (9)) overpredicted failure probability (was conservative).

For graphite-reactor-core structures, the stress gradients on flaws are a potential problem because flaws and microstructure can be large relative to the small fillet radii required for block-and-key construction (Figure 3). In addition, the material may not behave as a continuum in these regions because of the large grain size, which of course is a further complication, although this could possibly be handled with the Burchell model. The Bruckner-Foit analysis assumed that the material was a continuum. The handling of stress gradients around singularities (e.g., macroscopic cracks, sharp notches, zero-radius fillets, and bimaterial interfaces) is beyond the scope of this report.

3.9 Problems in and Recommendations for Predicting the Effects of Slots or Notches

Graphite bricks for reactors may be designed with a block-and-key construction (Figure 3(a)) to interlock the bricks and make a stable structure. This technique also allows for individual brick expansion and contraction. However, the graphite bricks may have various slots and protrusions with small-radius fillets. Large stress gradients can occur at these fillets and are a serious concern for the design engineer. Mitchell et al. (2003) tested L-shaped specimens (described in Sec. 1.4) with various fillet radii and could not correlate well with the predicted response using the two-parameter Weibull stress-volume integral with the PIA multiaxial theory (Eq. (21)). They used the Weibull parameters estimated from the rupture of bending bar specimens to predict the strength response of the L-shaped specimens. This study illustrates the limitations and caution that must be exercised when using statistical failure theories.

In Mitchell et al. (2003) the flexural bars failed in the typically energetic fashion of a brittle material, whereas the L-shaped specimens failed in a more stable crack-growth-controlled manner. A fracture mechanics analysis of the L-shaped specimen indicated that the stress intensity factor decreased with crack length, suggesting a stable crack growth mode of failure. The Weibull modulus from the L-shaped specimens also was significantly higher than that estimated from the flexure specimens, potentially indicating a difference in the mode of failure (including also the possibility that machining damage at the root of the fillet may have been greater than that at the surface of the flexural specimens). One of the lessons that may be learned in that study is that, when comparing results from one specimen geometry to another, a similar mode of failure should be maintained (consistency of approach). The fact that they were different raises questions about the fairness of the comparison. The failure theories reviewed herein assume a positive geometry[3]; therefore, positive geometry specimen tests should have been used consistently. A better comparison might have been if notched (with a finite fillet radius) flexural bars or notched cylindrical tensile specimens (that would likely fail in the more energetic fashion of a brittle material) were used rather than the L-shaped specimens. The authors herein conjecture that if Mitchell et al. had obtained the Weibull parameters from a particular radius of the L-shaped specimen and then subsequently applied these parameters to predict the failure response of the other fillet radii, better correlation to the experimental data would likely have been achieved.

Mitchell et al. also indicated a very high Weibull modulus of 54.4 for the zero-radius fillet of the L-shaped specimen. The high value may have been a consequence of the stress singularity, which probably acted as a large crack of a deterministic size. Choi and Salem (1992) show that strength scatter decreases when a deterministic crack size is introduced (in this case from an indenter), as was discussed in Section 1.4. The Mitchell et al. (2003) study illustrates a potential shortfall of the current statistical failure theories, and future modeling enhancements for stable crack growth should be considered. Note that Li and Fok (2009) also modeled the behavior of the L-shaped specimen from Mitchell et al. (2003) with interesting results, although it is not clear if they could fully explain the high-Weibull-modulus results from the zero-radius fillet of the L-shaped specimens.

It is the opinion of the authors herein that rupture data from notched tensile specimens or notched bending specimens (with a nonzero fillet radius) should be used to predict the probability of failure of the fillet regions of reactor bricks, and data results from flexural or tensile specimens should not be used for this purpose. Therefore, the statistical failure of a graphite brick should be predicted from a database

[3]Positive geometry: Stress intensity increases with increasing crack size, otherwise the crack gets arrested.

consisting of a combination of tensile-specimen, flexural-specimen, and notched-specimen (tensile and/or flexural) data. Also, the statistical failure theories reviewed herein were not developed to analyze stress singularities, such as sharp notches, zero-radius fillets, or cracks; therefore, they should not be applied without properly accounting for the singularity condition (a subject beyond the scope of this report). A final note is that Weibull methodology has been used to successfully predict the failure response of specimens that have stress concentration from tensile specimens that have no significant stress concentration. This was shown, for example, in Sharpe et al. (2008) for silicon carbide microtensile specimens. In that study, 3-mm-long microtensile specimens were used to successfully predict the strength response of microtensile specimens with a central circular hole that was 0.1 mm in diameter. Since the material was single crystal, continuum-based stress analysis was still operable at this size level.

3.10 Regarding Multiaxial Stresses and Anisotropic Strength

Multiaxial strength response and anisotropic strength response were discussed briefly in Sections 2.1.2.2 and 2.1.3, respectively. This was not a comprehensive study of either topic. However, the Batdorf-style approach that was presented appears to match the experimental data satisfactorily. The Burchell model has also been used to model the anisotropic strength response (Burchell et al. (2006)) using a PIA modeling approach, but those results are not reported herein.

3.11 Regarding the Burchell Model for Graphite

The Burchell (and Tucker-McLachlan) model was developed specifically for nuclear-grade graphite. The Burchell model combines a microstructural basis with a fracture mechanics approach to failure. Graphite is not considered to be a continuum in the model, even though a continuum-based stress solution is used. Data for several physical parameters are required, and the model may be fine tuned to match experimental fracture data. The Burchell model directly accounts for some R-curve behavior. The model does not consider flaw interaction, although it is not clear how important that omission is for graphite. Lattice simulations of notch sensitivity (Alava (2006)) show that this sensitivity depends on the size of the cracklike voids relative to the background defects (and probably also the density of cracklike voids).

The Burchell model depends on micrographs to obtain a characteristic pore-size distribution. That raises the possibility that rare, but ultimately strength-controlling, large flaws may not be sampled. This scenario was confirmed by Abe et al. (2003) in relating flaw-size populations to measured strength in alumina. They observed that scanning electron microscopy provided insufficient information on defects relevant to strength variation because only a small portion of a specimen could be examined in comparison to a transmission optical micrograph of a thinned-out section of a specimen, which was used to measure the size distribution of defects over a significantly larger volume. Therefore, to be useful for design to low probabilities of failure, a representative volume (or surface area) of material should be examined to characterize the distribution of the sizes of defects in the Burchell model.

The Burchell model is intriguing and has been reported to be quite successful in matching experimental results. However, a word of caution is in order. If the Burchell model shows that size effect decreases with increasing volume, this means that scatter in strength also decreases at larger volumes (see Eqs. (34) and (35) and Sec. 3.6.1). Using this model to predict strength for larger volumes and low probabilities of failure may result in a nonconservative design if scatter in graphite strength does not also decrease with increasing volume (increasing Weibull modulus with increasing volume).

The Burchell model should be developed further and incorporated in life-prediction codes such as CARES/Life (Nemeth et al. (2003, 2005)). It would be valuable to have available a software tool with the various statistical models of graphite failure in order to contrast and benchmark the various models.

3.12 Regarding Probabilistic Design

Probabilistic design is a very important feature of any life-prediction methodology for graphite. This means accounting for other sources of variation that may influence the failure probability of graphite components over their lifetime of service, including variability in thermomechanical loading, boundary conditions, and material properties (as well as variation of these properties over time including the effects of irradiation). The methodology to achieve this was demonstrated for ceramics and microelectromechanical systems by Reh et al. (2003), Jadaan and Trethewey (2006), Nemeth et al. (2007), and Luo et al. (2007). These papers attempt to analyze problems for a complete probabilistic design space. For the ANSYS/CARES probabilistic design system (Reh et al. (2003)), this means simulating the effect of variability in material properties, boundary conditions, and loading on component probability of failure, including simulating variability in Weibull parameters, accounting for billet-to-billet variations or uncertainties in the value of estimated Weibull parameters from specimen data. This methodology requires performing repeated simulations (for randomly chosen sets of conditions) in an optimized manner (so as to run as few a number of simulations as possible) to determine a distribution of failure probability.

3.13 Final Comments

The simplicity of the Weibull distribution is an attractive feature for the design engineer, and now a substantial body of knowledge has been developed regarding the methodology (parameter estimation, confidence bounds, data pooling, etc.) and how physical processes manifest themselves in the strength response that is approximated by the Weibull distribution. It is therefore premature to dismiss this distribution, or its variants (such as Batdorf), as not being appropriate for graphite design. Microstructurally based models of graphite also are important because they simulate the physics of the material system and provide further insight into material behavior and avenues for improving the material. Ultimately, multiple theories of material breakdown may be required to span the full range of potential and progressive failure modes. Also, the importance of an appropriate database (and an appropriately designed database) for tensile specimens, flexural specimens, notched specimens, and size-effect studies cannot be overemphasized.

The review of the literature cited herein indicates that significant progress has been made toward physically based statistical models that can explain failure across disparate material systems and that can accommodate the brittle-to-quasi-brittle spectrum of material failure modes. Ultimately, mathematically refined theories of fracture will be useful only to the extent that the associated stress analyses are equally accurate and that also includes considering the effect of nonlinear stress-strain response and bimodulus (different stress-strain response between tension and compression) material behavior.

This report has only addressed the issue of stochastic material strength independent of environment and time of exposure. Graphite-moderated reactors are intended to have a service life of 30 to 60 years, so durability and damage growth methodology is required to show at least a viable design estimate. Therefore, there is also a need to develop time-, cycle-, and environment-dependent reliability prediction models that can assess graphite performance over these extended time periods.

4.0 Conclusions

The fracture of nuclear-grade polycrystalline graphite is a function of the distribution, interaction, and growth kinetics of flaws of various forms and size scales. Graphite fracture strength is stochastic, and any theory of graphite failure must accommodate this fact. This report described various statistical models of brittle-constituent-controlled material failure. All these models assumed that material breakdown begins at inherent flaws or weak regions in the material. However, the various models differ in how material breakdown proceeds. This was broadly categorized into series-system or parallel-system models. Series-system models describe a weakest-link mode of material failure, and the Weibull, Batdorf, and Burchell

models were described. Parallel-system models describe the process of accumulating damage leading to ultimate material failure, and composite fiber-bundle models and lattice models were described. For parallel-system models, additional attention was given to the expected transition between brittle and quasi-brittle (ductile-like) behavior, particularly since nuclear-grade graphite is often described as quasi-brittle. Composite material modeling was included for the modeling insights it provides. Results from lattice simulations were included for a physics-based description of material breakdown.

The literature indicates that WLT modeling approaches cover a broad range of material systems; however, material systems with very strong disorder may not show WLT behavior until component sizes are very large. The Weibull distribution was argued to be the most appropriate statistical distribution for modeling the stochastic strength response of graphite. Consideration also was given to size effect and multiaxial strength response. Awareness of these modeling approaches provides additional perspective and potential avenues of inquiry that may be useful in selecting methodologies for designing graphite components by standards and regulatory organizations such as ASME International and the Nuclear Regulatory Commission.

Appendix A.—Uniform Defect Model Approximated as a Weibull Distribution

Weibull statistics are typically used to describe the behavior of classically brittle materials for tensile stress states only. This is appropriate because the WLT is a series system where a single event (uncontrolled crack propagation from a flaw) determines the integrity of the whole system. For compressive stress states, this model does not rigorously apply. The unequal principal compressive stresses ($\sigma_3 \leq \sigma_2 < \sigma_1$) produce shear stresses on arbitrarily oriented cracks that act against compressive normal forces on the crack face. This produces tensile stresses at the crack tips and the crack branches parallel to the direction of maximum compression. The crack growth is eventually arrested when the tension at the crack tip decreases below a critical level and an equilibrium condition is reached with the applied compression. A single event of crack extension, therefore, does not necessarily result in material failure. However, if a number of events of crack growth and arrest take place in a sufficiently confined region where they can join together and create what is known as a shear fault, then total failure ensues.

Weibull statistics and Batdorf methodology have been applied by Alpa (1985) to access material integrity in compression. This modeling scheme uses a WLT methodology to predict the first event of crack extension (initiation of damage). The Weibull modulus for compressive stress states and tensile stress states is assumed to be the same since the strength response is controlled by the same flaw population. Alpa's model predicts a Weibull size effect for compressive stresses similar to the tensile stress response. The basis for using the WLT to describe strength in compression is justifiably open to question. Kittl and Aldunate (1983) tested compact cement cylinders in compression, and a best-fit distribution could not be determined with a high level of confidence. Figure 30 shows lines of best fit to the 575 specimens tested for the normal, lognormal, and three-parameter Weibull distributions. Experiments measuring the compressive strength of specimens often show smaller scatter (higher Weibull modulus) and size effect than the tensile strength. The approach of employing separate Weibull moduli for tension and compression (described in Sec. 2.1.2.2) improves the correlation to measured data; however, the justification for doing this is somewhat arbitrary. The following is an argument that the uniform defect model (see Sec. 2.1.7) can be approximated as a Weibull distribution. This may help as a justification for using a Weibull distribution for strength in compressive stress states and for treating compressive failure and tensile failure as independent failure modes.

The crack-density function $\eta_V(\sigma_{1c})$ is defined to represent the average number of microcracks per unit volume with a critical mode I strength equal to or less than σ_{Ic}. A random volume flaw in a multiaxial stress field can be oriented such that there is a combination of a compressive normal force and a shearing force causing the critical mode stress intensity to be exceeded at the crack tips. The flaw is assumed to extend in a stable manner until its growth is eventually arrested. For an appropriately sized incremental volume element ΔV_d it is assumed that as the magnitude of the applied stress is increased, the number of critically oriented flaws that experience damage (stable crack extension) increase in accordance with the crack-density function. Each event of crack extension creates new surface within the incremental volume. When the total amount of new surface area per unit volume reaches a critical ratio, or alternatively, when the number of flaws n_d that experience growth within ΔV_d reaches a critical number n_{dc}, local material failure is assumed to occur. Therefore, a failure criterion for the RVE is constructed such that

$$\begin{aligned} n_d < n_{dc} &\text{ indicates that damage is not critical in } \Delta V_d \\ n_d \geq n_{dc} &\text{ indicates local material failure in } \Delta V_d \end{aligned} \tag{A1}$$

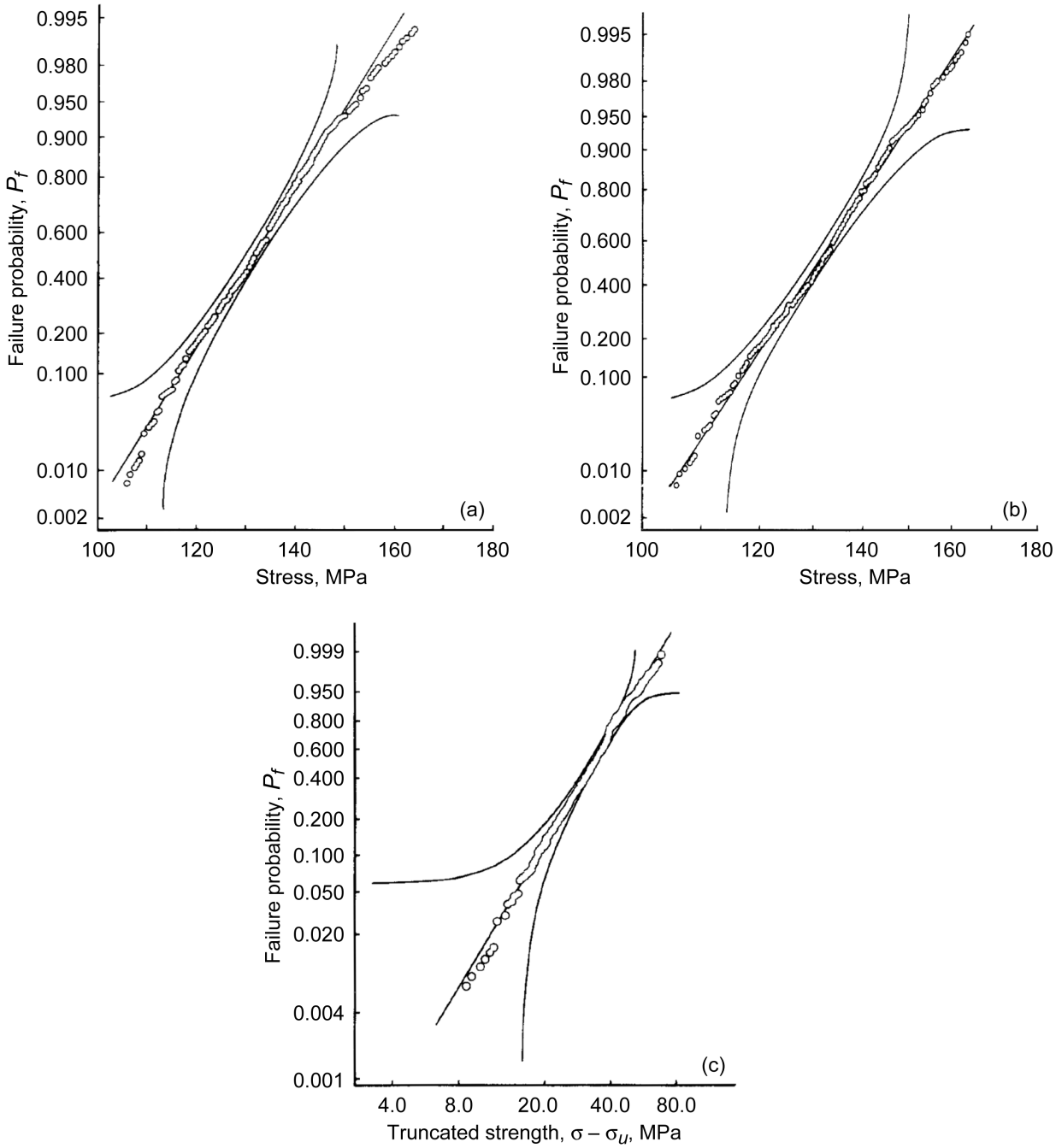

Figure 30.—Strength failure probability distributions versus strength of 575 cement cylinders tested in compression. Although statistical tests do not reject one distribution over another, the lognormal distribution subjectively appears to be slightly better than the normal distribution. (a) Shown in normal (gaussian) probability coordinates. (b) Shown in lognormal probability coordinates. (c) Shown in Weibull probability coordinates with a three-parameter distribution and a threshold stress σ_u of 97 MPa. Reproduced from Kittl and Aldunate (1983). Copyright Springer Publishing Company; used with permission.

for an applied compressive stress. In addition, some conservative and simplifying assumptions are made:

(1) The flaws are independently and uniformly distributed throughout the material volume
   (a) The defects arise at separate sites (there are no overlaps).
   (b) The number of defect occurrences in separate volumes are independent random variables.
   (c) The number of defect occurrences is independent of position.
(2) Local material failure constitutes component failure (or what could be defined as a damaged or rejected component).
(3) Crack growth is mutually exclusive—interactions between adjacent cracks are not considered (in other words, how the flaws interact and how the surrounding material is affected is not considered).
(4) ΔV_d is small (on the order of the critical crack length that spans the volume element).

Following Freudenthal's (1968) reasoning, assumption (1) allows for the construction of a spatial-point Poisson process (from which the Poisson distribution derives). The Poisson distribution models the probabilistic distribution of random particles in space or events in time. This probability distribution is an approximation to the binomial distribution for so-called rare events when the probability of occurrence of an event is close to zero. The Poisson distribution is represented as follows:

$$P\left(X = x\right) = \frac{\lambda^x e^{-\lambda}}{x!} \tag{A2}$$

$P(X = x)$ is the probability that the discrete random variable X takes on the values $x = 0, 1, 2, 3, ...$, and $\lambda = n P_{\text{event}}$, where n is the sample size and P_{event} is the probability of an event. As an aside, it is worthwhile to note the property that

$$e^{-\lambda} \sum_{x=0}^{\infty} \frac{\lambda^x}{x!} = 1 \tag{A3}$$

which validates that the Poisson distribution is a probability function.

The probability of failure in the material element ΔV_d is the probability that more than one flaw (at least n_{dc} number of flaws) grows within this incremental volume, and therefore for $\lambda = V_d \eta(\sigma_{Ic})$,

$$P_{f\{\Delta V_d\}} = P\left(X \geq n_{dc}\right) = e^{-\lambda} \sum_{x=n_{dc}}^{\infty} \frac{\lambda^x}{x!} \tag{A4}$$

or in terms of the survival probability

$$P_{s\{\Delta V_d\}} = P\left(X < n_{dc}\right) = e^{-\lambda} \sum_{x=0}^{(n_{dc}-1)} \frac{\lambda^x}{x!} \tag{A5}$$

Note that how the applied compressive stress acts to extend a crack is not considered. For $\lambda << 1$, then $e^{-\lambda} \cong 1$ and the higher order terms in Equation (A4) can be neglected. This allows Equation (A4) to be simplified as

$$P_{f\{\Delta V_d\}} \cong \sum_{x=n_{dc}}^{\infty} \frac{\lambda^x}{x!} \cong \frac{\lambda^{n_{dc}}}{n_{dc}!} \tag{A6}$$

If $\lambda = \Delta V_d \eta(\sigma_{Ic})$ is substituted into Equation (A6), then the elemental failure probability can be approximated by

$$P_{f\{\Delta V_d\}} \cong \frac{\left[\Delta V_d\, \eta(\sigma_{Ic})\right]^{n_{dc}}}{n_{dc}!} \tag{A7}$$

If a volume V is discretized into n incremental units such that $n = V/\Delta V_d$, the probability of survival of V is the product of the incremental probabilities of survival (see Eq. (1)):

$$\begin{aligned} P_{sV} &= \prod_{i=1}^{n}\left(P_{s\{\Delta V_d\}}\right)i = \prod_{i=1}^{n}\left(1 - P_{f\{\Delta V_d\}}\right)i \\ P_{sV} &\approx \prod_{i=1}^{n}\exp\left[-P_{f\{\Delta V_d\}}\right] = \exp\left[-\sum_{i=1}^{n} P_{f\{\Delta V_d\}}\right] \end{aligned} \tag{A8}$$

where the natural log exponential function can be substituted if $P_{f\{\Delta V_d\}}$ is small. Substituting Equation (A7) into (A8) yields

$$P_{sV} = \exp\left[-V\,\frac{\left(\Delta V_d\right)^{\left(n_{dc}-1\right)}\left[\eta\left(\sigma_{Ic}\right)\right]^{n_{dc}}}{n_{dc}!}\right] \tag{A9}$$

Substituting for the crack-density function $\eta\left(\sigma_{Ic}\right) = \left(\sigma_{Ieq}/\sigma_{oV}\right)^{m_V}$ where σ_{Ieq} describes an effective stress on the flaw from the applied compressive stress (see Eq. (23)) yields

$$P_{sV} = \exp\left[-V\left(\frac{\sigma_{Ieq}}{\left\{\dfrac{\sigma_{oV}\left(n_{dc}!\right)^{1/m_V n_{dc}}}{\left(\Delta V_d\right)^{\left(n_{dc}-1\right)/m_V n_{dc}}}\right\}}\right)^{m_V n_{dc}}\right] \tag{A10}$$

Finally substituting a constant term σ_{ocV} for the expression in the braces {…} and calling this term the scale parameter in compression yields

$$P_{sV} = \exp\left[-V\left(\frac{\sigma_e}{\sigma_{ocV}}\right)^{m_V n_{dc}}\right] \tag{A11}$$

Equation (A11) implies that, with the uniform defect model, failure strength can be approximated by a Weibull distribution with a Weibull modulus term, $m_V n_{dc}$, that is a multiple, n_{dc}, of the Weibull modulus m_V describing the power-law crack-density function exponent. This failure criterion posits significantly decreased scatter and size effect relative to the Weibull distribution with the exponent m_V.

The uniform defect model is a rudimentary model of compression failure, yet the Weibull exponent modified by n_{dc} has interesting parallels with the asymptotic behavior of Batdorf and Ghaffarian (1984) (see Figure 22) and Beyerlein and Phoenix (1996) (see Figure 23) at low probabilities of failure. The point of this exercise was to explore a basis where the Weibull distribution could be justified to describe strength in compression. On the practical side, there are several factors that may contribute to observed scatter in strength and, therefore, the value used for the compressive Weibull modulus $m_{cV} = m_V n_{dc}$ should be obtained from rupture experiments with compressive specimens. Also, strength scatter and size effect may not correlate well. This was reported by Kittl and Aldunate (1983), where no significant size effect

was detected (although the difference between the minimum and maximum volumes tested was not very large). Thus, the modified Weibull distribution of Watson and Smith (1985) to account for unexpectedly small-size effect is probably a good distribution to model strength in compression. The discussion to this point did not consider multiaxial stresses. The Batdorf unit sphere approach could be used to account for multiaxial stress states as described in Sections 2.1.2.1 and 2.1.2.2.

Appendix B.—Flaw Orientation Anisotropy and Stress Intensity Anisotropy

Flaw orientation anisotropy refers to the situation where a flaw has a higher likelihood of being oriented in one direction versus another. This means that a material will be stronger on average in one direction versus another. An isotropic brittle material is equally strong in any direction, and thus its flaws are randomly oriented. However, for components made by processes such as extrusion or hot pressing, which induce texture, a bias will exist in the distribution of processing flaws. Also, components finished by surface grinding will also contain machining damage in the form of cracks that are oriented parallel and transverse to the grinding direction. Salem et al. (1996) explored a methodology for modeling grinding damage. That work assumes that the machining flaws are all closely aligned in one direction. This was based on a more general approach developed by Buch et al. (1977) (specifically for graphite) and further explored by Nemeth (1989) for transversely isotropic strength response.

For volume-distributed flaws, flaw orientation anisotropy relative to a material coordinate system is modeled by introducing a probability density distribution $\wp$ into the Batdorf unit sphere formulation for P_{2V} in Equation (15). For one-half of the unit sphere,

$$P_{2V} = \int_0^{2\pi}\int_0^{\pi/2} \wp(\alpha,\beta) H\left(\sigma_{Ieq},\sigma_{Ic}\right)\sin\alpha \; d\alpha \; d\beta \tag{B1}$$

where

$$\wp(\alpha,\beta) = \frac{\zeta(\alpha,\beta)}{\int_0^{2\pi}\int_0^{\pi/2}\zeta(\alpha,\beta)\sin\alpha \; d\alpha\, d\beta} \tag{B2}$$

and

$$H\left(\sigma_{Ieq},\sigma_{Ic}\right) = 1 \qquad \sigma_{Ieq} \geq \sigma_{Ic}$$

$$H\left(\sigma_{Ieq},\sigma_{Ic}\right) = 0 \qquad \sigma_{Ieq} < \sigma_{Ic}$$

$\wp(\alpha,\beta)\sin\alpha \; d\alpha \; d\beta$ is the probability that a normal vector to the flaw plane is oriented at α,β within the intervals $(\alpha - d\alpha/2, \alpha + d\alpha/2)$ and $(\beta - d\beta/2, \beta + d\beta/2)$.

For a transversely isotropic strength response, ζ is only a function of α. Buch et al. (1977) introduced a cosine power function for $\zeta(\alpha) = [\cos(\xi\alpha)]^{\gamma}$ where ξ and γ are constants. This relation was modified by Nemeth (1989) to enhance the functional flexibility

$$\begin{aligned} \zeta(\alpha) &= \left[\cos(\xi\alpha)\right]^{\gamma} \qquad 0 \leq \alpha \leq \pi/(2\xi) \\ \zeta(\alpha) &= 0 \qquad\qquad\qquad \pi/(2\xi) < \alpha \leq \pi/2 \end{aligned} \tag{B3}$$

or alternatively,

$$\begin{aligned} \zeta(\alpha) &= 0 \qquad\qquad\qquad\qquad\qquad 0 \leq \alpha < \pi/2 - \pi/(2\xi) \\ \zeta(\alpha) &= \left[\sin\left(\xi\left\{\alpha - \left[\pi/2 - \pi/(2\xi)\right]\right\}\right)\right]^{\gamma} \qquad \pi/2 - \pi/(2\xi) \leq \alpha \leq \pi/2 \end{aligned} \tag{B4}$$

where ξ and γ are constants that control the degree of anisotropy, and $\xi \geq 1$ and $\gamma \geq 0$. When $\xi = 1$ and $\gamma = 0$, an isotropic strength response is obtained. Equations (B3) and (B4) are defined for one-half of the unit sphere (the top half of the unit sphere shown in Figure 31). In reference to Figure 31, Equation (B3) represents the "polar cap" or longitudinal distribution of flaws and Equation (B4) represents an

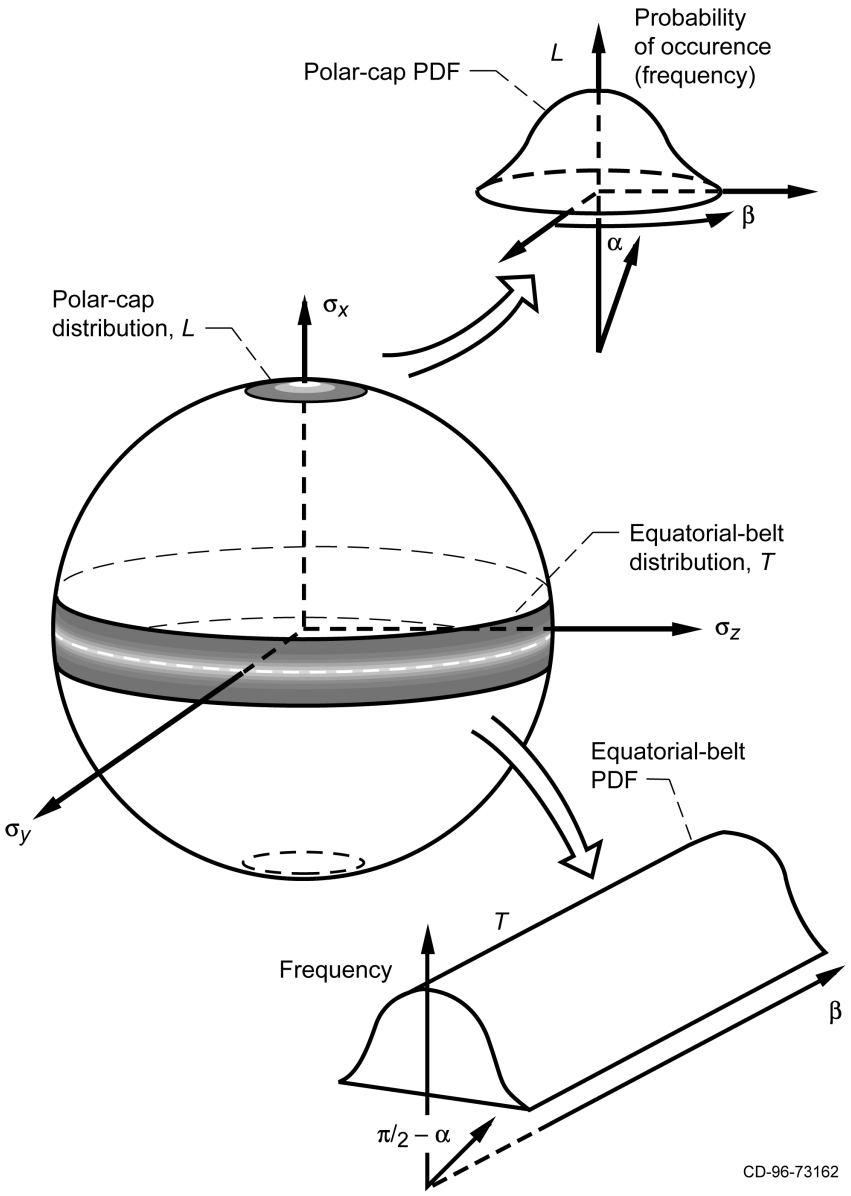

Figure 31.—Unit sphere with probability density distribution functions describing anisotropy of flaw orientation. Orientation is described with the normal to the crack plane. In this figure, two orientation functions are described: (1) a "polar-cap" distribution describing crack planes symmetrically distributed (centered) about a plane (in this case, the σ_y–σ_z plane) and (2) an "equatorial-belt" distribution, where crack planes are symmetrically distributed (centered along a line, in this case, the σ_x axis) and α and β are the angular coordinates.

"equatorial belt" or transverse distribution of flaws. The polar-cap distribution describes crack planes symmetrically distributed (centered) about a plane (in this case the σ_y–σ_z plane), and the equatorial-belt distribution describes crack planes symmetrically distributed (centered) along a line (in this case the σ_x axis). The separate polar-cap and equatorial-belt distributions were originally introduced to describe a unidirectionally fiber-reinforced composite where the polar cap represented the fiber strength distribution and the equatorial belt represented the matrix-fiber interface.

Similar to Equation (19) the strength anisotropy function can be more simply expressed as

$$P_{fV} = 1 - \exp\left[-\int_V \int_0^{2\pi} \int_0^{\pi/2} \wp(\alpha,\beta)\, \eta_V\left(\sigma_{\mathrm{I}eq}\right) \sin\alpha \; \mathrm{d}\alpha \; \mathrm{d}\beta \; \mathrm{d}V \right] \tag{B5}$$

and it should be noted that the crack-density function $\eta_V(\sigma_{\mathrm{I}c})$, as expressed in Equation (17), in this case has a normalized Batdorf crack-density coefficient $\bar{k}_{BV}$ that is a function both of the mixed-mode fracture criterion and the flaw orientation function for an applied uniaxial stress state.

Other quantities that can be made anisotropic with orientation using the Batdorf unit-sphere approach include the crack-density function η, the average size of the flaw, the critical stress intensity factor $K_{\mathrm{I}c}$, and the critical strength $\sigma_{\mathrm{I}c}$. Anisotropic $K_{\mathrm{I}c}$, flaw size, and critical strength $\sigma_{\mathrm{I}c}$ are functionally related quantities. For example anisotropic $K_{\mathrm{I}c}$ can be made functionally equivalent to anisotropic flaw size, and $K_{\mathrm{I}c}$ and $\sigma_{\mathrm{I}c}$ are directly related.

Batdorf (1973) approached strength anisotropy using the $\sigma_{\mathrm{I}c}$ strength ellipsoid approach (describing an ellipsoid rather than a unit sphere). Nemeth (1989) considered strength anisotropy using $K_{\mathrm{I}c}$, where $K_{\mathrm{I}c}$ was a function of the orientation angle on the unit sphere. The approach is similar to that developed for flaw orientation anisotropy described previously. The critical strength $\sigma_{\mathrm{I}c}$ is defined as the fracture strength of the crack in mode I loading and is directly proportional to $K_{\mathrm{I}c}$. Therefore, for anisotropic $K_{\mathrm{I}c}(\alpha,\beta) = (c\ \sigma_{\mathrm{I}c}(\alpha,\beta)) = [\sigma_{\mathrm{I}c\,\max} \bar{f}_{\mathrm{I}c}(\alpha,\beta)]$, where c is a constant, $\sigma_{\mathrm{I}c,\max}$ is the maximum value of $\sigma_{\mathrm{I}c}$ over the unit sphere (for all α,β), and $\bar{f}_{\mathrm{I}c}(\alpha,\beta)$ is a normalized function expressing the degree of anisotropy. For this approach, the unit sphere formulation described in Equations (13) to (19) in Section 2.1.2.2 is used except the Heaviside step function in Equation (18) is modified as follows

$$\begin{aligned} H\left(\sigma_{\mathrm{I}eq}, \sigma_{\mathrm{I}c}\right) &= 1 \quad \frac{\sigma_{\mathrm{I}eq}}{\bar{f}_{\mathrm{I}c}(\alpha,\beta)} \geq \sigma_{\mathrm{I}c,\max} \\ H\left(\sigma_{\mathrm{I}eq}, \sigma_{\mathrm{I}c}\right) &= 0 \quad \frac{\sigma_{\mathrm{I}eq}}{\bar{f}_{\mathrm{I}c}(\alpha,\beta)} < \sigma_{\mathrm{I}c,\max} \end{aligned} \tag{B6}$$

For a transversely isotropic response where anisotropy is only a function of angle α,

$$\bar{f}_{\mathrm{I}c}(\alpha) = 1 - \left|\cos\left(\xi_L \alpha\right)\right|^{\gamma_L} \left(1 - \frac{1}{r_L}\right) \qquad 0 \leq \alpha \leq \pi/\left(2\xi_L\right)$$

$$\bar{f}_{\mathrm{I}c}(\alpha) = 1 \qquad \pi/\left(2\xi_L\right) < \alpha < \pi/2 - \pi/\left(2\xi_T\right)$$

$$\bar{f}_{\mathrm{I}c}(\alpha) = 1 - \left|\sin\left\{\xi_T\left[\alpha - \left(\frac{\pi}{2} - \frac{\pi}{2\xi_T}\right)\right]\right\}\right|^{\gamma_T} \left(1 - \frac{1}{r_T}\right) \qquad \pi/2 - \pi/\left(2\xi_T\right) \leq \alpha \leq \pi/2 + \pi/\left(2\xi_T\right) \tag{B7}$$

where ξ_L, ξ_T, γ_L, γ_T, r_L, and r_T are constants. Equation (B7) is defined for the top half of the unit sphere as shown in Figure 31. The L subscript relates to the polar-cap strength anisotropy distribution for crack planes symmetrically distributed (centered) about a plane (in this case the σ_y–σ_z plane), and the T subscript relates to the equatorial-belt strength anisotropy distribution for crack planes symmetrically distributed (centered) along a line (in this case the σ_x axis) (see also Figure 31 for a reference frame).

Figure 16 shows an example using Equation (B7) to fit to experimental data for anisotropic K_{Ic} measured from a Knoop indenter. Figure 32 shows a hypothetical example of the predicted strength response for a uniaxial load on a unit volume rotated relative to the extrusion direction for shear-sensitive versus shear-insensitive flaws. Penny-shaped cracks (Eq. (20)) are assumed with a Shetty-shear-sensitivity coefficient $\bar{C} = 1.0$ for the shear-sensitive response and $\bar{C} = 100.0$ for the shear-insensitive response. A value of $\xi_L = 18.0$ was used such that the cosine function only spanned a 10° increment between $-5° \le \alpha \le 5°$, which provided a narrow distribution $\bar{f}_{Ic}(\alpha)$ such that the difference between a shear-sensitive and a shear-insensitive response is easily seen. This example was developed to show an approximately 25-percent anisotropy in strength. For the shear-insensitive response, $m_V = 10.0$, $\sigma_{oV} = 100.0$, $\bar{C} = 100.0$, $\bar{k}_{BV} = 21.92$, $\xi_L = 18.0$, and $r_L = 2.215$; and for the shear-sensitive response, $m_V = 10.0$, $\sigma_{oV} = 100.0$, $\bar{C} = 1.0$, $\bar{k}_{BV} = 3.921$, $\xi_L = 18.0$, and $r_L = 2.693$. The T population parameters are not active in this example ($\gamma_T = 0$, $r_T = 1.0$, and $\xi_T = 1.0$ (arbitrarily)).

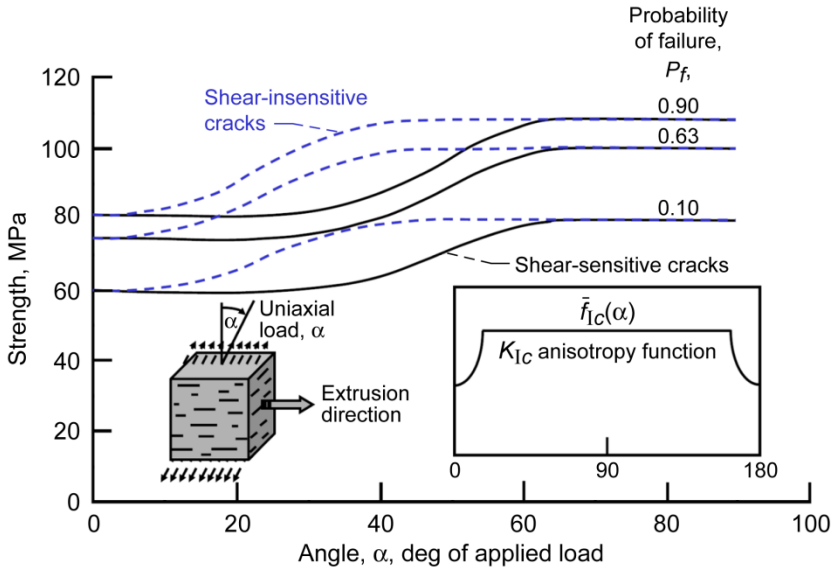

Figure 32.—Strength anisotropy example of a shear-sensitive and shear-insensitive response for a uniaxial load rotated at an angle relative to the extrusion direction. Anisotropy of the critical mode I stress-intensity factor, K_{Ic}, is assumed, which is also equivalent to the microcrack size being anisotropic.

Appendix C.—Interchangeability of Composite Stress With Fiber Stress in the Weibull Distribution

In a unidirectional composite where fiber strength controls the material failure and a Weibull distribution is used to describe the failure response based on fiber strength, for uniaxial loading a general form of the distribution may be expressed as

$$P_f(\sigma_{\text{fiber}}) = 1 - \exp\left\{-\left(\frac{\sigma_{\text{fiber}}}{\sigma_{o,\text{fiber}}}\right)^m\right\} \tag{C1}$$

If perfect bonding is assumed between the fibers and the matrix,

$$\varepsilon_{\text{composite}} = \varepsilon_{\text{matrix}} = \varepsilon_{\text{fiber}} \tag{C2}$$

If the fibers and matrix behave elastically,

$$\begin{aligned} \sigma_{\text{fiber}} &= E_{\text{fiber}}\varepsilon_{\text{fiber}} \\ \sigma_{\text{matrix}} &= E_{\text{matrix}}\varepsilon_{\text{matrix}} \end{aligned} \tag{C3}$$

The resultant load is

$$F_{\text{composite}} = \varepsilon_{\text{composite}}\left(E_{\text{fiber}}A_{\text{fiber}} + E_{\text{matrix}}A_{\text{matrix}}\right) \tag{C4}$$

where A is the cross-sectional area of the composite, A_{fiber} is the cross-sectional area of the fiber fraction of the composite, and A_{matrix} is the cross-sectional matrix fraction of the composite. The composite stress is

$$\begin{aligned} \sigma_{\text{composite}} &= \frac{F_{\text{composite}}}{A_{\text{composite}}} = \frac{\varepsilon_{\text{composite}}\left(E_{\text{fiber}}A_{\text{fiber}} + E_{\text{matrix}}A_{\text{matrix}}\right)}{A_{\text{fiber}} + A_{\text{matrix}}} \\ \sigma_{\text{composite}} &= \varepsilon_{\text{composite}}\,c_{\text{composite}} \end{aligned} \tag{C5}$$

Substituting Equations (C2) and (C3) into Equation (C1) yields

$$\begin{aligned} P_f(\sigma_{\text{fiber}}) &= 1 - \exp\left\{-\left(\frac{\varepsilon_{\text{composite}}E_{\text{fiber}}}{\varepsilon_{o,\text{fiber}}E_{\text{fiber}}}\right)^m\right\} = 1 - \exp\left\{-\left(\frac{\varepsilon_{\text{composite}}E_{\text{fiber}}}{\varepsilon_{o,\text{composite}}E_{\text{fiber}}}\right)^m\right\} \\ P_f(\sigma_{\text{fiber}}) &= 1 - \exp\left\{-\left(\frac{\varepsilon_{\text{composite}}}{\varepsilon_{o,\text{composite}}}\right)^m\right\} \end{aligned} \tag{C6}$$

since $\varepsilon_{o,\text{composite}} = \varepsilon_{o,\text{fiber}}$. Substituting Equation (C5) into (C6) yields

$$P_f\left(\sigma_{\text{fiber}}\right) = 1 - \exp\left\{-\left(\frac{\varepsilon_{\text{composite}}}{\varepsilon_{o,\text{composite}}}\right)^m\right\} = 1 - \exp\left\{-\left(\frac{\varepsilon_{\text{composite}}/c_{\text{composite}}}{\varepsilon_{o,\text{composite}}/c_{\text{composite}}}\right)^m\right\}$$

$$P_f\left(\sigma_{\text{fiber}}\right) = 1 - \exp\left\{-\left(\frac{\sigma_{\text{composite}}}{\sigma_{o,\text{composite}}}\right)^m\right\} \equiv P_f\left(\sigma_{\text{composite}}\right) \tag{C7}$$

Therefore, for a composite with fiber-controlled failure, if a Weibull distribution form is used, the failure probability expressed in terms of the composite stress $\sigma_{\text{composite}}$ and the failure probability expressed in terms of the fiber stress σ_{fiber} are equivalent: $\therefore P_f(\sigma_{\text{composite}}) = P_f(\sigma_{\text{fiber}})$.

Appendix D.—Symbols, Definitions, and Acronyms

D.1 Symbols

dA	$\sin\alpha\, d\alpha\, d\beta$ infinitesimal area on the surface of a unit radius sphere where $\sigma_{leq} \geq \sigma_{lc}$
$A_{composite}$	cross-sectional area of the composite
A_{fiber}	cross-sectional area of the fiber fraction in a composite
A_{matrix}	cross-sectional area of the matrix fraction in a composite
A_o	area of the grain
a	crack length or crack radius
a_μ	average crack length or crack radius
a_0	initial or preexisting crack size
b	average graphite grain size
$\bar{C}$	Shetty shear sensitivity constant
c	constant
$c_{composite}$	constant value
c_G	constant
c_1, c_2, c_3	constants
c_μ	mean concentration of inhomogeneities
D	constant ($D = 2$ for a two-dimensional network {~area}, $D = 3$ for a three-dimensional network {$\propto$ volume})
d	diameter of the specimen
E	Young's modulus of elasticity
E_{fiber}	Young's modulus of elasticity for composite fiber
E_{matrix}	Young's modulus of elasticity for composite matrix
exp	exponential function
$F_{composite}$	resultant load or force on composite
$f(\,)$	function
$f(x)$	real value function of x
$f(y)$	probability density function (PDF) of either k_s or u_c
$\bar{f}_{Ic}(\alpha,\beta)$	normalized anisotropy function of K_{Ic} or σ_{Ic} as a function of angles α and β
f_{-1}	first inverse moment of the probability distribution function
$G_{n_f}(x)$	bundle strength distribution for n_f number of fibers
$G_4(\sigma)$	bundle strength distribution for four fibers as a function of stress σ
H	Heaviside step function
H_{k,n_b}	composite strength distribution for k critical number of fiber breaks

$H_{n_f,n_b}(x)$	composite strength distribution
I	current
i	integer
j	integer; number of rows of grains that fracture
K_{I}	mode I stress-intensity factor
$K_{\mathrm{I}c}$	critical mode I stress-intensity factor
K_{R}	fracture toughness or fracture resistance
k	critical number of failure breaks
k_G	constant
km	modified Weibull modulus
k_s	stochastic spring constant
$\bar{k}_{BV}$	Batdorf uniaxial stress state normality constant for the volume-flaw failure mode
L	fiber length; length of composite material; system size
L_o	characteristic length
L_1, L_2	system sizes
ℓ_1, ℓ_2, ℓ_3	direction cosines
m	Weibull modulus
m^*	modified Weibull modulus
m_{cV}	Weibull modulus for the volume-flow failure mode for compressive stress states
m_{local}	local Weibull modulus or slope at a point of an arbitrary curve on a Weibull plot
m_V	Weibull modulus for the volume-flow failure mode
N	number of pores per unit volume
N_{eq}	equivalent number of links in a series
N_o	number of cracks per unit volume
n	integer; number of Bernoulli trials with success probability p; number of items in a set; number of bonds in a lattice system
n_b	number of mutually exclusive but linked bundles
n_{br}	number of broken bonds
n_c	critical number of bond breaks in a lattice system
n_d	number of flaws that experience growth within ΔV_d
n_{dc}	critical number of flaws that experience growth within ΔV_d
n_f	number of fibers
n_g	number of graphite grains in entire row ahead of crack tip
n_{indep}	maximum number of n bonds where spatial independence is maintained

n_o	constant
n_{sys}	product of n_f and n_b, which is the size of the composite system
n_δ	number of chains of height δ
$n_{\delta,o}$	characteristic value of n_δ
P	probability
$P(X = x)$	probability random variable X equals the value x
P_{event}	success probability or probability of an event
P_f	probability of failure ($P_f = 1 - P_s$)
P_{fi}	probability of failure in the i^{th} individual graphite grain
$(P_f)_i$	probability of failure of the i^{th} link
$P_f(\sigma_{composite})$	probability of failure of composite from $\sigma_{composite}$ stress
$P_f(\sigma_{fiber})$	probability of failure of fiber from σ_{fiber} stress
$P_{f,gr}$	grafting probability of failure
$P_{fi}(\sigma, a)$	probability of failure in the i^{th} individual graphite grain for crack size a and uniaxial stress σ
P_{fn_g}	probability of failure of n_g graphite grains
$P_{fn_g}(\sigma, a)$	probability of failure of n_g graphite grains for crack size a and uniaxial stress σ
P_{fV}	probability of failure of material volume
ΔP_{fV}	probability of failure of a crack with a strength between σ_{Ic} and $\sigma_{Ic} + \Delta\sigma_{Ic}$ in ΔV
P_{f,V_1}, P_{f,V_2}	probability of failure of volume 1, probability of failure of volume 2
$P_{f,V_1}(\sigma)$	probability of failure for value of σ for volume 1
$P_{f,V_2}(\sigma)$	probability of failure for value of σ for volume 2
$P_{f\{\Delta V_d\}}$	probability of failure for incremental volume element ΔV_d
P_s	reliability or probability of survival ($P_s = 1 - P_f$)
$P_{s,compressive}$	probability of survival from a compressive failure mode
$(P_s)_i$	probability of survival of the i^{th} link
$P_{s,tensile}$	probability of survival from a tensile failure mode
P_{sV}	probability of survival of material volume V
$P_{s\{\Delta V_d\}}$	probability of survival for incremental volume element ΔV_d
$P(x)$	distribution of fiber strength
ΔP_{1V}	probability of existence of a crack with strength between σ_{Ic} and $\sigma_{Ic} + \Delta\sigma_{Ic}$ in an incremental volume
P_{2V}	probability that a crack of critical strength will be oriented in a particular direction such that it will grow and cause failure
p	fraction of randomly chosen springs

p_{ce}	elastic response threshold (where removed members affect the elastic response of the system)
$\wp(\alpha, \beta)$	probability density distribution of flaw normals (oriented perpendicular to the plane of the flaw) and given by angles α and β
q	small, but nonzero, probability
r_d	distance from a broken fiber
r_L	constant (ratio) or parameter in K_{Ic} anisotropy function
r_T	constant (ratio) or parameter in K_{Ic} anisotropy function
$S(a)$	distribution of pore sizes—a function of a where a is crack size
S_d	scatter (standard deviation) in pore size distribution
S_μ	mean pore size
u	constant or parameter; constant between 1 and 2 in value
V	volume; voltage
ΔV	incremental volume
ΔV_d	incremental volume element
V_e	effective volume
V_{e1}, V_{e2}	effective volumes of body 1 and 2
V_o	characteristic volume
V_{ox}	characteristic volume for modified Weibull relation
V_{tot}	total volume of component
V_δ	cross section of volume of height δ for modified Weibull relation
$V_{\delta,o}$	characteristic value of V_δ for modified Weibull relation
V_1, V_2	uniformly stressed volumes of body 1 and 2
$W(x)$	composite material weakest-link characteristic probability distribution independent of n_f
$W(\sigma)$	characteristic probability distribution as a function of σ
w	span over which a uniform distribution of fuse breaking occurs
$w_c(L)$	boundary between brittle and ductile-like failure as a function of system size
w_o	threshold of w where single bond breakage causes system failure
X	discrete real-valued random variable
x	specific value of X; any variable; load per fiber
x, y, z	location in the body of the structure; Cartesian coordinate directions
x^*	the point where $x^*[1 - P(x^*)]$ is maximum
x_o	characteristic value of x
x_u	threshold value of x

α	orientation angle, angular coordinate
β	orientation angle, angular coordinate
Γ	gamma function
γ	constant or parameter in flaw orientation anisotropy function
γ_L	constant or parameter in K_{Ic} anisotropy function
γ_T	constant or parameter in K_{Ic} anisotropy function
Δ	increment
Δ_G	difference in σ/σ_μ from the mean to the value of σ/σ_μ where the probability of failure is 10^{-6} for the gaussian distribution
Δ_W	difference in σ/σ_μ from the mean to the value of σ/σ_μ where the probability of failure is 10^{-6} for the Weibull distribution
δ	incremental volume; average grain height or multiple of; ineffective length; stress transfer length
Σ	summation function; applied far-field multiaxial stress state
ε	strain
ε_c	critical strain
$\varepsilon_{composite}$	composite strain
ε_{fiber}	composite fiber strain
ε_{matrix}	composite matrix strain
$\varepsilon_{o,composite}$	Weibull scale parameter for composite strain
$\varepsilon_{o,fiber}$	Weibull scale parameter for composite fiber strain
$\zeta(\alpha)$	ζ as a function of angle α describing the anisotropy of flaw orientation
$\zeta(\alpha, \beta)$	function describing the anisotropy of flaw orientation where the normal direction to the flaw plane is given by angles α and β
$\eta(\sigma)$	crack-density function
$\eta_V(\sigma)$	crack-density function, number of flaws per unit volume with strength equal to or less than σ
$\eta_V(\sigma_{Ic})$	crack-density function for mode I strength, σ_{Ic}, of a flaw
θ	angle of individual graphite grain in relation to the crack tip
κ	constant or parameter
λ	parameter in Poisson distribution
ν	Poisson's ratio
ξ	constant or parameter in flaw orientation anisotropy function
ξ_L	constant or parameter in K_{Ic} anisotropy function
ξ_T	constant or parameter in K_{Ic} anisotropy function C
Π	product

π	pi, 3.14159
σ	applied uniaxial tensile stress
$\Delta\sigma$	increment of σ
$\sigma(x, y, z)$	uniaxial stress at location *x, y, z* in a body
$\sigma_{composite}$	composite stress
σ_{con}	constant
σ_e	effective stress for multiaxial stresses
$\sigma_{e,f}$	peak effective stress in component
σ_f	maximum stress in component; maximum stress in the component at failure
σ_{fiber}	composite fiber stress
σ_{f1}, σ_{f2}	σ_f for body 1 and 2
σ_{Ic}	critical mode I strength
$\sigma_{Ic}(x, y, z, \alpha, \beta)$	mode I far-field strength of a flaw located at coordinates *x*, *y*, and *z* and oriented at angles α and β
$\Delta\sigma_{Ic}$	increment of σ_{Ic}
$\sigma_{Ic\ max}$	maximum value of σ_{Ic} over the unit sphere
σ_{Ieq}	effective stress or equivalent stress
$\sigma_{Ieq\ max}$	maximum value of σ_{Ieq} over the unit sphere from the applied multiaxial stress Σ
σ_i	local tensile strength in incremental volume ΔV_i
σ_{matrix}	composite matrix stress
σ_n	applied far-field stress component normal to a crack face
σ_o	Weibull scale parameter
$\sigma_{o,composite}$	Weibull scale parameter for composite
σ_{ocV}	Weibull scale parameter for uniaxial compression
$\sigma_{o,fiber}$	Weibull scale parameter for fiber
$\sigma_{o,i}$	transformed Weibull scale parameter for principal stress direction denoted with direction cosines ℓ_1, ℓ_2, and ℓ_3
σ_{oV}	Weibull scale parameter for the volume-flaw failure mode normalized to unit volume
σ_{o1}, σ_{o2}, σ_{o3}	Weibull scale parameter σ_o for respective principal stresses σ_1, σ_2, σ_3
σ_{sd}	standard deviation of fiber strength
σ_u	threshold stress
σ_{uV}	threshold strength parameter for volume
σ_x, σ_y, σ_z	global coordinate system
$\sigma_{\delta,k}$	Weibull scale parameter for k^{th} Weibull line
σ_θ	Weibull characteristic strength

$\sigma_{\theta(\text{tensile specimen})}$	Weibull characteristic strength of reference tensile specimen
σ_{μ}	mean fracture strength
$\sigma_1, \sigma_2, \sigma_3$	principal stresses ($\sigma_1 \geq \sigma_2 \geq \sigma_3$)
τ	applied far-field shear stress on a crack face; shear stress acting on the oblique plane whose normal is determined by angles α and β
Φ	constant or exponent
ϕ	constant or parameter
φ	scaling constant between 0 and 1
φ^*	modified scaling constant between 0 and 1 depending on material system
φ_1, φ_2	scaling constants between 0 and 1
ψ	lattice model size effect constant
$\Omega(\Sigma,\sigma_{Ic})$	area of a solid angle projected onto a unit radius sphere in three-dimensional stress space for which $\sigma_{Ieq} \geq \sigma_{Ic}$ from an applied multiaxial stress state Σ
ω	coefficient of variation
ω_o	coefficient of variation
∞	infinity
!	factorial function

Subscripts

i	i^{th} value or i^{th} term
j	j^{th} value or j^{th} term
max	maximum
n	normal; n^{th} value
V	volume or a volume-based property (e.g., indicates volume-flaw analysis)
μ	average or characteristic
0	initial or starting value

D.2 Definitions

Batdorf	component reliability model using (typically) the Weibull distribution and fracture mechanics principles to account for the effect of multiaxial stress states on reliability (see Sec. 2.1.2.1)
Burchell	The Burchell model—combines fracture mechanics with a physics-based microstructural description of graphite failure (see Sec. 2.1.6)
extreme fiber stress	the location (point) in the body of the component where the stress is maximum (see σ_f)
fast fracture	component rupture in the absence of slow crack growth where strength is strictly controlled by the fracture toughness and the size, distribution, and orientation of inherent flaws

mode I	crack opening mode
mode II	crack sliding mode (in-plane shear)
mode III	crack tearing mode (out-of-plane shear)
R-curve	where fracture toughness K_R varies with crack size—typically increasing with crack size (see Sec. 2.1.4)
transient reliability analysis	predicting the probability of survival of a component while accounting for loads and temperatures that can vary over time
Weibull distribution	see Equations (4) and (8)

D.3 Acronyms and Initialisms

CARES	Ceramics Analysis and Reliability Evaluation of Structures
ELS	equal load sharing
FPZ	fracture process zone
HVDP	Hedgepeth and Van Dyke (1967) periodic LLS model
LEFM	linear elastic fracture mechanics
LLS	local load sharing
PIA	principle of independent action—a component reliability model based on the Weibull distribution that accounts for multiaxial stress states by using principal stresses applied independently of one another (see Eq. (21) in Sec. 2.1.2.2, Barnett et al. (1967), and Freudenthal (1968))
RFM	random fuse model
RSM	random spring model
RVE	representative volume element
WLT	weakest-link theory

References

Abe, Hiroya, et al.; 2003: Flaw Size Distribution in High-Quality Alumina. J. Am. Ceram. Soc., vol. 86, no. 6, pp. 1019–1021.

Abernethy, R.B.; 2008: quote cited from http://www.barringer1.com/wa.htm Accessed Oct. 22, 2010.

Abernethy, R.B., et al.; 1983: Weibull Analysis Handbook; Final Technical Report. AD–A143100 (AFWAL–TR–83–2079).

Afferrante, L.; Ciavarella, M.; and Valenza, E.; 2006: Is Weibull's Modulus Really a Material Constant? Example Case With Interacting Collinear Cracks. Int. J. Solids Struct., vol. 43, pp. 5147–5157.

Alava, Mikko J.; Nukala, Phani K.V.V.; and Zapperi, Stefano; 2006: Statistical Models of Fracture. Advan. Phys., vol. 55, nos. 3–4, pp. 349–476.

Alpa, G.; 1984: On a Statistical Approach to Brittle Rupture for Multiaxial States of Stress. Engrg. Fract. Mechan., vol. 19, no. 5, pp. 881–901.

Arai, T.; and Oku, T.: 1979: The Effect of Nonlinear Stress-Strain Relationship on the Bend Strength of Isotropic Graphite. J. Nuclear Materials, vol. 79, issue 1, pp. 227–234.

Babcock, S.G., et al.; 1972: Dynamic Biaxial and Elevated-Temperature Properties of ATJ–S Graphite. Proceedings of the Conference on Continuum Aspects of Graphite Design, CONF–701105.

Barnett, Ralph L., et al.; 1967: Fracture of Brittle Materials Under Transient Mechanical and Thermal Loading. AFFDL–TR–66–220.

Barringer & Associates, Inc.; 2009: SuperSMITH Weibull Probability Plotting Software. http://www.barringer1.com/wins.htm. Accessed Oct. 22, 2010.

Batdorf, Samuel B.; 1973: A Statistical Theory for the Fracture of Transversely Isotropic Brittle Materials of Moderate Anisotropy. Air Force Report SAMSO–TR–73–361, Aerospace Report TR–0074(4450–76–1, NTIS AD–770 982.

Batdorf, S.B.; 1975: Fracture Statistics of Brittle Materials With Intergranular Cracks. Nuclear Engrg. Design, vol. 35, pp. 349–360.

Batdorf, S.B.; 1978a: Fracture Statistics of Polyaxial Stress States. Fracture Mechanics, Nicholas Perrone, ed., University Press of Virginia, Charlottesville, VA, pp. 579–591.

Batdorf, S.B.; 1978b: New Light on Weibull Theory. Nuclear Engrg. Design, vol. 47, no. 2, pp. 267–272.

Batdorf, S.B.; 1982: Tensile Strength of Unidirectionally Reinforced Composites—I. J. Reinforced Plastics Composites, vol. 1, no. 2, pp. 153–164.

Batdorf, S.B.; and Crose, J.G.; 1974: A Statistical Theory for the Fracture of Brittle Structures Subjected to Nonuniform Polyaxial Stresses. J. Appl. Mech. Trans. ASME, vol. 41, no. 2, pp. 459–464.

Batdorf, S.B.; and Ghaffarian, Reza; 1982: Tensile Strength of Unidirectionally Reinforced Composites—II. J. Reinforced Plastics Composites, vol. 1, no. 2, pp. 165–176.

Batdorf, S.B.; and Ghaffarian, Reza; 1984: Size Effect and Strength Variability of Unidirectional Composites. Int. J. Fracture, vol. 26, no. 2, pp. 113–123.

Batdorf, S.B.; and Heinisch, H.L., Jr.; 1978: Weakest Link Theory Reformulated for Arbitrary Fracture Criterion. J. Am. Ceram. Soc., vol. 61, no. 7, pp. 355–358.

Batrouni, G. George; and Hansen, Alex; 1998: Fracture in Three-Dimensional Fuse Networks. Phy. Rev. Letter, vol. 80, no. 2, pp. 325–328.

Battiste, R.; Burchell, T.; and Strizak, J; 2010: Biaxial Strength Testing of NBG–18 Graphite in Fourth Stress Quadrant. Oak Ridge National Laboratory, ORNL/TM–2010/143.

Bazant, Zdenek P.; and Li, Z.; 1995: Modulus of Rupture: Size Effect Due to Fracture Initiation in Boundary Layer. J. Structural Engrg., vol. 121, no. 4, pp. 739–746.

Bazant, Zdenek P.; and Pang, Sze-Dai; 2007: Activation Energy Based Extreme Value Statistics and Size Effect in Brittle and Quasibrittle Fracture. J. Mechan. Physics Solids, vol. 55, pp. 91–131.

Bazant, Z.P.; and Planas, Jaime; 1998: Fracture and Size Effect in Concrete and Other Quasibrittle Materials. CRC Press, Boca Raton, FL.

Beale, Paul D.; and Srolovitz, David J.; 1988: Elastic Fracture in Random Materials. Phys. Rev. B., vol. 37, no. 10, pp. 5500–5507.

Beyerlein, Irene J.; and Phoenix, S. Leigh; 1996: Statistics for the Strength and Size Effects of Microcomposites With Four Carbon Fibers in Epoxy Resin. Compos. Sci. Technol., vol. 56, no. 1, pp. 75–92.
Beyerlein, Irene J.; and Phoenix, S. Leigh; 1997: Statistics of Fracture for an Elastic Notched Composite Lamina Containing Weibull Fibers—Part II. Probability Models of Crack Growth. Eng. Fract. Mech., vol. 57, nos. 2–3, pp. 267–299.
Brocklehurst, J.E.; 1977: Fracture in Polycrystalline Graphite. Chemistry and Physics of Carbon, P.L. Walker and P.J. Thrower, eds., Marcel Dekker, New York, NY, vol. 13, pp. 146–272.
Brocklehurst, J.E.; and Darby, M.I.; 1974: Concerning the Fracture of Graphite Under Different Test Conditions. Mater. Sci. Eng., vol. 16, nos. 1–2, pp. 91–106.
Broek, David; 1982: Elementary Engineering Fracture Mechanics. Martinus Nijhoff, The Hague, Netherlands.
Broutman, L.J.; Krishnakumar, S.M.; and Mallick, P.K.; 1970: Effects of Combined Stresses on Fracture of Alumina and Graphite. J. Amer. Ceram. Soc., vol. 53, no. 12, pp. 649–654.
Brückner-Foit, A.; Hülsmeier, P.; and Sckuhr, M.; 2000: Limitations of the Weibull Theory in Stress Fields With Pronounced Stress Gradients. ASME 2000–GT–0663.
Buch, J.D.; 1976: Mechanical Behavior Model for Graphites. ASTM STP–605, p. 124.
Buch, J.D.; Crose, J.G.; and Robinson, E.Y.; 1977: Failure Criteria in Graphite Program; Final Report. AFML–TR–77–16. (Available from the Air Force Material Laboratory.)
Burchell, T.D.; 1986: Studies of Fracture in Nuclear Graphite. Ph.D. Thesis, University of Bath, UK.
Burchell, Timothy D.; 1996: A Microstructurally Based Fracture Model for Polygranular Graphites. Carbon, vol. 34, no. 3, pp. 297–316.
Burchell, Timothy D., ed.; 1999: Carbon Materials for Advanced Technologies. Pergamon, Amsterdam, Netherlands.
Burchell, Tim; Yahr, Terry; and, Battiste, Rick; 2006: Modelling the Multiaxial Strength of Nuclear Graphite. Proceedings HTR2006: 3rd International Topical Meeting on High Temperature Reactor Technology, E00000206, Johannesburg, South Africa.
Chakrabarti, Bikas K.; and Benguigui, L. Gilles; 1997: Statistical Physics of Fracture and Breakdown in Disordered Systems. Oxford University Press, Oxford, U.K.
Chao, Luen-Yuan; and Shetty, Dinesh K.; 1990: Equivalence of Physically Based Statistical Fracture Theories for Reliability Analysis of Ceramics in Multiaxial Loading. J. Amer. Ceram. Soc., vol. 73, no. 7, pp. 1917–1921.
Chao, Luen-Yuan; and Shetty, Dinesh K.; 1992: Extreme-Value Statistics Analysis of Fracture Strengths of a Sintered Silicon Nitride Failing From Pores. J. Am. Ceram. Soc., vol. 75, no. 8, pp. 2116–2124.
Choi, S.R.; and Gyekenyesi, J.P.; 1999: Elevated-Temperature “Ultra” Fast Fracture Strength of Advanced Ceramics: An Approach to Elevated-Temperature “Inert” Strength. J. Eng. Gas Turbines Power, vol. 121, no. 1, pp. 18–24.
Choi, Sung R.; and Salem, Jonathan A.; 1992: Indentation Flaw Formation and Strength Response of Silicon Nitride Ceramics at Low Indentation Loads. J. Mat. Sci. Lett., vol. 11, no. 21, pp. 1398–1400.
Coleman, Bernard D.; 1957: A Stochastic Process Model for Mechanical Breakdown. J. Rheol., vol. 1, no. 1, pp. 153–168.
Connecticut Reserve Technologies, Inc.; 2009: WeibPar 4.1 User Guide. Version 4.1. http://www.weibpar.com Accessed Oct. 22, 2010.
Cook, R.F.; and Clarke, D.R.; 1988: Fracture Stability, R-Curves and Strength Variability. Acta Metall., vol. 36, no. 3, pp. 555–562.
Cooper, N.R.; 1988: Probabilistic Failure Prediction of Rocket Motor Components. Ph.D. Dissertation, Royal Military College of Science.
Corbin, Normand D., et al.; 1988: Material Development in the Silicon Nitride-Silicon Carbide Whisker System. Proceedings of the Twenty-sixth Automotive Technology Development Contractors’ Coordination Meeting, Series P–219, pp. 235–242.

Curtin, W.A.; 1997: Toughening in Disordered Brittle Materials. Phys. Rev. B, vol. 55, no. 17, pp. 11270–11276.
Curtin, W.A.; and Scher, H.; 1990a: Brittle Fracture in Disorder Materials. A Spring Network Model. J. Mater. Res., vol. 5, no. 3, pp. 535–553.
Curtin, W.A.; and Scher, H.; 1990b: Mechanics Modeling Using a Spring Network. J. Mater. Res., vol. 5, no. 3, pp. 554–562.
Daniels, H.E.; 1945: The Statistical Theory of the Strength of Bundles of Threads. I. Proc. Roy. Soc. Ser. A, vol. 183, no. 995, pp. 405–435.
Danzer, R., et al.; 2007: Fracture Statistics of Ceramics—Weibull Statistics and Deviations From Weibull Statistics. Eng. Fract. Mech., vol. 74, no. 18, pp. 2919–2932.
Danzer, Robert, et al.; 2008: Fracture of Ceramics. Adv. Eng. Mat., vol. 10, no. 4, pp. 275–298.
de Arcangelis, L.; and Herrmann, H.J.; 1989: Scaling and Multiscaling Laws in Random Fuse Networks. Phys. Rev. B, vol. 39, no. 4, pp. 2678–2684.
de Arcangelis, L.; and Redner, S.; 1985: Random Fuse Model for Breaking Processes. J. Phys. (Paris) Lett., vol. 46, no. 13, pp. 585–590.
de Arcangelis, L.; Redner, S.; and Coniglio, A.; 1986: Multiscaling Approach in Random Resistor and Random Superconducting Networks. Phys. Rev. B, vol. 34, no. 7, pp. 4656–4673.
Diaz, G.; Kittl, P.; and Martinez, V.; 1999: On the Determination of Flaw Size Distribution in Brittle Materials. Ciencia Abierta, no. 7. http://cabierta.uchile.cl/revista/7/flaw.htm Accessed Oct. 22, 2010.
Duffy, S.F.; Palko, J.L.; and Gyekenyesi, J.P., 1993: Structural Reliability Analysis of Laminated CMC Components. J. Eng. Gas Turbines Power (NASA TM–103685), vol. 115, no. 1, pp. 103–108.
Duxbury, P.M.; Beale, P.D.; and Leath, P.L.; 1986: Size Effects of Electrical Breakdown in Quenched Random Media. Phys. Rev. Lett., vol. 57, no. 8, pp. 1052–1055.
Duxbury, P.M.; and Leath, P.L.; 1987: The Failure Distribution in Percolation Models of Breakdown. J. Phys. A: Math. Gen., vol. 20, pp. L411–L415.
Duxbury, P.M.; Leath, P.L.; and Beale, Paul D.; 1987: Breakdown Properties of Quenched Random Systems: The Random-Fuse Network. Phys. Rev. B, vol. 36, no. 1, pp. 367–380.
Epstein, Benjamin; 1948: Application of the Theory of Extreme Values in Fracture Problems. J. Am. Stat. Assoc., vol. 43, no. 243, pp. 403–412.
Erdogan, F.; and Sih, G.C.; 1963: On the Crack Extension in Plates Under Plane Loading and Transverse Shear. J. Basic Eng., vols. 85–86, Series D, pp. 519–525.
Evans, A.G.; 1978: General Approach for the Statistical Analysis of Multiaxial Fracture. J. Amer. Ceram. Soc., vol. 61, nos. 7–8, pp. 302–308.
Feng, Shechao; and Sen, Pabitra N.; 1984: Percolation on Elastic Networks: New Exponent and Threshold. Phys. Rev. Lett., vol. 52, no. 3, pp. 216–219.
Fisher, Ronald Aylmer, Sir; and Tippett, L.H.C.; 1928: Limiting Forms of the Frequency Distribution of the Largest of Smallest Member of a Sample. Proc. Cambridge Philos. Soc., vol. 24, pp. 180–190.
Freudenthal, Alfred M.; 1968: Statistical Approach to Brittle Fracture. Fracture: An Advanced Treatise, H. Liebowitz, ed., Vol. II, pp. 592–619.
General Atomics; 1988: Graphite Design Handbook. U.S. Department of Energy, DOE–HTGR–88111.
Generation IV International Forum; 2009: Nuclear Energy Systems for the Future. http://gif.inel.gov/ Accessed Oct. 22, 2010.
Greenstreet, W.L.; 1968: Mechanical Properties of Artificial Graphites—A Survey Report. ORNL–4327. http://www.osti.gov/bridge//product.biblio.jsp?query_id=0&page=0&osti_id=4809139
Gücer, D.E.; and Gurland, J.; 1962: Comparison of the Statistics of Two Fracture Modes. J. Mech. Phys. Solids, vol. 10, pp. 365–373.
Gyekenyesi, J.P.; and Nemeth, N.N.; 1987: Surface Flaw Reliability Analysis of Ceramic Components With the SCARE Finite Element Postprocessor Program. J. Eng. Gas Turbines Power, vol. 109, no. 3, pp. 274–281.
Hansen, Alex; Hinrichsen, Einar L.; and Roux, Stephane; 1991: Scale-Invariant Disorder in Fracture and Related Breakdown Phenomena. Phys. Rev. B, vol. 43, no. 1, pp. 665–678.

Hansen, A.; and Roux, S.; 2000: Statistics Toolbox for Damage and Fracture. Damage and Fracture of Disordered Materials, Dusan Krajcinovic and Jan Van Mier, eds., Springer, New York, pp. 17–101.
Hansen, A.; Roux, S.; and Herrmann, H.J.; 1989: Rupture of Central-Force Lattices. J. Phys. France, vol. 50, pp. 733–744.
Harlow, D. Gary; and Phoenix, S. Leigh; 1978a: The Chain-of-Bundles Probability Model for the Strength of Fibrous Materials I: Analysis and Conjectures. J. Compos. Mat., vol. 12, pp. 195–214.
Harlow, D.G.; and Phoenix, S.L.; 1978b: The Chain-of-Bundles Probability Model for the Strength of Fibrous Materials II: A Numerical Study of Convergence. J. Compos. Mat., vol. 12, pp. 314–334.
Harlow, D.G.; and Phoenix, S.L.; 1981a: Probability Distributions for the Strength of Composite Materials I: Two-Level Bounds. Int. J. Fract., vol. 17, no. 4, pp. 347–372.
Harlow, D.G.; and Phoenix, S.L.; 1981b: Probability Distributions for the Strength of Composite Materials II: A Convergent Sequence of Tight Bounds. Int. J. Fract., vol. 17, no. 6, pp. 601–630.
Hedgepeth, John M.; and Van Dyke, Peter; 1967: Local Stress Concentrations in Imperfect Filamentary Composite Materials. J. Compos. Mater., vol. 1, no. 3, pp. 294–309.
Hellen, T.K.; and Blackburn, W.S.; 1975: The Calculation of Stress Intensity Factors for Combined Tensile and Shear Loading. Int. J. Fract., vol. 11, no. 4, pp. 605–617
Herrmann, Hans J.; Hansen, Alex; and Roux, Stephane; 1989: Fracture of Disordered, Elastic Lattices in Two Dimensions. Phys. Rev. B, vol. 39, no. 1, pp. 637–648.
Herrmann, Hans J.; and Roux, Stephane, eds.; 1990: Statistical Models for the Fracture of Disordered Media. Elsevier Science Pub., Amsterdam, Netherlands.
Hidalgo, Raul Cruz, et al.; 2002: Fracture Model With Variable Range of Interaction. Phys. Rev. E, vol. 65, no. 4, pp. 046148/1–046148/8.
Ho, F.; 1979: A Modified Weibull Theory for the Strength of Granular Brittle Material. General Atomic Company Series GA–A 15228.
Hoel, Paul G.; Port, Sidney C.; and Stone, Charles J.; 1971: Introduction to Probability Theory. Houghton Mifflin Company, Boston, MA, p. 69.
Holt, M.J.; 2010: Issues of Scale and the Functionality of Polygranular Graphite Components. The University of Hull, Department of Engineering. http://www.hull.ac.uk/MAPP/graphite Accessed Nov. 1, 2010
Homan, F.J.; and Kasten, Paul R.; 1980: High-Temperature Gas-Cooled Reactor Base-Technology Program Annual Progress Report for Period Ending December 31, 1979. ORNL–5643, Contract No. W-7405-eng-26.
Ichikawa, Masahiro; 1991: Proposal of an Approximate Analytical Expression of Maximum Energy Release Rate of a Mixed Mode Crack in Relation to Reliability Evaluation of Ceramic Components. J. Soc. Mat. Sci. Jpn., vol. 40, no. 449, pp. 224–227.
Idaho National Laboratory, Oak Ridge National Laboratory, and Argonne National Laboratory; 2005: Next Generation Nuclear Plant Research and Development Program Plan. Idaho National Engineering and Environmental Laboratory, Idaho Falls, ID, INEEL/EXT–05–02581. http://www.inl.gov/technicalpublications/Documents/3028298.pdf Accessed Oct. 22, 2010.
Ishihara, Masahiro; Takahashi, Tsuneo; and Hanawa, Satoshi; 2001: Applicability of Advanced Design Method of Graphite Components by Microstructure-Based Brittle Fracture Model. Transactions, SMiRT 16, paper #1920, Washington, DC.
Jadaan, Osama; and Trethewey, Jeremy; 2006: Reliability of High Temperature Lightweight Valve Train Components in a Total Probabilistic Design Environment. Ceram. Eng. Sci. Proc., vol. 27, no. 2, pp. 533–542.
Jayatilaka, Ayal De S.; 1979: Fracture of Engineering Brittle Materials. Applied Science Publishers, London, England.
Jayatilaka, A. De S.; and Trustrum, K.; 1977: Statistical Approach to Brittle Fracture. J. Mat. Sci., vol. 12, no. 7, pp. 1426–1430.
Jenkins, G.M.; 1962: Fracture in Reactor Graphite. J. Nucl. Mater., vol. 5, no. 3, pp. 280–286.

Johnson, C.A.; 1983: Fracture Statistics of Multiple Flaw Distributions. Fracture Mechanics of Ceramics, Vol. 5—Surface Flaws, Statistics, and Microcracking, R.C. Bradt, et al., eds., Plenum Press, New York, NY, pp. 365–386.
Johnson, C.A.; and Tucker, William T.; 1994: Weibull Estimators for Pooled Fracture Data. Life Prediction Methodologies and Data for Ceramic Materials, ASTM STP–1201, C.R. Brinkman and S.F. Duffy, eds., pp. 250–264.
Jortner, J.; 1972: Biaxial Mechanical Properties of AXF–5Q Graphite to 4000°F. Proceedings of the Conference on Continuum Aspects of Graphite Design, CONF–701105, pp. 514–532.
Kahng, B., et al.; 1988: Electrical Breakdown in a Fuse Network With Random, Continuously Distributed Breaking Strengths. Phys. Rev. B, vol. 37, no. 13, pp. 7625–7637.
Kaiser, Joseph; 1950: An Investigation Into the Occurrence of Noises in Tensile Tests. Ph.D. Thesis, Munich Technische Hochschule. 1964 Translation. (Previously cited in Untersuchungen Uber das Auftreten Von Gerauschen Beim Zugversuch. Ph.D. Thesis, Technische Hochschule, Munich, Germany, 1950.)
Kantor, Yacov; and Webman, Itzhak; 1984: Elastic Properties of Random Percolating Systems. Phys. Rev. Lett., vol. 52, no. 21, pp. 1891–1894.
Kasten, P.R., et al.; 1989: High-Temperature Gas-Cooled Reactor Technology Development Program, Annual Progress Report for Period Ending December 31, 1987. DOE–HGTR–88272 (ORNL–6502).
Kendall, K., et al.; 1986: Influence of Toughness on Weibull Modulus of Ceramic Bending Strength. J. Mater. Res., vol. 1, no. 1, pp. 120–123.
Kennedy, C.R.; 1987: Statistical Characterization of Three Grades of Large-Billet Graphites: Stackpole 2020, Union Carbide TS1792, and Toyo Tanso IG11. DOE–HGTR–87–010 (ORNL/TM–10457).
Kittl, P.; and Aldunate, R.; 1983: Compression Fracture Statistics of Compacted Cement Cylinders. J. Mat. Sci., vol. 18, no. 10, pp. 2947–2950.
Knibbs, R.H.; 1967: Fracture in Polycrystalline Graphite. J. Nucl. Mater., vol. 24, pp. 174–187.
Kuo, Chia-Chyuan; and Phoenix, S. Leigh; 1987: Recursions and Limit Theorems for the Strength and Lifetime Distributions of a Fibrous Composite. J. Appl. Probab., vol. 24, no. 1, pp. 137–159.
Landis, Chad M.; Beyerlein, Irene J.; and McMeeking, Robert M.; 2000: Micromechanical Simulation of the Failure of Fiber Reinforced Composites. J. Mech. Phys. Solids, vol. 48, no. 3, pp. 621–648.
Li, Haiyan; and Fok, Alex Siu-Lun; 2009: An Analytical Study on the Effects of Strain Gradient on the Fracture Statistics of Quasi-Brittle Materials. J. Nucl. Mater., vol. 394, nos. 2–3, pp. 136–143.
Li, Y.S.; and Duxbury, P.M.; 1987: Size and Location of the Largest Current in a Random Resistor Network. Phys. Rev. B, vol. 36, no. 10, pp. 5411–5419.
Li, Y.S.; and Duxbury, P.M.; 1989: From Moduli Scaling to Breakdown Scaling: A Moment-Spectrum Analysis. Phys. Rev. B, vol. 40, no. 7, pp. 4889–4897.
Liu, Chi-Chao; 1997: A Comparison Between the Weibull and Lognormal Models Used to Analyse Reliability Data. Ph.D. Thesis, University of Nottingham.
Losty, H.H.W.; and Orchard, J.S.; 1962: The Strength of Graphite. Proceedings of the Fifth Biennial Conference on Carbon, Pergamon Press, New York, NY, pp. 519–532.
Lu, C.; Danzer, R.; and Fischer, F.; 2005: Effects of Pore/Grain-Size Interaction and Porosity on the Fracture of Electroceramics. Fracture Mechanics of Ceramics: Active Materials, Nanoscale Materials, Composites, Glass, and Fundamentals. R.C. Bradt, et al., eds., Springer, New York, NY, pp. 411–420.
Luo, X.; Srinivasan, G.V.; and Tredway, W.K.; 2007: Reliability Prediction of Monolithic Structural Ceramics With Uncertainties. ASME GT2007–27935.
Mahesh, Sivasambu; Beyerlein, Irene J.; and Phoenix, S. Leigh; 1999: Size and Heterogeneity Effects on the Strength of Fibrous Composites. Phys. D, vol. 133, nos. 1–4, pp. 371–389.
Mahesh, S.; and Phoenix, S.L.; 2004: Absence of a Tough-Brittle Transition in the Statistical Fracture of Unidirectional Composite Tapes Under Local Load Sharing. Phys. Rev. E: Stat. Nonlinear Soft Matter Phys., vol. 69, no. 2, pp. 026102–1 to 026102–23.

Mahesh, Sivasambu; Phoenix, S. Leigh; and Beyerlein, Irene J.; 2002: Strength Distributions and Size Effects for 2D and 3D Composites With Weibull Fibers in an Elastic Matrix. Int. J. Fract., vol. 115, no. 1, pp. 41–85.
Margetson, J.; 1976: A Statistical Theory of Brittle Failure for an Anisotropic Structure Subjected to a Multiaxial Stress State. AIAA–1976–632.
Matsuo, Yataro; 1981: A Probabilistic Analysis of the Brittle Fracture Loci Under Bi-Axial Stress State: 1st Report, In the Case of Tension Being Dominant. Bull. JSME, vol. 24, no. 188, pp. 290–294.
McClintock, Frank A.; 1973: Statistics of Brittle Fracture. Fracture Mechanics of Ceramics, Vol. 1, R.C. Bradt, D.P.H. Hasselman, and F.F. Lange, eds., Plenum Press, New York, NY, pp. 93–116.
Mitchell, B.C., et al., 2003: The Mechanical Testing of Nuclear Graphite. J. Nucl. Mater., vol. 322, nos. 2–3, pp. 126–137.
Meeker, William Q.; and Escobar, Luis A.; 1998: Statistical Methods for Reliability Data. Wiley, New York, NY.
Mrozowski, S.; 1956: Mechanical Strength, Thermal Expansion and Structure of Cokes and Carbons. Proceedings of the First and Second Conferences on Carbon. Stanislaw W. Mrozowski and L.W. Phillips, eds., University of Buffalo, Buffalo, NY.
Munz, Dietrich; 2007: What Can We Learn From R-Curve Measurements? J. Am. Ceram. Soc., vol. 90, no. 1, pp. 1–15.
Munz, Dietrich; and Fett, Theo; 1999: Ceramics: Mechanical Properties, Failure Behaviour Materials Selection. Springer, Berlin, Germany.
Nemeth, Noel N.; 1989: Concepts of LEFM Applied to Fast Fracture Statistics to Predict the Reliability of an Anisotropic Brittle Material Experiencing Multiaxial Loading. Unpublished draft report available from author.
Nemeth, Noel N.; and Bratton, Robert L.; 2010: Overview of Statistical Models of Fracture for Nonirradiated Nuclear-Graphite Components. Nucl. Eng. Des., vol. 240, no. 1, pp. 1–29.
Nemeth, Noel N., et al.; 1993: Designing Ceramic Components for Durability. Amer. Ceram. Soc. Bull., vol. 72, no. 12, pp. 59–69.
Nemeth, Noel N., et al.; 2003: CARES/Life Ceramics Analysis and Reliability Evaluation of Structures Life Prediction Program. NASA/TM—2003-106316.
Nemeth, Noel N., et al.; 2007: Fabrication and Probabilistic Fracture Strength Prediction of High-Aspect-Ratio Single Crystal Silicon Carbide Microspecimens With Stress Concentration. Thin Sol. Fi. (NASA/TM—2005-213986), vol. 515, no. 6, pp. 3283–3290.
Nemeth, Noel N., et al.; 2011: Pooled Weibull Analysis of Legacy H–451 Graphite Specimen Rupture Data—Full Report. To be published as a NASA Technical Memorandum.
Nemeth, Noel N.; Jadaan, Osama M.; and Gyekenyesi, John P.; 2005: Lifetime Reliability Prediction of Ceramic Structures Under Transient Thermomechanical Loads. NASA/TP—2005-212505.
Nukala, P.K.V.V.; and Simunovic, S.; 2004: Scaling of Fracture Strength in Disordered Quasi-Brittle Materials. Eur. Phys. J. B, vol. 37, no. 1, pp. 91–100.
Nukala, Phani Kumar; Zapperi, Stefano; and Simunovic, Srdan; 2005: Statistical Properties of Fracture in a Random Spring Model. Phys. Rev. E: Stat. Nonlinear Soft Matter Phys., vol. 71, no. 6, pp. 066106–1 to 066106–11.
Nukala, Sirisha, et al.; 2006: Crack-Cluster Distributions in the Random Fuse Model. Phys. Rev. E: Stat. Nonlinear Soft Matter Phys., vol. 73, no. 3, pp. 036109–1 to 036109–6.
Otani, H.; Phoenix, S.L.; and Petrina, P.; 1991: Matrix Effects on Lifetime Statistics for Carbon Fibre-Epoxy Microcomposites in Creep Rupture. J. Mat. Sci., vol. 26, pp. 1955–1970.
Pai, Shantaram S.; and Gyekenyesi, John P.; 1988: Calculation of Weibull Strength Parameters and Batdorf Flaw-Density Constants for Volume- and Surface-Flaw-Induced Fracture in Ceramics. NASA TM–100890.
Pears, C.D.; and Sanders, H.G.; 1970: A Strength Analysis of a Polygraphite. Part II. AFML-TR-69-204-Pt-2.

Peirce, Frederick Thomas; 1926: Tensile Tests for Cotton Yarns—"The Weakest Link," Theorems on the Strength of Long and of Composite Specimens. J. Text. Inst., vol. 17, pp. T355–T368.
Phoenix, S.L.; 2007: Personal communication, Cornell University, Ithaca, NY, July 27.
Phoenix, S.L.; and Beyerlein, I.J.; 2000a: Statistical Strength Theory for Fibrous Composite Materials. Comprehensive Composite Materials, Vol. I, Anthony Kelly and Carl Zweben, eds., Elsevier, pp. 559–639.
Phoenix, S. Leigh; and Beyerlein, Irene J.; 2000b: Distributions and Size Scalings for Strength in a One-Dimensional Random Lattice With Load Redistribution to Nearest and Next-Nearest Neighbors. Phys. Rev. E: Stat. Phys. Plasmas Fluids Relat. Interdisciplin. Top., vol. 62, no. 2, pp. 1622–1645.
Phoenix, S.L.; Ibnabdeljalil, M.; and Hui, C.-Y.; 1997: Size Effects in the Distribution for Strength of Brittle Matrix Fibrous Composites. Int. J. Solids Struct., vol. 34, no. 5, pp. 545–568.
Pinner, Joe; 2010: Fort St. Vrain Power Station History, Overview. http://www.fsvfolks.org/FSVHistory_2.html, Accessed Nov. 1, 2010
Planas, J.; 1995: Crack Growth in an Elastic Medium With Random Crack Growth Resistance. Report No. 95-jp03, Departamento de Ciencia de Materiales, ETS de Ingenieros de Caminos, Universidad Politecnica de Madrid, Ciudad Universitaria sn. 28040 Madrid, Spain, 1995.
Price, R.J.; 1976: Statistical Study of the Strength of Near-Isotropic Graphite. General Atomic Project 3224 (GA–A13955 and UC–77).
Quinn, G.D.; 2007: Fractography of Ceramics and Glasses. NIST Special Publication 960–16.
Quinn, George D.; and Bradt, Richard C.; 2007: On the Vickers Indentation Fracture Toughness Test. J. Am. Ceram. Soc., vol. 90, no. 3, pp. 673–680.
Ramachandran, Nageswaram; Chao, Luen-Yuan; and Shetty, Dinesh K.; 1993: R-Curve Behavior and Flaw Insensitivity of Ce-TZP/Al_2O_3 Composite. J. Am. Ceram. Soc., vol. 76, no. 4, pp. 961–969.
Reh, Stefan; Palfi, Tamas; and Nemeth, Noel N.; 2003: Probabilistic Analysis Techniques Applied to Lifetime Reliability Estimation of Ceramics. Proceedings of the JANNAF 39th Combustion Subcommittee, 27th Airbreathing Propulsion Subcommittee, 21st Propulsion Systems Hazards Subcommittee, and 3rd Modeling and Simulation Subcommittee Joint Meeting, CPIA–JSC–CD–24.
Rickerby, D.G.; 1980: Theoretical Aspects of the Statistical Variation of Strength. J. Mat. Sci., vol. 15, no. 10, pp. 2466–2470.
Rose, A.P.G.; and Tucker, M.O.; 1982: Fracture Criterion for Nuclear Graphite. J. Nucl. Mater., vol. 110, nos. 2–3, pp. 186–195.
Rosen, B.W.; 1964: Tensile Failure of Fibrous Composites. AIAA J., vol. 2, no. 11, pp. 1985–1991.
Roux, Stephane, et al.; 1988: Rupture of Heterogeneous Media in the Limit of Infinite Disorder. J. Statistical Phys., vol. 52, nos. 1–2, pp. 237–244.
Roux, Stephane, et al.; 1991: Fuse Model on a Randomly Diluted Hierarchical Lattice. Phys. A: Math. Gen., vol. 24, pp. 1625–1642.
Sahimi, Muhammad; 1998: Non-Linear and Non-Local Transport Processes in Heterogeneous Media: From Long-Range Correlated Percolation to Fracture and Materials Breakdown. Phys. Rep., vol. 306, nos. 4–6, pp. 213–395.
Sahimi, Muhammad; and Arbabi, Sepehr; 1993: Mechanics of Disordered Solids. II. Percolation on Elastic Networks With Bond-Bending Forces. Phys. Rev. B, vol. 47, no. 2, pp. 703–712.
Sahimi, Muhammad; and Goddard, Joe D.; 1986: Elastic Percolation Models for Cohesive Mechanical Failure in Heterogeneous Systems. Phys. Rev. B, vol. 33, no. 11, pp. 7848–7851.
Salem, J.A., et al.; 1996: Reliability Analysis of Uniaxially Ground Brittle Materials. J. Eng. Gas Turbines Power, vol. 118, no. 4, pp. 863–871.
Schmidt, A.; 2000: Reliability Analysis of Graphite Structures, Part I: Theory. Westinghouse Reaktor GmbH, Project 910PMRB08, Report GBRA 050 306.
Schmidt, Anton; 2003: Regulation for the Design of the Internals of the High Temperature Reactor, Version May 2003. Westinghouse Reaktor GmbH, Project EE–03–3089–ENGSPM, Report GBRA 065 942, Preliminary Report.

Scop, Peter M.; and Argon, Ali S.; 1967: Statistical Theory of Strength of Laminated Composites. J. Compos. Mater., vol. 1, no. 1, pp. 92–99.
Sharpe, William N., Jr., et al., 2008: Fracture Strength of Single-Crystal Silicon Carbide Microspecimens at 24 °C and 1000 °C. J. Microelectromech. Sys., vol. 17, no. 1, pp. 244–254.
She, S.; and Landes, J.D.; 1993: Statistical Analysis of Fracture in Graphite. Int. J. Fract., vol. 63, no. 2, pp. 189–200.
Shetty, D.K.; 1987: Mixed-Mode Fracture Criteria for Reliability Analysis and Design With Structural Ceramics. J. Eng. Gas Turbines Power, vol. 109, no. 3, pp. 282–289.
Shetty, Dinesh K.; and Wang, Jr-Sheng; 1989: Crack Stability and Strength Distribution of Ceramics That Exhibit Rising Crack-Growth-Resistance (R-Curve) Behavior. J. Am. Ceram. Soc., vol. 72, no. 7, pp. 1158–1162.
Shih, T.T.; 1980: Evaluation of the Probabilistic Approach to Brittle Design. Eng. Fract. Mech., vol. 13, no. 2, pp. 257–271.
Smith, M.C.; 1972: Deformation and Fracture Mechanisms in Polycrystalline Graphites. Proceedings of the Conference on Continuum Aspects of Graphite Design, OSTI ID 4665905, CONF–701105.
Smith, Richard Lyttleton; 1979: Limit Theorems for the Reliability of Series-Parallel Load-Sharing Systems. Ph.D. Thesis, Cornell University.
Smith, R.L.; 1980: Probability Model for Fibrous Composites With Local Load Sharing. Proc. R. Soc. London, Ser. A, vol. 372, no. 1751, pp. 539–553.
Smith, Richard L.; 1982: The Asymptotic Distribution of the Strength of a Series-Parallel System With Equal Load-Sharing. Ann. Prob., vol. 10, no. 1, pp. 137–171.
Smith, R.L., et al., 1983: Lower-Tail Approximations for the Probability of Failure of Three-Dimensional Fibrous Composites With Hexagonal Geometry. Proc. R. Soc. Lond. Ser. A, vol. 388, pp. 353–391.
Smith, R.L.; and Phoenix, S.L.; 1981: Asymptotic Distributions for the Failure of Fibrous Materials Under Series-Parallel Structure and Equal Load-Sharing. J. Appl. Mech. Trans. ASME, vol. 48, no. 1, pp. 75–82.
Sookdeo, Steven; Nemeth, Noel N.; and Bratton, Robert L.; 2008: Reliability Assessment of Graphite Specimens Under Multiaxial Stresses. NASA/TM—2008-215204.
Strizak, J.P.; 1991: The Effect of Volume on the Tensile Strength of Several Nuclear-Grade Graphites. The Status of Graphite Development for Gas Cooled Reactors, IAEA–TECDOC–690, pp. 233–241.
Tang, P.Y.; 1979: Recommendation of a Triaxial Failure Theory for Graphite. General Atomic Report GA–A–15333.
Taylor, R., et al.; 1967: The Mechanical Properties of Reactor Graphite. Carbon, vol. 5, pp, 519–531.
Tennery, V.J.; and Ferber, M.K.; 1989: Fracture Strength Analysis of Silicon Nitride and Silicon Carbide Ceramics From an International Cooperative Research Program. Presented at the Annual Automotive Technology Development Contractors Coordination Meeting, Dearborn, MI.
Thoman, D.R.; Bain, L.J.; and Antle, C.E.; 1969: Inferences on the Parameters of the Weibull Distribution. Technomet., vol. 11, no. 3, pp. 445–460.
Toyo Tanso USA, Inc.: Grade IG–11, EDM Isotropic Graphite. http://www.ttu.com/Grade_IG-11.html Accessed Oct. 22, 2010.
Tsai, Stephen W.; and Wu, Edward M.; 1971: A General Theory of Strength for Anisotropic Materials. J. Compos. Mater., vol. 5, no. 1, pp. 58–80.
Tucker, M.O.; and McLachlan, N.; 1993: Fracture and Microstructure of Graphites. J. Phys. D: Appl. Phys., vol. 26, no. 6, pp. 893–907.
Tucker, M.O.; Rose, A.P.G.; and Burchell, T.D.; 1986: The Fracture of Polygranular Graphites. Carbon, vol. 24, no. 5, pp. 581–602.
Uchimura, H.; Kokaji, A.; and Kaji, M.; 1992: Evaluation of Fast Fracture Strength of Ceramic Components Under Multiaxial Stress States. ASME Paper 92–GT–384.

U.S. DOE Nuclear Energy Research Advisory Committee and Generation IV International Forum; 2002: A Technology Roadmap for Generation IV Nuclear Energy Systems, Ten Nations Preparing Today for Tomorrow's Energy Needs. http://gif.inel.gov/roadmap/pdfs/gen_iv_roadmap.pdf, Accessed Nov. 1, 2010

U.S. Department of Energy; 2008: Energy Efficiency & Renewable Energy, Industrial Technologies Program. http://www1.eere.energy.gov/industry/bestpractices/process_heat.html Last updated Apr. 16, 2008, Accessed Oct. 22, 2010.

Wapedia, 2009: Generalized Extreme Value Distribution. http://wapedia.mobi/en/Generalized_extreme_value_distribution Accessed Oct. 22, 2010.

Watson, A.S.; and Smith, R.L.; 1985: Examination of Statistical Theories for Fibrous Materials in the Light of Experimental Data. J. Mat. Sci., vol. 20, no. 9, pp. 3260–3270.

Weibull, Waloddi; 1939a: A Statistical Theory of the Strength of Materials. Ingeniorsvetenskapsakademiens Handlingar, no. 151.

Weibull, Waloddi; 1939b: The Phenomenon of Rupture in Solids. Ingeniorsvetenskapsakademiens Handlingar, no. 153.

Weibull, Waloddi; 1951: A Statistical Distribution Function of Wide Applicability. J. Appl. Mech. Trans. ASME, vol. 18, pp. 293–297.

Wetherhold, R.C.; 1983: Statistics of Fracture of Composite Materials Under Multiaxial Loading. Ph.D. Thesis, University of Delaware.

Wikipedia, 2010: Generalized Extreme Value Distribution. http://en.wikipedia.org/wiki/Extreme_value_distribution Accessed Oct. 22, 2010.

Yahr, G.T., et al., 1993: Multiaxial Tests of H–451 Graphite. ORNL/NPR–93/13, vol. 1, Oct. Available from Carbon Materials Technology Group, Oak Ridge National Laboratory.

Zapperi, Stefano; and Nukala, Phani Kumar V.V.; 2006: Fracture Statistics in the Three-Dimensional Random Fuse Model. Int. J. Fract., vol. 140, nos. 1–4, pp. 99–111.

Zapperi, Stefano; Vespignani, Alessandro; and Stanley, H. Eugene; 1997: Plasticity and Avalanche Behaviour in Microfracturing Phenomena. Nature, vol. 388, pp. 658–660.

Zweben, C.; and Rosen, B.W.; 1970: Statistical Theory of Material Strength With Application to Composite Materials. J. Mech. Phys. Solids, vol. 18, no. 3, pp. 189–206.

REPORT DOCUMENTATION PAGE	Form Approved OMB No. 0704-0188

1. REPORT DATE *(DD-MM-YYYY)*	2. REPORT TYPE	3. DATES COVERED *(From - To)*
01-03-2011	Technical Memorandum	

4. TITLE AND SUBTITLE
Statistical Models of Fracture Relevant to Nuclear-Grade Graphite: Review and Recommendations

5a. CONTRACT NUMBER

5b. GRANT NUMBER

5c. PROGRAM ELEMENT NUMBER

6. AUTHOR(S)
Nemeth, Noel, N.; Bratton, Robert, L.

5d. PROJECT NUMBER

5e. TASK NUMBER

5f. WORK UNIT NUMBER
WBS 392259.02.03.0683.11

7. PERFORMING ORGANIZATION NAME(S) AND ADDRESS(ES)
National Aeronautics and Space Administration
John H. Glenn Research Center at Lewis Field
Cleveland, Ohio 44135-3191

8. PERFORMING ORGANIZATION REPORT NUMBER
E-16798-1

9. SPONSORING/MONITORING AGENCY NAME(S) AND ADDRESS(ES)
National Aeronautics and Space Administration
Washington, DC 20546-0001

10. SPONSORING/MONITOR'S ACRONYM(S)
NASA

11. SPONSORING/MONITORING REPORT NUMBER
NASA/TM-2011-215805

12. DISTRIBUTION/AVAILABILITY STATEMENT
Unclassified-Unlimited
Subject Category: 39
Available electronically at http://gltrs.grc.nasa.gov
This publication is available from the NASA Center for AeroSpace Information, 443-757-5802

13. SUPPLEMENTARY NOTES
This report is an expanded version of Nemeth, Noel N.; and Bratton, Robert L.; 2010: Overview of Statistical Models of Fracture for Nonirradiated Nuclear-Graphite Components. Nucl. Eng. Des., vol. 240, no. 1, pp. 1-29.

14. ABSTRACT
The nuclear-grade (low-impurity) graphite needed for the fuel element and moderator material for next-generation (Gen IV) reactors displays large scatter in strength and a nonlinear stress-strain response from damage accumulation. This response can be characterized as quasi-brittle. In this expanded review, relevant statistical failure models for various brittle and quasi-brittle material systems are discussed with regard to strength distribution, size effect, multiaxial strength, and damage accumulation. This includes descriptions of the Weibull, Batdorf, and Burchell models as well as models that describe the strength response of composite materials, which involves distributed damage. Results from lattice simulations are included for a physics-based description of material breakdown. Consideration is given to the predicted transition between brittle and quasi-brittle damage behavior versus the density of damage (level of disorder) within the material system. The literature indicates that weakest-link-based failure modeling approaches appear to be reasonably robust in that they can be applied to materials that display distributed damage, provided that the level of disorder in the material is not too large. The Weibull distribution is argued to be the most appropriate statistical distribution to model the stochastic-strength response of graphite.

15. SUBJECT TERMS
Graphite; Strength; Flexural strength; Nuclear electric power generation

16. SECURITY CLASSIFICATION OF:			17. LIMITATION OF ABSTRACT	18. NUMBER OF PAGES	19a. NAME OF RESPONSIBLE PERSON
a. REPORT	b. ABSTRACT	c. THIS PAGE			STI Help Desk (email:help@sti.nasa.gov)
U	U	U	UU	115	19b. TELEPHONE NUMBER *(include area code)* 443-757-5802